C. L. M. POUW

PARAMAGNETIC SPIN-LATTICE RELAXATION IN MANGANESE, CHROMIUM AND COBALT COMPOUNDS STUDIED WITH NON-RESONANCE TECHNIQUES AT STRONG MAGNETIC FIELDS

PARAMAGNETIC SPIN-LATTICE RELAXATION
IN MANGANESE, CHROMIUM AND COBALT COMPOUNDS
STUDIED WITH NON-RESONANCE TECHNIQUES
AT STRONG MAGNETIC FIELDS

PARAMAGNETIC SPIN-LATTICE RELAXATION IN MANGANESE, CHROMIUM AND COBALT COMPOUNDS STUDIED WITH NON-RESONANCE TECHNIQUES AT STRONG MAGNETIC FIELDS

PROEFSCHRIFT

TER VERKRIJGING VAN DE GRAAD VAN DOCTOR IN DE WISKUNDE EN NATUURWETENSCHAPPEN AAN DE RIJKSUNIVERSITEIT TE LEIDEN, OP GEZAG VAN DE RECTOR MAGNIFICUS DR. A.E. COHEN, HOOGLERAAR IN DE FACULTEIT DER LETTEREN, VOLGENS BESLUIT VAN HET COLLEGE VAN DEKANEN TE VERDEDIGEN OP WOENSDAG 22 OKTOBER 1975 TE KLOKKE 15.15 UUR

door

Clemens Leonardus Maria Pouw
geboren te Ter Aar in 1947

Dutch Efficiency Bureau - Pijnacker

PROMOTOR: *PROF. DR. N.J. POULIS*

DIT PROEFSCHRIFT IS TOT STAND GEKOMEN

ONDER LEIDING VAN *DR. A.J. VAN DUYNEVELDT*

ISBN 90 6231 003 6

addunt,mutant, adimunt,reponũt repetunt,recudunt, oſtendunt, nonũ in annum premunt,nec unq̃ ſibi ſatiſſaci/unt,ac futile præmiũ,nempe laudẽ,eam q̃ perpaucorũ, tanti emunt, tot uigiliꝭ, ſomniq̃,rerum omniũ dulciſſimi, tanta iactura,tot ſudoribus,tot crucibus.

Desiderius Erasmus, *Stultitiae Laus*
(Iohannes Frobenius, Basel, 1515)

Aan Carla

De illustratie op de omslag stelt voor: de Natuurfilosoof, naar de originele tekening van Hans Holbein de Jongere in de marge van het uit 1515 daterende Bazelse exemplaar van Erasmus' *Lof der Zotheid*.

CONTENTS

PREFACE

In the study of paramagnetic spin-lattice relaxation phenomena two types of research may be recognised. The first successful measurements were performed with non-resonance techniques, in which the differential susceptibility is studied at relatively low frequencies (<1 MHz). The relaxation parameters obtained in that way represent the relaxation behaviour averaged over all populated energy levels. The fundamental theoretical work on spin-lattice relaxation is specifically related to those cases in which the paramagnetic ion can be considered as isolated, a situation that is best approached in highly dilute magnetic materials. From the inapplicability of non-resonance techniques to measurements on magnetically highly diluted materials it can be understood that many of the earlier non-resonance data are not in accordance with the theoretical predictions.

The progress in modern electronics enabled the use of resonance techniques, the second type of paramagnetic relaxation research. With these methods, operating at microwave frequencies, it became possible to obtain information on the actual population difference between a selected pair of energy levels. The theoretical predictions on spin-lattice relaxation times were verified regularly in highly diluted systems. A drawback of the resonance techniques is that they are restricted usually to one, or a few, frequencies and, as a consequence, to one, or a few, magnetic fields. A study of the field dependence of the relaxation times with the resonance methods is therefore rather elaborate. Particularly, the striking field dependence of the direct spin-lattice relaxation process was rarely observed.

Since the application of strong magnetic fields, it has been demonstrated that the non-resonance technique may be applied successfully in the examination of the direct process in concentrated materials. The non-resonance method is particularly suited for the measurement of the field dependence of the relaxation time. At strong magnetic fields the paramagnetic ions may be considered as isolated from each other even in concentrated materials and the observed relaxation times agree with the theoretical predictions. However, the identification of the direct relaxation process suffers from inaccuracies

due to the influence of the phonon bottleneck. This effect arises because at the temperatures of liquid helium, where the measurements are performed, the lattice oscillations are not always capable of a rapid energy transport from the magnetic spin system towards the cooling liquid. Such a bottleneck is not expected if the experiments are performed at, for instance, the temperatures of liquid hydrogen.

In the present research, non-resonance techniques have been applied in the investigation of spin-lattice relaxation times. The examination of the field dependence of the relaxation times at strong magnetic fields has been extended to the temperature range of liquid hydrogen.

In chapter I the microscopic theory of spin-lattice relaxation has been reviewed. A survey of the theoretical foundations of the non-resonance method is given in chapter II, together with the experimental facilities. In chapter III the investigation of spin-lattice relaxation times in various manganese and chromium compounds is presented. It is demonstrated that the direct spin-lattice relaxation process can be studied adequately by using a non-resonance method at liquid hydrogen temperatures and strong external magnetic fields. The direct and the Raman process of the manganese and chromium salts showed the behaviour as predicted for multilevel systems. A comparison between the results in the various compounds gives a reasonable agreement with the theoretical predictions. The relaxation behaviour in three cobalt Tutton salts is reported in chapter IV. Measurements at liquid hydrogen temperatures and strong magnetic fields revealed the existence of a field dependent Raman process as predicted for an isolated Kramers doublet already in one of the pioneering papers on spin-lattice relaxation phenomena, but not experimentally verified until now.

CHAPTER I

MICROSCOPIC THEORY OF SPIN-LATTICE RELAXATION

1.1 *Paramagnetism*

A paramagnetic substance contains ions with a permanent magnetic dipole moment, which are randomly oriented, independent from each other. The application of an external magnetic field on such a system results in a net magnetic moment. The magnetic moment of an ion - or atom - arises from the orbital angular momentum and the spin angular momentum of the electrons in incomplete shells. The nucleus itself has a magnetic moment also, but usually this moment is negligible compared to the magnetic moments of the electrons. Incomplete electron shells may occur in the elements of the transition groups in the periodic system, as for instance the iron group with an incomplete 3d shell and the rare earths group with an incomplete 4f shell.

If a paramagnetic system, consisting of N magnetic dipoles, is placed in a constant external magnetic field H, a magnetization M is induced. For an energy spectrum of the dipoles that consists of a number of low lying energy levels with a distance between consecutive levels much smaller than the thermal energy kT, the magnetization is given by [1]:

$$M = NgJ\mu_B B_J(gJ\mu_B H/kT) \qquad (1)$$

with the Brillouin function

$$B_J(x) = \frac{2J+1}{2J}\coth\left(\frac{2J+1}{2J}x\right) - \frac{1}{2J}\coth\left(\frac{1}{2J}x\right),$$

in which g is the Landé splitting factor, J the total angular momentum quantum number and μ_B the Bohr magneton. In calculating the magnetization as given by eq.(1) higher energy levels, giving rise to the so-called 'Van Vleck' temperature independent paramagnetism, are neglected. In the limiting case $g\mu_B H \ll kT$ the expression for the magnetization may be simplified to:

$$M = Ng^2 J(J+1)\mu_B^2 H/3kT. \qquad (2)$$

The quotient M/H is called the static susceptibility χ. Eq.(2) is known as the Curie law, generally written as $\chi = C/T$, in which C is the Curie constant being equal to:

$$C = Ng^2J(J + 1)\mu_B^2/3k.$$

In many paramagnetic compounds, with interactions between the ions, a better approximation of the experimentally observed relation between the static susceptibility and the temperature is obtained by the Curie-Weiss law:

$$\chi = C/(T-\theta) \qquad (3)$$

in which θ is the Curie-Weiss constant.

1.2 *Spin-lattice relaxation*

1.2.1 *Paramagnetic relaxation.* The expressions given above for the magnetization and the susceptibility are only valid for magnetic systems in thermal equilibrium with their surroundings. The time required to establish equilibrium, if, for instance, the external magnetic field is varied, was neglected. Generally, the magnetization of a paramagnetic substance does not follow a change of one of the external conditions instantaneously. This effect is called paramagnetic relaxation.

It has become common to refer to the system of magnetic moments of a paramagnetic substance as the spin system. All non-magnetic properties of the paramagnetic material as lattice vibrations, are contained in the so-called lattice system. The spin system is not necessarily in internal equilibrium. In order to establish an equilibrium situation relaxation effects within the spin system may occur under the agency of e.g. dipole-dipole or exchange interactions. We assume the characteristic time constant to reach such an equilibrium to be short compared to the relaxation phenomena that will be discussed below. So we consider only spin systems in internal equilibrium. According to quantum statistical theory the populations of the energy levels of the spin system can be represented by a Boltzmann distribution with a characteristic temperature T_S, the spin temperature. For a spin system that is thermally isolated from its surroundings, a variation in one of the external conditions leads to a change of the spin temperature because a redistribution of the populations of the energy levels requires the exchange of energy. Interaction of the spin system with the lattice vibrations provides a

mechanism to exchange energy with the lattice system and a redistribution of the populations of the energy levels of the spin system can occur. This effect is called spin-lattice relaxation. The redistribution of the energy level population after a change in the magnetic field is coupled with a change of the magnetization. Phenomenologically, the response of the magnetization after a variation in one of the external conditions may be given as:

$$dM/dt = (M_o - M)/\tau \qquad (4)$$

in which M_o is the equilibrium magnetization and the time constant τ may be identified as the spin-lattice relaxation time.

1.2.2 *Transition probability*. The spin-lattice relaxation time is connected with the probability that transitions occur between the energy states of the spin system. We will derive the relation between the transition probability and the spin-lattice relaxation time for a simple system consisting of N paramagnetic ions that have only two possible energy states $|a\rangle$ and $|b\rangle$ with energies E_a and E_b. As mentioned above, the spin temperature is defined as:

$$n_b/n_a = e^{-(E_b - E_a)/kT_S}$$

in which n_b and n_a are the number of spins in states $|b\rangle$ and $|a\rangle$, respectively ($n_a + n_b = N$). If the spin system is in thermal equilibrium with the lattice, T_S equals the lattice temperature T_L and thus

$$N_b/N_a = e^{-(E_b - E_a)/kT_L},$$

the capitals N_a and N_b correspond to the equilibrium populations. The probabilities of a transition from $|a\rangle$ to $|b\rangle$, and reverse, are represented by w_{ab} and w_{ba} respectively. The change in population of the levels per unit time can be written as:

$$dn_a/dt = -w_{ab}n_a + w_{ba}n_b = -dn_b/dt. \qquad (5)$$

If the spin system is in thermal equilibrium with the lattice there is a certain probability that transitions between the energy states occur also, but the net change in the populations is zero:

$$dN_a/dt = dN_b/dt = -w_{ab}N_a + w_{ba}N_b = 0.$$

Starting from eq.(5) and omitting some algebraic steps finally leads to:

$$d(n_a - n_b)/dt = (w_{ab} + w_{ba}) \{(N_a - N_b) - (n_a - n_b)\}. \qquad (6)$$

As the magnetization in a simple two level system is proportional to the difference between the populations of the energy states, comparison of eq.(6) with eq.(4) directly yields:

$$1/\tau = w_{ab} + w_{ba}. \qquad (7)$$

A complicated relaxation behaviour arises in the case that more than two energy levels are populated. For a system with p energy levels E_p the expression for the spin-lattice relaxation time becomes [2]:

$$1/\tau = \sum_{n,m=1}^{p} (E_n - E_m)^2 w_{nm} / (2 \sum_{n} E_n^2). \qquad (8)$$

The expression for the relaxation time of the simple two level system follows directly from the above relation with p = 2.

In practise, the relaxation time is studied as a function of magnetic field and temperature. These dependences of τ may be predicted by calculation of the transition probabilities. We consider a system consisting of magnetic ions, placed in a lattice. Transitions between the electronic states of an ion may be induced under the agency of a time dependent perturbation. Such a time dependent perturbation exists due to the presence of thermal vibrations in the crystal lattice. These lattice vibrations, usually described by phonons, cause the interatomic spacings in the lattice to vary continuously. The relative motion of the atoms modulates the interatomic interactions, as for instance the crystalline field potential at the site of the magnetic ion, the dipole-dipole coupling between neighbouring magnetic ions or the exchange interactions. Thus the effect of the lattice vibrations may be transferred to the magnetic ion. In general, the perturbation potential at the site of a magnetic ion, surrounded by n neighbours can be written as:

$$V_{perturbation} = V(\vec{r}_1, \vec{r}_2, \ldots\ldots \vec{r}_n) - V(\vec{r}_1{}^o, \vec{r}_2{}^o, \ldots\ldots \vec{r}_n{}^o)$$

in which $V(\vec{r}_1^{\,o}, \vec{r}_2^{\,o}, \ldots\ldots \vec{r}_n^{\,o})$ is the static value of the interaction potential due to the atoms at relative distances $\vec{r}_n^{\,o}$ and $V(\vec{r}_1, \vec{r}_2, \ldots\ldots \vec{r}_n)$ the potential after a relative displacement of the atoms $\vec{r}_n^{\,o} - \vec{r}_n = \Delta\, r_n(t)$ (a function of time!). If this displacement is small, the perturbation potential may be written in a series expansion in $\Delta r_j(t)$ as:

$$V_{\text{perturbation}} = V' + V'' + \ldots\ldots$$

$$= \sum_{j=1}^{n} V_j \Delta r_j(t) + \tfrac{1}{2} \sum_{jj'=1}^{n} V_{jj'} \Delta r_j(t) \Delta r_{j'}(t) + \ldots\ldots \qquad (9)$$

where $V_j = (\partial V/\partial r_j)_{r_j = r_j^{\,o}}$ and $V_{jj'} = (\partial^2 V/\partial r_j \partial r_{j'})_{r_j = r_j^{\,o},\, r_{j'} = r_{j'}^{\,o}}$.

In general, the probability per unit time for a transition of the system of ions plus lattice from a state $|\alpha\rangle$ to $|\beta\rangle$ is given by [3]):

$$w_{\alpha\beta} = (2\pi/\hbar)\,|\langle\beta|V'|\alpha\rangle|^2 \rho(E) +$$

$$(2\pi/\hbar)\left[\,|\langle\beta|V''|\alpha\rangle|^2 + \Big|\sum_{\gamma} \langle\beta|V'|\gamma\rangle\langle\gamma|V'|\alpha\rangle/(E_\alpha - E_\gamma)\Big|^2\right] \rho(E'). \qquad (10)$$

The energy density of the final state is represented by the terms $\rho(E)$ and $E_\alpha - E_\gamma$ is the energy difference between the initial state $|\alpha\rangle$ and an intermediate state $|\gamma\rangle$. The first and second order perturbations V' and V'' between lattice vibrations and magnetic ion are written in eq.(9) as the product of two terms. The first term describes the rate of change of the interaction between the magnetic ion and the neighbours, the second one represents the variation of the positions of these neighbours with time due to the lattice vibrations. The wave functions describing the combined system can also be written as the direct product of the wave functions of the magnetic ion and the lattice, if the interaction between the magnetic ion and the lattice vibrations is weak. Thus the matrix element $\langle\beta|V'|\alpha\rangle$ in eq.(10) becomes:

$$\sum_j \langle b|V_j|a\rangle\langle q|\Delta r_j(t)|p\rangle$$

and a similar factorisation is allowed for $\langle\beta|V''|\alpha\rangle$. As a consequence, the expression for the transition probability contains matrix elements involving the properties of the lattice vibrations. In the next paragraph we will review

some general aspects of the theory of lattice vibrations that are important in deriving the transition probability.

1.2.3 *Phonons.* In the phonon description of the lattice vibrations it is assumed that the lattice is composed of quantised modes, each representing a simple harmonic oscillator. The quantum of the lattice vibrational field is referred to as phonon [4]). A vibrational state of the lattice is specified by a set of numbers p_i with $i = 1,\ldots 3n$ (n is the total number of the atoms in the lattice), which represent the number of phonons in each mode ω_i, with energy $\hbar\omega_i$. A typical state function for a given vibrational state is $|p_1,p_2,\ldots\ldots p_{3n}>$ (abbreviation $|\ldots p_i\ldots>$). The occupation number p_i is given by Bose-Einstein statistics:

$$p_i = 1/(e^{\hbar\omega_i/kT_L} - 1).$$

This number can be expressed also in terms of the annihilation operator a_i and the creation operator $a_i^\dagger$. The annihilation operator a_i has the effect of reducing the number of phonons in mode ω_i by one, while all other occupation numbers remain unchanged. Similarly, $a_i^\dagger$ increases p_i by one. Thus:

$$a_i|\ldots p_i\ldots> = p_i^{\frac{1}{2}}|\ldots p_i-1\ldots>$$

$$a_i^\dagger|\ldots p_i\ldots> = (p_i+1)^{\frac{1}{2}}|\ldots p_i+1\ldots.>$$

and the eigenvalue of the operator $a_i^\dagger a_i$ is p_i. The total Hamiltonian for the lattice may be written now as:

$$\mathcal{H}_L = \sum_i \hbar\omega_i(p_i+\tfrac{1}{2}) = \sum_i \hbar\omega_i(a_i^\dagger a_i+\tfrac{1}{2}).$$

The relative displacements of neighbouring atoms in a lattice can be expressed in terms of the annihilation and creation operator in the long wave approximation [4]). Omitting the, at present, irrelevant constants one may write:

$$\sum_j \Delta r_j(t) \propto (\hbar/2M)^{\frac{1}{2}} \sum_i \omega_i^{\frac{1}{2}} v^{-1}(a_i+a_i^\dagger),$$

in which v is the velocity of sound in the crystal and M the lattice mass.

In order to calculate the density of states of the phonons one usually

assumes the Debije model. In this model, the crystal is represented by an isotropic elastic continuum with wavelengths, long compared to the interatomic spacings. The distribution of the phonons is given by:

$$\rho(\omega) = (1/2\pi^2)(2v_t^{-3}+v_l^{-3})\omega^2 V$$

where v_l and v_t are the longitudinal and transversal velocities of sound in the material and V is the volume of the crystal. The maximum number of vibrational modes is 3n and thus the distribution $\rho(\omega)$ is cut off at a maximum frequency ω_m, given by:

$$\omega_m^3 = (18\pi^2 n/V)(2v_t^{-3}+v_l^{-3})^{-1}. \qquad (11)$$

The maximum frequency is related to the so-called Debije temperature Θ_D by $\hbar\omega_m = k\Theta_D$.

1.2.4 *The direct spin-lattice relaxation process.* The expression for the transition probability $w_{\alpha\beta}$ as given in eq.(10) consists of three terms. Each of these terms corresponds to a relaxation process with its characteristic temperature and field dependence of τ. We consider a single magnetic ion that has energies E_a or E_b ($E_b - E_a = E_{ba} > 0$) corresponding to the states $|a\rangle$ and $|b\rangle$. Then the first term of eq.(10), giving rise to a single-phonon spin-lattice relaxation process, may be written as:

$$w_{ab} = (2\pi/\hbar)|\sum_j \langle b|V_j|a\rangle\langle q|\Delta r_j(t)|p\rangle|^2 \rho(E).$$

This transition probability involves the increase of the energy of the magnetic spin with E_{ba} due to the annihilation of a phonon having the same energy, so that the population of the phonon mode $\omega_i = E_{ba}/\hbar$ is reduced by one. A schematic view of this so-called direct process is given in fig. 1. The energy density $\rho(E)$ can be expressed in the phonon distribution $\rho(\omega)$ as [5]:

$$\rho(E) = (1/\hbar)\rho(\omega)\delta(E_{ba}/\hbar - \omega)$$

in which a Dirac delta function is used to restrict to phonons of frequency $E_{ba}/\hbar$ only. Summation over all phonon modes and applying the Debije model for $\rho(\omega)$ finally leads to:

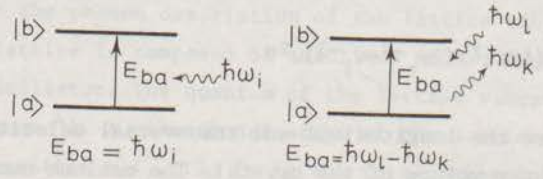

Fig. 1 Schematic diagrams indicating the direct and the Raman relaxation processes.

$$w_{ab} = (3/2\pi\hbar\rho v^5)|\sum_j \langle b|V_j|a\rangle|^2 (E_{ba}/\hbar)^3 p_i,$$

where ρ is the density of the crystal. In this expression the difference between the longitudinal and transversal velocities of sound has been neglected ($v_l = v_t = v$). Following an analogous derivation, the transition probability for the reverse process, with a spin flipping from $|b\rangle$ to $|a\rangle$ and the simultaneous emission of a phonon, becomes:

$$w_{ba} = (3/2\pi\hbar\rho v^5)|\sum_j \langle a|V_j|b\rangle|^2 (E_{ba}/\hbar)^3 (p_i + 1).$$

Addition of w_{ab} and w_{ba}, according to eq.(7), directly leads to the spin-lattice relaxation rate:

$$\tau_{direct}^{-1} = (3/2\pi\hbar^4\rho v^5)|\sum_j \langle a|V_j|b\rangle|^2 E_{ba}^3 \coth(E_{ba}/2kT). \qquad (12)$$

The energy E_{ba} is equal to $g\mu_B H$ if the energy splittings are caused by an external magnetic field H only, so the field and temperature dependence of τ_{direct} may be found from:

$$\tau_{direct}^{-1} = AH^3 \coth(g\mu_B H/2kT). \qquad (13)$$

The hyperbolic cotangent simplifies to $2kT/g\mu_B H$ if $g\mu_B H \ll kT$, thus in such cases:

$$\tau^{-1}_{direct} = A'TH^2.$$

1.2.5 *The Raman spin-lattice relaxation process.* The number of phonons in a frequency interval $d\omega$ about a certain frequency ω is equal to $\rho(\omega)p(\omega)d\omega$. In the Debije phonon model this expression becomes proportional to $\omega^2/(e^{\hbar\omega/kT} - 1)d\omega$, a function that reaches a maximum value at $\hbar\omega \approx kT$. This implies that, if the energy of the phonons in a certain mode is small compared to kT, also the number of phonons in that mode is small. Usually the energy level splitting between the spin states is small compared to kT and as a consequence, the phonon spectrum is not optimally used in the direct relaxation process. The much more abundant phonons near the peak of the energy distribution ($\hbar\omega \approx kT$) are available for the second order processes. These processes, given by the second term of eq.(10) result in the creation and the annihilation of two phonons, so that the energy difference between these two phonons equals the energy level splitting between the spin states. Thus, second order processes which are expected to be less effective may dominate over the, first order, direct process because of the large number of available phonons. Such a two-phonon process is analogous to the Raman effect in optical spectroscopy and therefore referred to as Raman process. A schematic view of the Raman process is given in fig. 1.

The transition probability for the Raman process between a spin state $|a\rangle$ and $|b\rangle$ involving two phonons $\hbar\omega_l$ and $\hbar\omega_k$, so that $\hbar\omega_l - \hbar\omega_k = E_{ba}$, may be written as:

$$w_{ab} = (2\pi/\hbar) \left[\left| \sum_{jj'} \langle b|V_{jj'}|a\rangle \right|^2 + \left| \sum_{jj'c} \frac{\langle b|V_j|c\rangle\langle c|V_{j'}|a\rangle}{E_a - E_c} \right|^2 \right]$$

$$|\langle q|\Delta r_j(t)|p\rangle\langle q'|\Delta r_{j'}(t)|p'\rangle|^2 (1/\hbar)\rho(\omega_l)\rho(\omega_k)$$

$$\delta\{(E_{ba}/\hbar) - (\omega_l - \omega_k)\}d\omega_k \, d\omega_l .$$

The first contribution arises from the second order term V" of the perturbation potential, the other from V' in second order perturbation theory. As this last perturbation operator has to act twice, it is necessary to interact through the intermediary of an excited state $|c\rangle$. The summation in the above expression is over all intermediate states $|c\rangle$. The principle of conservation of energy is

required only between the initial and the final state, and not between the initial and intermediate or between intermediate and final state. This leads to a large uncertainty of the energy in the intermediate state, which can be regarded therefore as a virtual state. When the two-phonon process involves a relaxation via a real intermediate state, the principle of energy conservation holds for both steps. This process, that is known as the Orbach process [5]), will not be discussed further here. By straightforward calculation the following expression for the Raman relaxation time is obtained:

$$\tau_{Raman}^{-1} = (9/8\pi^3 v^{10}\rho^2)(e^{E_{ba}/kT} + 1)$$

$$\int \frac{(E_{ba}/\hbar + \omega_k)^3\ \omega_k^3 e^{\hbar\omega_k/kT}}{(e^{\hbar\omega_k/kT} - 1)(e^{(\hbar\omega_k + E_{ba})/kT} - 1)} \Big[\Big| \sum_{jj'} \langle a|V_{jj'}|b\rangle \Big|^2 +$$

$$\Big| \sum_{jj'c} \langle a|V_j|c\rangle\langle c|V_{j'}|b\rangle \Big\{ \frac{1}{\hbar\omega_k + \tfrac{1}{2}E_{ba} - \Delta_c} - \frac{1}{\hbar\omega_k + \tfrac{1}{2}E_{ba} + \Delta_c} \Big\} \Big|^2 \Big] d\omega_k, \qquad (14)$$

in which Δ_c represents the energy level splitting between the intermediate state $|c\rangle$ and state $|b\rangle$. In the case that $\Delta_c >> kT$, the phonon energy $\hbar\omega_k$ may be neglected compared totemperatures, while τ_{Raman}^{-1} honons participating in the Raman process have energies $\hbar\omega \cong kT$. Then, with $E_{ba} << kT$, the temperature and field dependence of the Raman relaxation time becomes:

$$\tau_{Raman}^{-1} = BH^0T^7J_6(\Theta_D/T) \qquad (15)$$

in which $J_6(\Theta_D/T)$ is one of the integrals

$$J_n(\Theta_D/T) = \int_0^{\Theta_D/T} x^n e^x/(e^x - 1)^2 dx \qquad (16)$$

with $x = \hbar\omega/kT$. These integrals are constant for $T << \Theta_D$ and proportional to T^{1-n} for $T >> \Theta_D$. So the Raman relaxation rate τ_{Raman}^{-1} varies as T^7 at low temperatures, while $\tau_{Raman}^{-1} \propto T^2$ at the highest temperatures. In the region $0.1\Theta_D < T < \Theta_D$ the exponent decreases continuously from 7 towards 2.

1.3 *The spin-lattice interaction mechanism*

In the derivation of the dependence of spin-lattice relaxation times on magnetic field and temperature as presented in the foregoing section, we passed quickly over the mechanism that is responsible for the interaction between the lattice and the spin system. In his pioneering paper on spin-lattice relaxation phenomena, Waller [6]) proposed the interaction mechanism to be the result of the thermal modulation of the magnetic dipolar interaction. This theory leads to much longer relaxation times than observed experimentally. Al'tshuler [7]) modified the theory many years later, but the numerical agreement with experiment is still not very satisfactory. Kronig [8]) and Van Vleck [9]) supposed the modulation of the crystalline field to be of major importance, leading generally to shorter relaxation times than with the Waller-Al'tshuler theory. Both theories will be reviewed.

1.3.1 *The Waller-Al'tshuler (WA) interaction mechanism.* The first numerical calculation of spin-lattice relaxation times as presented by Waller [6]) in 1932, deals with a coupling between the spin system and the lattice via the modulation of the magnetic dipoler interaction of the ions under influence of the lattice vibrations. The magnetic dipole interaction between an ion i and its neighbours j at a distance $\vec{r}_{ij}$ is given by:

$$V_{dipole} = \sum_j \left[(\vec{\mu}_i.\vec{\mu}_j)/r_{ij}^3 - 3(\vec{\mu}_i.\vec{r}_{ij})(\vec{\mu}_j.\vec{r}_{ij})/r_{ij}^5\right] \qquad (17)$$

with $\vec{\mu}$ representing the magnetic dipole moments of the ions. The magnetic field at the site of one magnetic ion due to the magnetic dipole moments of neighbouring magnetic ions fluctuates because the distance $\vec{r}_{ij}$ between the ions is varied continuously by the lattice vibrations. An oscillating magnetic field is produced that may induce a transition of a single spin between the energy levels of the spin system. Al'tshuler modified this theory by taking into account the simultaneous re-orientation of two spins [7]). In that case the exchangable energy at a magnetic field H amounts to $2g\mu_B H$. Thus, for the WA interaction mechanism the field and temperature dependence of τ_{direct} has to be written as:

$$\tau_{direct}^{-1} = A_{WA\ I} H^3 \coth(g\mu_B H/2kT) + A_{WA\ II} H^3 \coth(2g\mu_B H/2kT), \qquad (18)$$

where the first term represents the single spin flip and the second one the simultaneous transition of two spins. The coefficients $A_{WA\ I}$ and $A_{WA\ II}$ can be calculated by applying the dipolar interaction potential as given in eq.(17) into the general formula τ_{direct} (eq.(12)). The result is [7]:

$$A_{WA\ I} = (4\pi^3 Z g^7 \mu_B^7 / 3h^4 \rho v^5 r_o^6) S(2S + 1)(S + 1)^2, \text{ and} \qquad (19a)$$

$$A_{WA\ II} = (128\pi^3 Z g^7 \mu_B^7 / 3h^4 \rho v^5 r_o^6)(2S + 1)^2 (S + 1)^2, \qquad (19b)$$

in which r_o is the equilibrium distance between nearest neighbour magnetic ions and Z the number of nearest neighbours. The quantity Z in the coefficients $A_{WA\ I}$ and $A_{WA\ II}$ is responsible for a concentration dependence of the relaxation times. The mechanism may be of importance if for instance the magnetic ions have large magnetic moments and are present in large concentrations.

The relaxation time for the Raman process in the WA interaction theory is proportional to $T^{-7} J_6^{-1}(\Theta_D/T)$ as given in eq.(15). A complete expression for the coefficient B in the Waller-Al'tshuler theory will not be discussed.

1.3.2 *The Kronig-Van Vleck (KVV) interaction mechanism.* Kronig [8] and Van Vleck [9] supposed the interaction mechanism between lattice and spins to arise from the modulation of the electrical crystalline field through the motion of the atoms surrounding the magnetic ion. The orbital states of a magnetic ion may be split by an electrical crystal field. Via the spin-orbit coupling the spin states are influenced indirectly by a fluctuation of the electrical field.

The electrical field at the site of a magnetic ion is found by solving Laplace's equation, $\Delta V = 0$. The magnitude of the orbit-lattice interaction can be estimated by adapting the static theory of the crystalline field to the dynamic case [9]. The matrix elements in the general formulas for τ_{direct} and τ_{Raman} (eqs.(12) and (14), respectively) describing the spin-lattice interaction, have to be evaluated for each specific case of a magnetic ion in a given configuration. As a consequence of the complexity of describing the orbit-lattice interaction, this can be done only for simple systems in specific approximations. A discussion of the detailed calculation procedures will be omitted here. It is more important to point out the implications of the KVV interaction mechanism for the field and temperature dependence of τ.

According to Kramers' theorem [10], an operator that is invariant under time reversal (e.g. an electrostatic operator) can not connect time reversed states of half-integral quantum number. The perturbation potential in the KVV theory is of electrical nature. In non-Kramers ions (ions with an even number of electrons) the energy levels are not time conjugates of each other. In such cases the orbit-lattice interaction can induce transitions between these levels. As a consequence, the field and temperature dependences of the relaxation times in non-Kramers ions may be given by eq.(13) for the direct process and by eq.(15) for the Raman process. For ions with an odd number of electrons (Kramers ions) the degeneracy of the energy levels, which occur in doublets, can not be lifted by the electrical crystalline field. A time-odd operator, as for instance an external magnetic field, is required to lift this degeneracy. Then an electrostatic operator may induce transitions within the doublets, but for the prediction of temperature and field dependences of τ one can not use the simple eqs.(12) and (14), as will be shown in the next subsections.

a) *The field and temperature dependence of the relaxation times for an isolated Kramers doublet.* We consider a system with a Kramers doublet $|\pm a/2\rangle$ as ground state and an excited doublet $|\pm c/2\rangle$ at a distance $\Delta_c >> kT$. Thus only one Kramers doublet is effectively populated, and direct transitions within this doublet cannot occur because in first order $\langle -a/2|V_{el}|a/2\rangle = 0$ as a consequence of Kramers' theorem. A magnetic field mixes the excited state into the ground state. Then the ground state wave functions become [5]:

$$|-a/2\rangle' = |-a/2\rangle - g\mu_B H \frac{\langle \pm c/2|J|-a/2\rangle}{\Delta_c} |\pm c/2\rangle \qquad (20a)$$

$$|+a/2\rangle' = |+a/2\rangle - g\mu_B H \frac{\langle \pm c/2|J|+a/2\rangle}{\Delta_c} |\pm c/2\rangle. \qquad (20b)$$

If $\langle +c/2|J|+a/2\rangle \neq 0$, then $\langle +c/2|J|-a/2\rangle = 0$. This follows because a is an odd integer and J can at most connect states differing in quantum number by ± 1. Thus, if in the ground state $|-a/2\rangle'$ the $|-c/2\rangle$ excited state is mixed, then in $|+a/2\rangle'$ only $|+c/2\rangle$ of the excited doublet occurs, or reverse. These wave functions have to be applied into the matrix element in eq.(12). Using the time reversal properties this matrix element becomes, to first order in H, [5]:

$$\langle -a/2|V_j|+a/2\rangle' = \langle -a/2|V_j|+a/2\rangle - (2g\mu_B H/\Delta_c)\langle -c/2|J|-a/2\rangle\langle -a/2|V_j|c/2\rangle.$$

The first term is zero and thus the direct relaxation rate (eq.(12)) involves an extra H^2 dependence:

$$\tau_{direct}^{-1} = A_1 H^5 \coth(g\mu_B H/2kT). \tag{21}$$

In the case $g\mu_B H \ll kT$, this expression simplifies to:

$$\tau_{direct}^{-1} = A_1' T H^4.$$

The consequences of time degeneracy are more complicated for the Raman process, because τ_{Raman} is composed of two terms (see eq.(14)), one arising from the second order term $V_{jj'}$, the other from V_j acting twice in second order perturbation theory. Similar arguments as mentioned above apply for the matrix element $\langle -a/2|V_{jj'}|+a/2\rangle$. So this term in τ_{Raman}^{-1} shows up an extra H^2 dependence also:

$$\tau_{Raman}^{-1} = CH^2 T^7 J_6(\Theta_D/T). \tag{22}$$

The matrix element containing the first order perturbation potential does not vanish, because each term $\langle a/2|V_j|c/2\rangle$, etc. relates states of different doublets. Calculating the matrix elements for V_j acting twice in second order perturbation theory, one obtains for the second term between the square brackets in eq.(14):

$$\Big| \sum_{jj'c} \frac{\langle -a/2|V_j|c/2\rangle\langle c/2|V_{j'}|a/2\rangle}{\hbar\omega_k - \Delta_c} + \sum_{jj'c} \frac{\langle -a/2|V_{j'}|-c/2\rangle\langle -c/2|V_j|a/2\rangle}{-\hbar\omega_k - \Delta_c} \Big|^2. \tag{23}$$

From the time reversal symmetry it follows directly that the products of the matrix elements in the two numerators are equal, but of opposite sign [5]). This effect is the so-called Van Vleck cancellation. Consequently, the sum of the two terms in eq.(23) vanishes except for the difference in the denominators, and the above expression, that replaces the second term between the square brackets in eq.(14), becomes:

$$\sum_{jj'c} \langle -a/2|V_j|c/2\rangle\langle c/2|V_{j'}|a/2\rangle \frac{2\hbar\omega_k}{(\hbar\omega_k)^2 - \Delta_c^2}. \tag{24}$$

In the case $\Delta_c \gg kT$, $\hbar\omega_k$ may be neglected compared to Δ_c, giving an extra factor $(\hbar\omega_k)^2$ in the integral of eq.(14). This results in an extra T^2 term for the

Raman relaxation rate:

$$\tau^{-1}_{Raman} = B_1 H^0 T^9 J_8(\Theta_D/T), \qquad (25)$$

with $J_8(\Theta_D/T)$ being one of the integrals defined by eq.(16).

b) *The field and temperature dependence of* τ *for a multilevel system.* The above $\tau(T,H)$ dependences in the KVV theory were derived for an isolated Kramers doublet. In a Kramers ion with a zero field splitting between the doublets that is small compared to kT, in other words with $\Delta_c \ll kT$, more than one doublet is effectively populated. This is what we mean by a multilevel system. The major difference between such a system and the two level system considered above, is that the simple relation between the relaxation time and the transition probabilities (eq.(7)) no longer holds. The relation in the case of a multilevel system is given in eq.(8). The relaxation time is composed of the several contributions from the transitions between the populated energy levels. Our main interest on the moment lies in the behaviour of τ as a function of magnetic field and temperature. Only the like dependences of the transition probabilities have to be evaluated, because they are identical for each possible transition.

Blume and Orbach [11]) calculated for the direct process in a multilevel system that transitions between the doublets are more effective than the transitions within doublets. In such cases an external magnetic field is not a necessary condition in order to induce transitions by the orbit-lattice interaction. This means that the extra H^2 factor in the expression for the direct relaxation rate does not occur, thus:

$$\tau^{-1}_{direct} = A_2 H^3 \coth(g\mu_B H/2kT). \qquad (26)$$

This expression is identical to the general expression of eq.(13), but A_2 may be a rather complicated function of the separate transition probabilities.

The same arguments would lead for the Raman process in a multilevel system to the general expression of eq.(15). But due to the Van Vleck cancellation the expression as given by eq.(24) has to be included in the second term between square brackets of eq.(14). Then the condition $\Delta_c \ll kT$ implies that Δ_c may be neglected compared to the phonon energy $\hbar\omega_k$, resulting in an extra factor T^{-2} in the Raman relaxation rate:

$$\tau_{Raman}^{-1} = B_2 H^0 T^5 J_4(\Theta_D/T) \qquad (27)$$

with $J_4(\Theta_D/T)$ one of the integrals defined by eq.(16). In the presence of an external magnetic field the term in eq.(14) containing the matrix element $\langle a|V_{jj'}|b\rangle$ leads to the $H^2T^7J_6(\Theta_D/T)$ dependence of τ_{Raman}^{-1} as given by eq.(22). An experimental verification of such a field and temperature dependence of the Raman relaxation time in multilevel systems is not found. Therefore, this term will not be considered further.

c) *The field dependence of the Raman process for non-isolated ions.* The above field and temperature dependences of τ in the theory of the KVV interaction mechanism are derived for the specific case of an isolated magnetic ion. The interaction with neighbouring magnetic ions (cf. the WA interaction mechanism) is not taken into account. At the site of the magnetic ion an internal magnetic field may be produced under influence of e.g. dipolar or exchange interactions with neighbouring ions. In practise, the situation of an isolated ion may be achieved in highly diluted systems, or in magnetic fields much stronger than the internal field, where the spins will be coupled much more strongly to the magnetic field than to each other.

The internal field value is given by $(b/C)^{\frac{1}{2}}$, where C is Curie's constant and b is defined by the high temperature approximation of the specific heat at constant magnetization, $c_M = b/T^2$. The coefficient b includes the contributions to the specific heat due to e.g. dipole-dipole coupling, exchange interaction or hyperfine interaction. At magnetic fields of the order of the internal field, the field dependence of the Raman relaxation time is described phenomenologically by the Brons-Van Vleck relation [9,12]:

$$\tau_{Raman}^{-1}(H) = \tau^{-1}(0)(b/C + pH^2)/(b/C + H^2) \qquad (28)$$

with p a constant of approximately 0.5. A detailed theoretical discussion of this relation is given in ref.13. According to the Brons-Van Vleck relation, the Raman relaxation time increases with a factor of $1/p$ ($\simeq 2$) upon increasing H. At magnetic fields $H \gg (b/C)^{\frac{1}{2}}$, the Raman relaxation time becomes field independent and the theory of the isolated ions applies. A similar correction for the direct process can be omitted here, as this process is observed only in magnetic fields much stronger than the internal field.

CHAPTER II

THE DETERMINATION OF RELAXATION TIMES

The present research deals with investigations of relaxation phenomena by means of non-resonance techniques, or more precisely by means of studying the a.c. susceptibility. In this chapter we will review the relation between the a.c. susceptibility and the relaxation time, while we also recall the other physical quantities that follow from a.c. susceptibility measurements. A survey of the available experimental facilities will be given in the last section.

2.1 *The relation between susceptibility and relaxation time*

2.1.1 *Thermodynamical theory of spin-lattice relaxation.* The determination of spin-lattice relaxation times by means of non-resonance techniques is based upon a thermodynamical model, as proposed by Casimir and Du Pré [14]).
The magnetic spin system and the lattice system (chapter I) are assumed to be in internal equilibrium, characterised by the temperatures T_S and T_L, respectively. The energy flow between these systems is considered to be proportional to the temperature difference $T_S - T_L$, thus:

$$đQ/dt = -\alpha(T_S - T_L). \tag{29}$$

This assumption can only be made if the temperature difference $T_S - T_L$ is small compared to both T_L and T_S. The first law of thermodynamics, applied to a magnetic spin system, can be written as:

$$đQ = dU + MdH, \tag{30}$$

in which U represents the internal energy of the system. If the external magnetic field is kept constant, the time derivative of eq.(30) becomes:

$$đQ/dt = (\partial U/\partial T_S)_H dT_S/dt = c_{H_S} dT_S/dt, \tag{31}$$

in which c_{H_S} is the heat capacity of the magnetic spin system at constant magnetic

field. So, by means of the eqs.(29) and (31) one may write:

$$dT_S/dt = (T_L - T_S)\alpha/c_{H_S}. \qquad (32)$$

In chapter I the relaxation time τ was defined from:

$$dM/dt = (M_o - M)/\tau$$

which, in the case that the magnetization is characterised by a Curie law, can be written as:

$$\frac{d}{dt}(CH/T_S) = CH(1/T_L - 1/T_S)/\tau. \qquad (33)$$

The time derivative of the left hand part of eq.(33) is also equal to:

$$-(CH/T_S^2)dT_S/dt,$$

thus:

$$dT_S/dt = -T_S^2(1/T_L - 1/T_S)/\tau \simeq (T_L - T_S)/\tau. \qquad (34)$$

The last simplification being correct if the assumption with eq.(29) is valid. A comparison of eq.(32) and eq.(34) shows that:

$$\tau = c_{H_S}/\alpha.$$

This relation is of general validity and not restricted to the case that the magnetization obeys Curie's law for which it is derived above [15].

The relation between τ and c_{H_S} enables the determination of relaxation times from a.c. susceptibility measurements. For a magnetic system a variation in the external magnetic field results in a variation of the magnetization. If this variation is caused by an oscillating field (angular frequency ω and amplitude h) one may write in the complex notation:

$$H(t) = H_c + h(\omega)\exp(i\omega t) \qquad (35a)$$

and consequently:

$$M(t) = M_o + m(\omega)\exp(i\omega t) \qquad (35b)$$

and

$$T_S = T_L + \theta(\omega)\exp(i\omega t)\,. \tag{35c}$$

The complex differential susceptibility $\bar{\chi}$ (= $\chi' - i\chi''$), which is defined as dM/dH, is equal to m/h. Substitution of the time derivatives of eqs.(35) into

$$dT_S/dt = (\partial T_S/\partial H)_M dH/dt + (\partial T_S/\partial M)_H dM/dt$$

yields θ in eq.(35c) in terms of m and h:

$$\theta = (\partial T_S/\partial H)_M h + (\partial T_S/\partial M)_H m.$$

The basic assumption of the thermodynamical model as given by eq.(29) may now be rewritten as:

$$đQ/dt = -\alpha\{(\partial T_S/\partial H)_M h + (\partial T_S/\partial M)_H m\}\exp(i\omega t). \tag{36}$$

On the other hand, $đQ/dt$ may be derived from the first law of thermodynamics. Using the standard formulas of thermodynamics, in which M and H take the place of p and V, respectively, one finally arrives at:

$$đQ/dt = c_{H_S}(\partial T_S/\partial M)_H dM/dt + c_{M_S}(\partial T_S/\partial H)_M dH/dt. \tag{37}$$

The heat capacities of the spin system at constant magnetic field and constant magnetization (c_{H_S} and c_{M_S}, resp.) are given by:

$$c_{H_S} = (\partial U/\partial T_S)_H = -T_S(\partial M/\partial T_S)_H(\partial H/\partial T_S)_{S'} \tag{38a}$$

$$c_{M_S} = (\partial U/\partial T_S)_M = T_S(\partial H/\partial T_S)_M(\partial M/\partial T_S)_{S'} \tag{38b}$$

where S' represents the entropy. By comparing the right hand sides of eqs.(36) and (37) and omitting the algebra, one obtains:

$$\bar{\chi} = m/h = (\partial M/\partial H)_{T_S}\{(c_{M_S}/c_{H_S}) + (c_{H_S} - c_{M_S})/c_{H_S}(1 + i\omega c_{H_S}/\alpha)\}. \tag{39}$$

The quantity $(\partial M/\partial H)_{T_S}$ defines the isothermal susceptibility χ_T. From eqs.(38)

it follows:

$$c_{M_S}/c_{H_S} = (\partial M/\partial H)_S/(\partial M/\partial H)_{T_S},$$

$(\partial M/\partial H)_S$, being the adiabatic susceptibility χ_{ad}. Thus,

$$c_{M_S}/c_{H_S} = \chi_{ad}/\chi_T$$

and together with the relation $\tau = c_{H_S}/\alpha$, eq.(39) can be written as:

$$\chi'(\omega) = \chi_{ad} + (\chi_T - \chi_{ad})/(1 + \omega^2\tau^2) \qquad (40a)$$

$$\chi''(\omega) = (\chi_T - \chi_{ad})\omega\tau/(1 + \omega^2\tau^2). \qquad (40b)$$

The eqs.(40) are known as the Casimir-Du Pré relations. Apart from describing the frequency behaviour of χ' and χ'', they also indicate what kind of susceptibility one measures at extremely high or low frequencies: as a function of frequency, χ' decreases from χ_T to χ_{ad}. If the external magnetic field is zero, $c_{H_S} = c_{M_S}$ and thus $\chi_{ad} = \chi_T$ which also equals the static differential susceptibility χ_o. The Casimir-Du Pré relations represent for $\chi(\omega)$ a semi-circle in the complex plane, as can be seen by elimination of $\omega\tau$ in eqs.(40). One can derive the relaxation time τ from this so-called Argand diagram [16]) as the reciprocal value of the angular frequency corresponding to the top of the semi-circle. In practise, χ''/χ_o (absorption) is plotted against χ'/χ_o (dispersion). A typical example of such an Argand diagram is shown in fig. 2a.

Another quantity that can be determined from a.c. susceptibility measurements is the internal field value. The heat capacities c_{M_S} and c_{H_S} as given above are related to each other by:

$$c_{H_S} = c_{M_S} - T(\partial M/\partial T)_H(\partial H/\partial T)_M,$$

as can be derived from eqs.(38) by applying simple thermodynamics. For a magnetic substance, following the Curie-Weiss law (eq.(3)), one obtains:

$$c_{H_S}/c_{M_S} = 1 + CH^2T/c_{M_S}(T - \theta)^3.$$

c_{M_S} may be written as b/T^2 in the high temperature approximation (see 1.3.2c) and

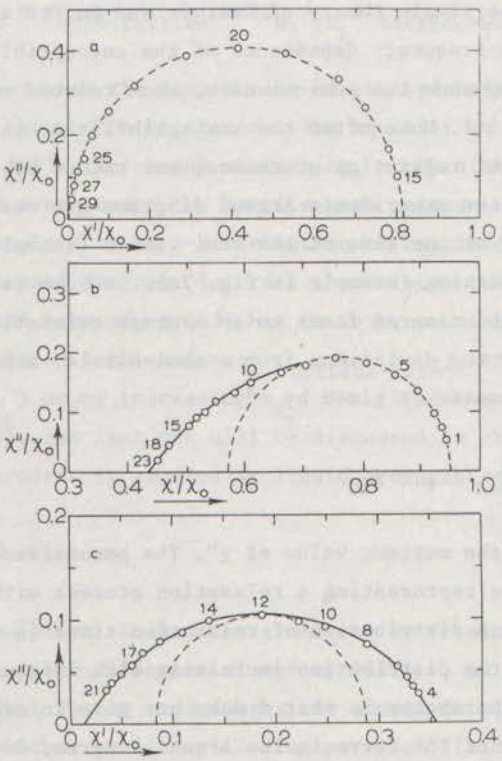

Fig. 2 Differential susceptibilities in the complex plane (Argand diagram) for manganese sulphate tetrahydrate. The broken lines represent semi-circles according to eqs.(40). The numbers are related to the measuring frequencies by $f(n) = (\sqrt{2})^n \times 0.324$ *Hz.*
a) $T = 14.03$ *K,* $H = 30$ *kOe, b)* $T = 2.00$ *K,* $H = 4$ *kOe,*
c) $T = 2.00$ *K,* $H = 20$ *kOe.*

c_{M_S}/c_{H_S} equals χ_{ad}/χ_T, thus:

$$\chi_{ad} = \chi_T/\{1 + H^2(T/T-\theta)^3/(b/C)\}. \qquad (41)$$

Measuring χ_{ad} ($= \chi'$ at frequencies $\omega >> \tau^{-1}$) as a function of magnetic field and temperature yields a value for b/C and the Curie-Weiss constant θ. The value of the internal field is given by $(b/C)^{\frac{1}{2}}$ (see 1.3.2c).

In some cases the simple theory of Casimir and Du Pré as reviewed above, fails to describe the frequency dependence of the susceptibilities. For example, the Argand diagram may show two semi-circles, each related to a separate relaxation mechanism [17]). More often the susceptibilities can not be described by a discrete number of relaxation processes, but rather by a distribution of relaxation times. In our experiments Argand diagrams are observed with an asymmetric broadening at one side of the semi-circle (example in fig. 2b) or with a symmetric flattening (example in fig. 2c). In such cases the top of the curve in the Argand diagram leads to an average relaxation time. In order to have a measure for the deviations from a semi-circle, a parameter d is introduced. This parameter is given by [18]):

$$d = 1 - 2\chi''_{max}/(\chi_T - \chi_{ad}) \qquad (42)$$

in which χ''_{max} equals the maximum value of χ''. The parameter d varies between 0 and 1. A semi-circle representing a relaxation process with one time constant corresponds to $d = 0$. A distribution of relaxation times is characterized by $d \neq 0$, the width of the distribution increasing with increasing d. A disadvantage of this parameter is that d does not give information about the symmetry or asymmetry of the curve in the Argand diagram. On the other hand, our experiments will concentrate on situations with minimal deviations in the Argand diagrams, and d is only used to indicate whether the quoted relaxation times represent a single time constant or not.

2.1.2 *The phonon bottleneck.* In the foregoing paragraph we tacitly assumed the lattice temperature to be constant. This situation is achieved when the lattice has always the temperature of the surrounding cooling liquid, in other words, if the lattice heat capacity may be assumed to be infinite. This assumption is no longer fulfilled if the energy exchange between the phonons and the cooling liquid is insufficient to keep the surplus or shortage of the energy of the phonon system negligible. Such a situation may occur if the relaxation proceeds via the direct process, in which only phonons of one specific mode are affected. These so-called resonant phonons form a separate system with finite heat capacity between the spin system and the other phonons

which are in thermal equilibrium with the cooling liquid. On the basis of this extension of the thermodynamical model of Casimir and Du Pré, Stoneham [19] derived a relation for the observed (spin-bath) relaxation time:

$$\tau_{observed} = \tau_{spin\text{-}lattice} + (c_{H_S}/c_{H_L})\tau_{lattice\text{-}bath}. \qquad (43)$$

This equation demonstrates the lengthening of the spin-lattice relaxation time, an effect known as the phonon bottleneck. The equilibrium in the phonon system can be restored by inelastic phonon scattering, or by direct energy exchange with the bath. As a consequence the lattice-bath relaxation time varies over the crystal. The result will be a distribution of relaxation times and thus a flattening in the Argand diagram. In order to minimize the effect of the phonon bottleneck the second term of eq.(43) has to be kept small. This can be realised by measuring on powdered samples (small $\tau_{lattice\text{-}bath}$), on magnetically diluted compounds (small c_{H_S}) or by increasing c_{H_L}. The first two possibilities were verified earlier [18], the last one will be discussed in chapter III where the direct relaxation process is studied at liquid hydrogen temperatures.

2.2 *Experimental facilities*

2.2.1 *Measuring equipment.* Relaxation times can be determined from the frequency dependence of the complex differential susceptibility, as was demonstrated in the preceding section. In our experiments the sample is placed in a constant magnetic field on which a small oscillating parallel field is superimposed.

Between 1 kHz and 1 MHz the susceptibility is found by measuring the change of the selfinductance of a coil, if a magnetic material is inserted. This selfinductance is measured in a bridge circuit consisting of four coils in a Wheatstone bridge configuration. The coils are identical pairs, but wound in opposite directions. One pair of coils, forming one branch of the bridge, is placed in the cryostat. The other pair of coils is placed in a heavy brass box, together with compensating elements as variable resistors and capacitors. The bridge circuit is balanced in its linear range. If a magnetic sample is moved in the cryostat from the centre of the upper coil to the centre of the lower one, or reverse, two different out-of-balance signals are obtained. The difference between the two output signals is proportional to the complex susceptibility of the sample. The in- and out-phase components of the output signal are separated by two synchronous detectors, thus enabling an instantaneous measurement of χ' and χ''. A detailed description of all features

of this measuring system, in all its complexity, is given by De Vries [20].

In the low frequency range (0.3Hz - 15kHz) a complicated bridge circuit is not needed. In this case the susceptibilities are measured by means of the change in the mutual inductance between two coils due to a magnetic compound inside the coil system. Around one primary coil two equivalent secondary coils, next to each other, are wound in opposite directions. When a sample is moved between the centres of the two secondary coils, the variation in output signal is proportional to the susceptibility of the sample. This output signal is led via a low noise transformer (Princeton Applied Research Corporation type TM 190) to a lock-in amplifier (PAR model 124 L) with a two phase accessory (PAR model 127). The primary coil is fed by the PAR 124 L via a low frequency amplifier.

2.2.2 *Magnets*. Several magnets were used to produce the required constant magnetic fields. A 40 years old watercooled solenoid provided the weak magnetic fields (H_{max} = 4.2 kOe). The efficiency factor H/i equals 22.52 Oe/A; the magnet is fed from a 200 A-100 V stabilized Standard Electric & Transforma rectifier, with a stability of 0.005% and a ripple current of less than 20 mA. The homogeneity of this magnet is better than 1% over 250 mm axial distance.

In order to generate strong magnetic fields, two superconducting coils were available The characteristic features of these magnets are given in table I. Both coils are energised from a Hewlett-Packard d.c. power supply type 6260B (10 V-100 A) used in remote resistor-controlled voltage-stabilized mode. The superconducting magnets are used with an extra inner cryostat, the tail of which is reaching inside the magnet coils. A schematic view of such a set-up is given in fig. 3.

Table I

	superconducting coil 1	superconducting coil 2
length	142.0 mm	142.2 mm
clear bore	51.0 mm	28.2 mm
axial homogeneity	0.1% over 57 mm	0.5% over 40 mm
efficiency factor H/i	0.462 kOe A^{-1}	1.025 kOe A^{-1}
quench field at 4.2 K	28 kOe	52 kOe
quench field at 1.5 K	36 kOe	62 kOe
wire type	IMI Niomax FM A61/40	IMI Niomax S25/40
number of windings	6274	12565

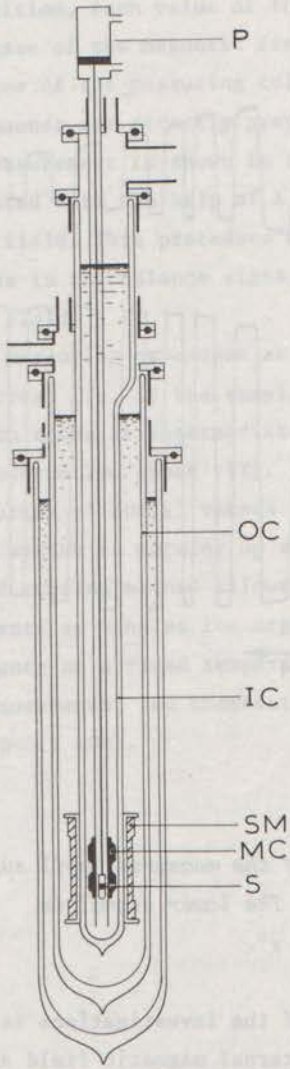

Fig. 3 Schematic view of a cryostat with superconducting coil. The inner cryostat (IC) contains the measuring coil system (MC) with the sample (S). This sample is moved between the centres of the measuring coils by means of a pneumatic system (P). The tail of the inner cryostat is reaching inside the superconducting magnet (SM), which is placed in the outer cryostat (OC). The whole assembly is contained in a third cryostat with liquid nitrogen.

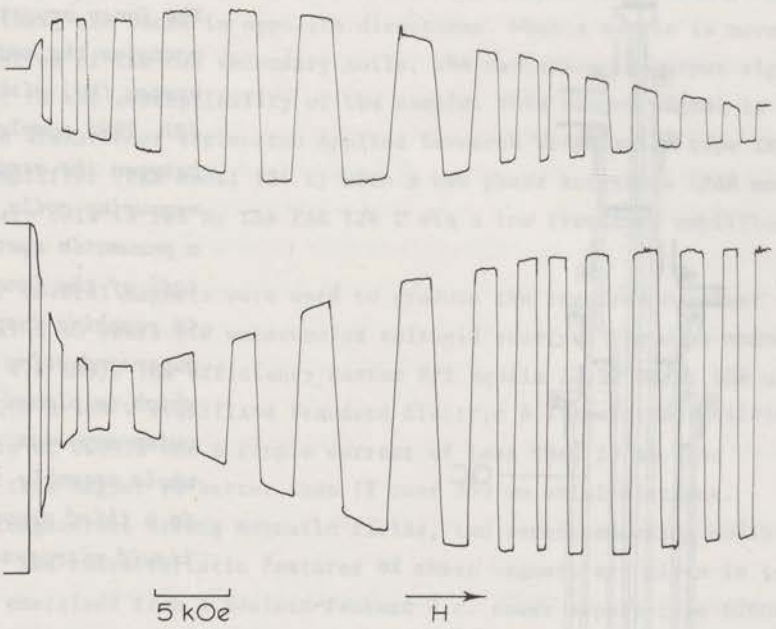

Fig. 4 Example of the output voltages of the measuring coil system as a function of magnetic field. The lower signal is proportional to χ', the other to χ''.

2.2.3 *Measuring procedure*. The main purpose of the investigations is to determine relaxation times as a function of external magnetic field and temperature. As discussed in 2.1.1 the relaxation time is obtained from the frequency dependence of the real and imaginary part of the complex susceptibility. So a.c. susceptibilities have to be measured as a function of frequency, magnetic field and temperature. The measuring procedure is such that at a fixed temperature and frequency the magnetic field is varied continuously. This is repeated for a number of frequencies at the same temperature. Such a set of results yields $\tau(H)$ at one temperature. From repeating the whole procedure for a number of temperatures one finally obtains $\tau(H,T)$.

During the determination of $\chi(\omega)$, the rate of change of the external magnetic field has to be small compared to the measuring frequency, the relaxation time of the sample and the response time of the electronics. Under this condition, each value of the magnetic field is quasi-stationary. During the increase of the magnetic field the sample is moved periodically between the centres of the measuring coils. The differences in output voltage obtained in this manner are directly proportional to χ' and χ''. A typical example of such a measurement is shown in fig. 4. The open parts in such curves are interpolated with the help of a continuous curve obtained with decreasing magnetic field. This procedure eliminates long term instabilities due to variations in the balance signal under the influence of the strong external magnetic field.

The measuring procedure as described above can be used only at fixed temperatures, i.e. if the sample is in direct contact with a cooling liquid. The relaxation times at intermediate temperatures may be needed in order to obtain enough information about $\tau(T)$. This is done by evaporating the cooling liquid and measuring χ' and χ'' versus H at one frequency while the assembly of sample and coil system is warming up slowly by the heat input from outside. This so-called running method allows a determination of $\tau(T)$ from these one-frequency measurements as long as the Argand diagram is known in enough detail from measurements at a fixed temperature. Magneto-caloric effects may influence such measurements, and therefore we only used this technique at weak magnetic fields ($H<4.2$ kOe).

CHAPTER III

PARAMAGNETIC SPIN-LATTICE RELAXATION IN MULTILEVEL SYSTEMS

The original theory of Kronig and Van Vleck on the spin-lattice relaxation mechanism in Kramers ions was derived for transitions within an isolated doublet, leading to the well-known temperature and field dependences given by $\tau^{-1} \propto TH^4$ for the direct process and $\tau^{-1} \propto T^9$ for the Raman process (section 1.3.2). In the case where the distance to the next doublet is much smaller than kT, the situation is obtained in which more than one doublet is effectively populated (multilevel system). A more complicated relaxation behaviour with a number of relaxation paths arises, since transitions between the doublets become effective. This was pointed out already by Van Vleck [9], but Blume and Orbach [11,21] emphasized the consequences for the field and temperature dependences of the relaxation times leading to the expressions reviewed in section 1.3.2b. Thus the observed relaxation time is expected to be given as:

$$\tau^{-1} = AH^3\coth(g\mu_B H/2kT) + BT^5 J_4(\Theta_D/T), \qquad (44)$$

the first term representing the direct process ($\tau^{-1} \propto TH^2$ if $g\mu_B H \ll kT$), the second one the Raman process.

The hydrated manganese (Mn^{2+}) salts can be reckoned among the multilevel systems, because their zero field splitting within the $^6S_{5/2}$ ground state is of the order of 0.1 cm^{-1}. The characteristic temperature and field dependence of the relaxation time was verified in two of such salts [22]. The direct relaxation process in three hydrated manganese salts is presented here (section 3.1). In order to examine the influence of covalency between the magnetic ion and the surrounding atoms, the field and temperature dependences of τ of a fourth manganese compound (Cs_3MnCl_5) are determined (section 3.2).

The ground state of the Cr^{3+} ion is $^4F_{3/2}$, which in the hydrated salts is split into two doublets with a separation of approximately 0.1 cm^{-1}. So such chromium salts are expected to fall into the category of the multilevel systems also. The direct and Raman relaxation process in three hydrated chromium salts have been investigated (section 3.3). Finally, some general conclusions concerning the spin-lattice relaxation in multilevel systems are discussed, with an attempt to explain

the numerical differences (section 3.4).

3.1 *The direct spin-lattice relaxation process in three hydrated manganese salts*

3.1.1 *Introduction.* The paramagnetic spin-lattice relaxation times of manganese salts have been the object of many studies. In weak external magnetic fields, the temperature dependence of these times in manganese Tutton salt and hydrated manganese fluosilicate was characterized by a $T^5 J_4(\Theta_D/T)$ Raman process above 10 K [22,23], while at liquid helium temperatures no agreement with theoretical predictions was achieved [24]. In manganese fluosilicate the investigation was extended to strong magnetic fields and as a result the direct relaxation process was observed above 10 kOe at liquid helium temperatures [25]. So far, the experimentally observed temperature and field dependences of τ agree with the theoretical predictions for a multilevel system based on the Kronig-Van Vleck interaction mechanism between the lattice vibrations and the magnetic ions. However, at liquid helium temperatures the relaxation mechanism in weak magnetic fields is influenced by impurities that create fast relaxing centres, while at strong fields the phonon bottleneck influences the observed relaxation times. At liquid hydrogen temperatures in weak magnetic fields usually the Raman process is observed and the influence of fast relaxing centres may be neglected, while the phonon bottleneck is not expected to be present at strong fields. Therefore, a study of the field dependence of relaxation times at liquid hydrogen temperatures, which can now be achieved, may lead directly to a reliable determination of the direct relaxation process. The manganese sulphate tetrahydrate was added to the above mentioned manganese salts, as relaxation times from ESR measurements on this salt [26,27] were thought to confirm the Waller-Al'tshuler interaction mechanism, while to the contrary non-resonance measurements [28,29] did not differ essentially from the results on the other manganese salts. From the present experiments a thorough comparison between the direct relaxation processes in the three equivalent manganese compounds is possible.

3.1.2 *Experimental results.* The observed relaxation times at liquid helium temperatures and strong magnetic fields may be influenced by the occurrence of the phonon bottleneck. This implies that the lattice (phonon system) is not always in thermal equilibrium with the cooling liquid. As a consequence the observed relaxation times are lengthened and a flattening in the Argand diagrams arises. By reducing the crystal size of the samples phonon-bottleneck effects will decrease. An average size of 0.1 mm was demonstrated to be adequate in order to minimize

phonon-bottleneck effects without creating secondary effects such as crystal dehydration, etc. [18]). For this reason most measurements presented in this section were performed on powdered samples with an average grain size of 0.1 mm. The phonon bottleneck will not be present at liquid hydrogen temperatures, so the existence of an anisotropy in the direct relaxation process may be examined at these temperatures. Such measurements were performed on single crystals of manganese fluosilicate.

A survey of the measurements is given successively for manganese fluosilicate, manganese Tutton salt and manganese sulphate tetrahydrate with a review of earlier results and some crystallographic data.

a) *Manganese fluosilicate hexahydrate.* The fluosilicate hexahydrates belong to a group of crystals with general formula $M''SiF_6.6H_2O$, in which M'' is a bivalent ion of the iron group. The compound manganese fluosilicate ($MnSiF_6.6H_2O$) forms crystals with hexagonal structure (a = 9.70 Å, c = 9.80 Å) [30]). The crystalline field at the site of the manganese ion is nearly cubic with a small trigonal distortion along the crystal c axis. The three doublets of the orbital ground state have energies 0.036, 0.009 and -0.045 cm^{-1} with respect to the unresolved ^6S state [31]).

Spin-lattice relaxation times of both $MnSiF_6.6H_2O$ and some magnetically diluted $Mn_xZn_{1-x}SiF_6.6H_2O$ samples have been investigated over a wide range of temperatures [23]). These measurements were all performed in external magnetic fields smaller than 4 kOe. The temperature dependence of the relaxation rate above 10 K was confirmed to be $T^5J_4(\Theta_D/T)$, in agreement with the theoretical prediction for the Raman process in multilevel systems. Later, the investigation of relaxation times at liquid helium temperatures was extended to strong magnetic fields [25]). Above 10 kOe the relaxation times showed the quadratic field dependence of the direct process and could be described by $\tau^{-1} = 0.30\ TH^2$ (H in kOe, T in K).

In the present research, the measurements have been extended to liquid hydrogen temperatures in order to study the direct relaxation process over a wide range of temperatures. The samples were made from ordinary laboratory chemicals (pro analysi), because in earlier experiments no strong influence of chemical impurities as in the manganese Tutton salt [24]) was noticed in the manganese fluosilicate [23]). Two single crystals were grown from the same solution (sample C_1 and C_2). A powdered sample was obtained by crushing single crystals to a powder (sample P_1, average crystal diameter 0.1 mm). During the experiments another sample was needed. Crystallites that came out of a solution were used and crushed, so that the average crystal diameter of this sample was 0.1 mm (sample P_2). A powdered sample, magnetically

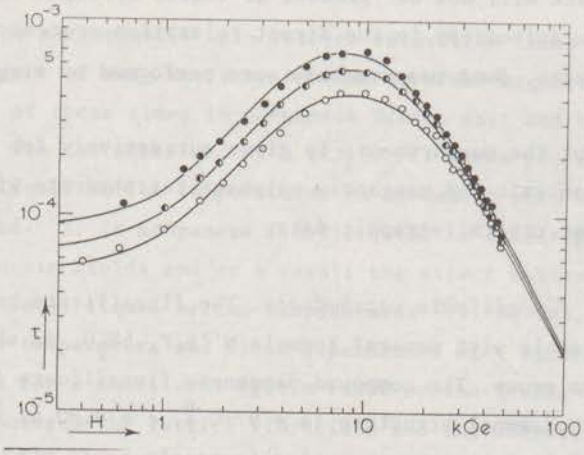

Fig. 5 Relaxation time as a function of the external magnetic field for a single crystal of manganese fluosilicate (sample C_1, H⊥c axis); ● : T = 14.10 K, ◐ : T = 14.91 K, ○ : T = 16.09 K. Full lines are computer fits according to eq.(53).

diluted with zinc, was obtained directly from the aqueous solution and turned out to be $Mn_xZn_{1-x}SiF_6.6H_2O$, with x = 0.07 (sample 7%).

The measurements on single crystals were performed with the external magnetic field perpendicular to the crystallographic c axis (sample C_1) and parallel to the c axis (sample C_2). A complete set of τ versus H curves, obtained at different liquid hydrogen temperatures on sample C_1 is given in fig. 5. At different temperatures the τ versus H curves exhibit an identical form. At weak magnetic fields τ increases strongly with increasing magnetic field, about a factor of 6 between 0.6 and 6 kOe. Above this field value, τ decreases continuously, at first slowly but above 20 kOe the observed relaxation times may be given as $\tau \propto H^{-1.9}$. The behaviour of the relaxation times obtained on sample C_2 was identical to that given in fig. 5: a strong increase in weak fields and $\tau \propto H^{-1.9}$ above 20 kOe. In order to compare the τ versus H curves for the different directions of the magnetic field, the results at 14.1 K for C_1(H⊥c) and C_2(H//c) are given together in fig. 6a (open triangles). In weak magnetic fields no significant difference between the two directions was observed, but above 15 kOe the relaxation

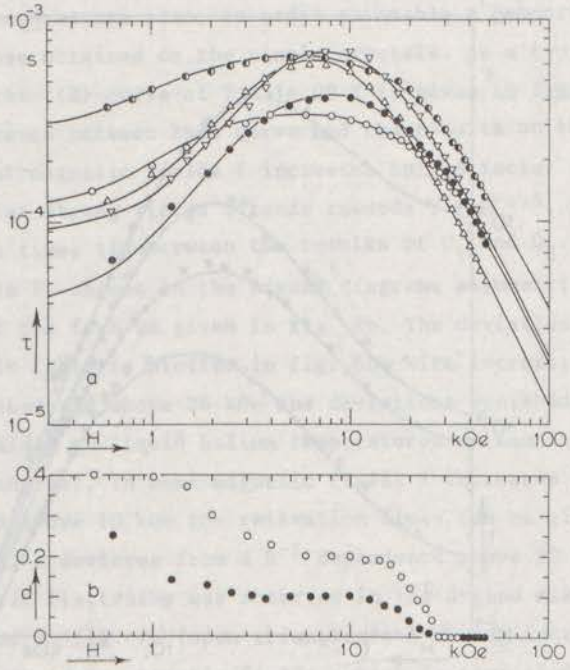

Fig. 6 Relaxation time (a) and deviation parameter (b) as a function of magnetic field at T = 14.1 K for various manganese fluosilicate samples; ▽ :C_1(H⊥c axis), △ :C_2(H//c axis), ○ :P_1, ● :P_2, ◐ :7%, ——: computer fits according to eq.(53). Relaxation times that do not correspond to a d value in b were obtained from semi-circles in the Argand diagram, thus d = 0.

times of sample C_1 are about a factor of 1.7 longer than those of C_2. The external magnetic field was applied parallel to the c axis of C_1 also, in order to exclude a possible systematic difference between the relaxation times of the two samples. The results were identical to those on C_2, so it may be concluded that there is an anisotropy of the relaxation times at strong magnetic fields for manganese fluosilicate. It should be noted that, for both samples, the susceptibilities in the Argand diagrams led to semi-circles (as given by the example in fig. 2a) over the whole field range.

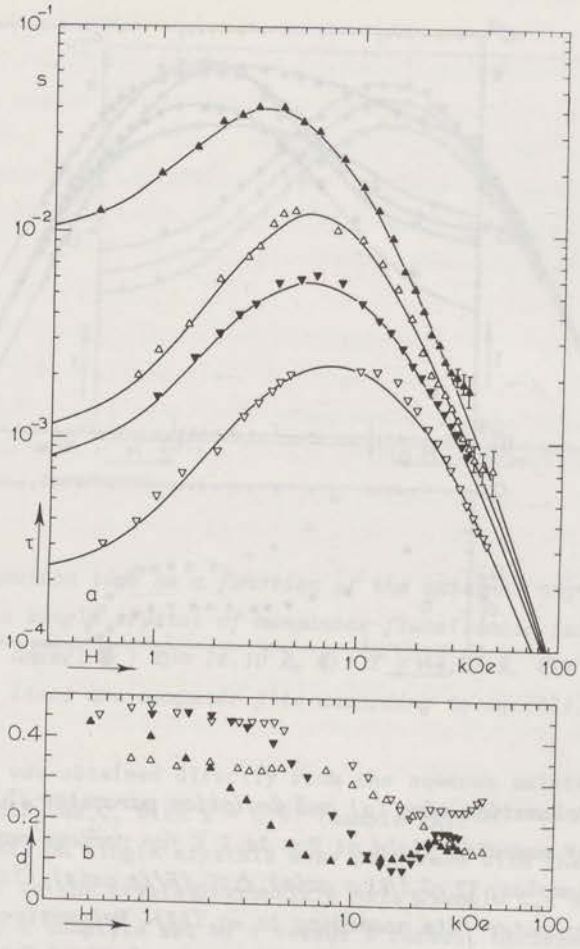

Fig. 7 Relaxation time (a) and deviation parameter (b) as a function of magnetic field for powdered $MnSiF_6.6H_2O$ at T = 2.0(△,▲) and T = 4.2 K(▽,▼). Open symbols: sample P_1, closed symbols: sample P_2,——— : computer fits acc. to eq.(53).

At liquid helium temperatures, the curves in the Argand diagrams were strongly flattened, with an increasing deviation parameter d (eq.(42)) at strong fields, due to the influence of the phonon bottleneck in the single crystals. Therefore, the relaxation behaviour for the crystals C_1 and C_2 was not examined at liquid helium

temperatures. At these temperatures the direct relaxation process has to be determined from measurements on powdered samples in order to exclude the phonon-bottleneck effects. The investigation on powdered samples was performed at liquid hydrogen temperatures also, in order to enable a comparison between these results and those obtained on the single crystals. As a typical result of such a measurement, the $\tau(H)$ curve at T = 14.09 K is given in fig. 6a (sample P_1, symbol ○). The difference between this curve and the results on the single crystals is noticeable, at weak magnetic fields τ increases only a factor of 3 with increasing field and at strong fields τ tends towards $\tau \propto H^{-1.5}$. At the strongest fields the relaxation times lie between the results of C_1 and C_2. The measurements on sample P_1 showed in the Argand diagrams asymmetric deviations from a semi-circle of the form as given in fig. 2b. The deviation parameter as a function of magnetic field is plotted in fig. 6b. With increasing magnetic field the asymmetry diminished and above 26 kOe the deviations vanished.

The results obtained at liquid helium temperatures on sample P_1 are given in fig. 7a (open triangles). In weak magnetic fields τ increases as a function of magnetic field and above 10 kOe the relaxation times can be given as $\tau^{-1} \propto H^2$. However, at T = 2.0 K, τ deviates from a H^{-2} dependence above 30 kOe. In the whole field range a symmetric flattening was observed in the Argand diagrams. The deviation parameter is indicated in fig. 7b (open triangles). A strong increase of this deviation parameter at strong magnetic fields, which is typical for the occurrence of the phonon bottleneck, is not observed. So it may be concluded that the phonon bottleneck does not dominate in the relaxation process, although minor effects due to a bad heat exchange between the spins and the cooling liquid can not be excluded. The above mentioned deviations at T = 2.0 K above 30 kOe have to be ascribed to the less accurate determination of the relaxation time because χ_T is small due to the effect of saturation.

In performing the measurements on P_1 it was noticed that the relaxation times at liquid helium temperatures below 10 kOe became shorter in the course of time, approaching a factor of 2 if the sample was kept at room temperature for one week. The deviation parameter did not change. Such a shortening was not observed during the measurements on single crystals. One may conclude that crushing single crystals introduces a distribution of relaxation times of which the average time constant changes in time. From measurements on cobalt fluosilicate it is known that a powder, if it is grown directly from the solution, exhibits fewer physical impurities, and thus less fast relaxation centres [18]). It was not possible to prepare such a powder, but in order to minimize the influence of crystal cracks etc., a powder with an average crystal diameter 0.1 mm was obtained, using

that which came from the solution with a slightly larger average crystal diameter (sample P_2). To reduce the influence of the changes on the weak field relaxation behaviour as a function of time, the experiments on sample P_2 were performed within a few days, while the sample was stored at liquid nitrogen temperature.

From the results at different liquid helium temperatures, the τ versus H curves at T = 4.20 and 1.96 K are given in fig. 7a (symbol ▼ and ▲, resp.), while the corresponding deviation parameters are given in fig. 7b. The average relaxation times exhibit, as a function of magnetic field, the same form as with sample P_1, with $\tau \propto H^{-2}$ above 10 kOe, but the relaxation times are longer. At liquid hydrogen temperatures the spin-lattice relaxation times of both powders coincided above 20 kOe. The τ versus H curve at T = 14.00 K is given in fig. 6a (closed circles). In weak magnetic fields the shape of the curve is identical to the curves of the single crystals, the values of the relaxation times are a factor of 1.5 shorter. In strong magnetic fields τ tends towards $\tau \propto H^{-1.7}$ and is only slightly shorter than the relaxation times of sample C_1 ($H \perp c$ axis). In weak magnetic fields an asymmetric broadening was observed in the Argand diagrams, which vanished above 25 kOe. The d versus H curve is shown in fig. 6b (symbol ●). In the field range where the relaxation times coincide, d = 0 for both P_1 and P_2, while at liquid helium temperatures in strong fields, where $d \neq 0$, different values of τ are observed.

The influence of reducing the magnetic concentration on the relaxation times was studied on sample 7% at liquid hydrogen temperatures. The relaxation times at T = 14.08 K are given in fig. 6a (symbol ◐). The τ(H) behaviour is analogous to that observed for sample P_1, but the absolute values of τ are about a factor of 2 larger. Over the whole field range the susceptibilities formed semi-circles in the Argand diagrams, so d = 0.

b) *Manganese ammonium Tutton salt.* The Tutton salts form a group of isomorphous monoclinic crystals with general formula $M''M'_2(S'O_4)_2.6H_2O$, in which M'' is Mg, Zn or any divalent cation of the 3d group, M' is a monovalent cation e.g. NH_4, K, Rb and S' is S or Se [32]). The manganese Tutton salts are stable only with ammonium as the monovalent cation ($Mn(NH_4)_2(SO_4)_2.6H_2O$). The nearly tetragonal crystal field splits the ground sextet of the free manganese ion into three spin-doublets at 0.093, -0.016 and -0.077 cm^{-1} respectively [31]).

The temperature dependence of spin-lattice relaxation times in manganese ammonium Tutton salt has been investigated extensively in weak magnetic fields [24]). The importance of the influence of fast relaxation centres caused by magnetic and

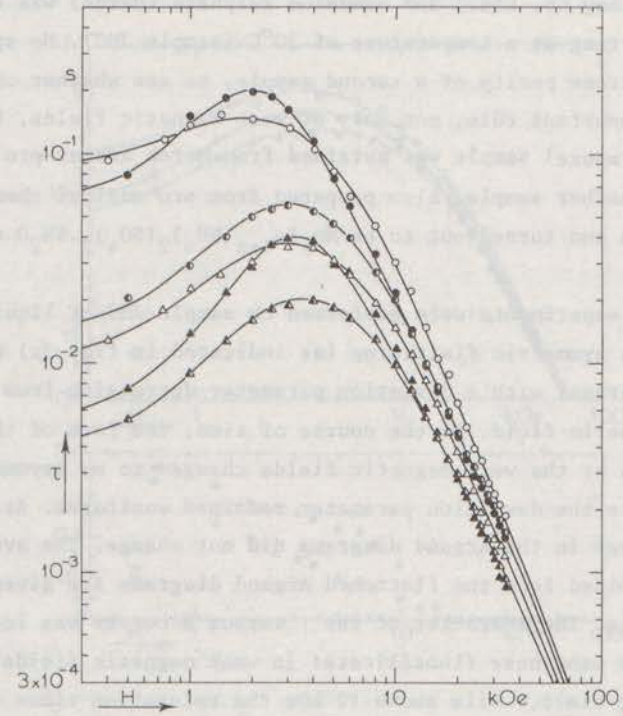

Fig. 8 Relaxation time versus magnetic field for manganese ammonium Tutton salt at T = 4.2 K (triangles) and T = 2.0 K (circles). Open symbols: sample JMC, half-closed symbols: sample MA, closed symbols: sample 11.5%. The full lines are computer fits according to eq.(53).

non-magnetic impurities on the relaxation times in weak fields was demonstrated. At temperatures above 10 K, these authors concluded that a $T^{-7}J_6^{-1}(\Theta_D/T)$ dependence of the relaxation time was valid, but reanalysis of the same results shows that a description with $\tau \propto T^{-5}J_4^{-1}(\Theta_D/T)$, as predicted for the Raman process in multilevel systems, prevails [22]).

The investigation has now been extended to strong magnetic fields at both liquid helium and liquid hydrogen temperatures. All measurements were performed on powdered samples with an average crystal diameter of 0.1 mm. One sample was

prepared from spectroscopically pure chemicals to reduce the influence of chemical impurities on the relaxation times. A solution of manganese sulphate (Johnson & Matthey Co. Ltd.) and ammonium sulphate (Merck) was evaporated under continuous stirring at a temperature of 30°C (sample JMC). No special attention was paid to extreme purity of a second sample, to see whether chemical impurities play such an important rôle, not only at weak magnetic fields, but also at strong fields. This 'impure' sample was obtained from Merck Analar pro analysi chemicals (sample MA). Another sample, also prepared from pro analysi chemicals, was diluted with Zn and turned out to be $Mn_xZn_{1-x}(NH_4)_2(SO_4)_2.6H_2O$ with x = 0.115 (sample 11.5%).

The first experiments were performed on sample JMC at liquid helium temperatures. A symmetric flattening (as indicated in fig. 2c) was observed in the Argand diagrams, with a deviation parameter decreasing from 0.2 to 0.1 with increasing magnetic field. In the course of time, the form of the curves in the Argand diagrams at the weak magnetic fields changed to an asymmetric broadening (fig. 2b), while the deviation parameter remained unaltered. At strong magnetic fields the curves in the Argand diagrams did not change. The average relaxation times as determined from the flattened Argand diagrams are given in fig. 8 by the open symbols. The character of the τ versus H curves was identical to those observed on the manganese fluosilicate: in weak magnetic fields τ increased with increasing field, while above 10 kOe the relaxation times tended towards $\tau \propto H^{-2.0}$.

Measurements at various liquid hydrogen temperatures were performed with a time interval of about half a year between the measurements, but no deviations from a semi-circle were observed in the Argand diagrams. As a typical result, the τ versus H curve at T = 15.00 K is displayed in fig. 9a (open circles). In weak increasing magnetic fields τ increases by a factor of two, above 15 kOe the relaxation times tend towards $\tau \propto H^{-1.7}$.

In order to examine the influence of impurities on the relaxation times, the measurements were repeated on the less pure sample MA. The results at T = 4.20 and 1.98 K are given in fig. 8 (symbol ▼ and ◐, respectively). The character of the field dependence of τ is the same as in sample JMC. Below 5 kOe the relaxation times are about a factor of two shorter than those observed for sample JMC at corresponding fields, confirming the effect of impurities, but also at strong fields the relaxation times of sample MA are shorter, although the difference is less pronounced. The effect of the impurities can be observed also from the deviations in the Argand diagrams. In the whole field range d is about a factor of 1.5 larger for sample MA than for sample JMC. At liquid

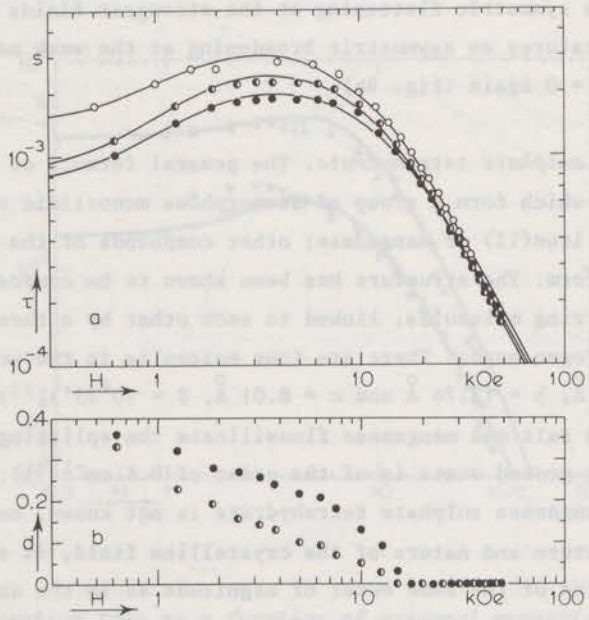

Fig. 9 Relaxation time (a) and deviation parameter (b) versus magnetic field for $Mn(NH_4)_2(SO_4)_2.6H_2O$ at T = 15.0 K. ○: sample JMC, ◐: sample MA, ●: sample 11.5%, ———— : computer fits acc. to eq.(53). Omitted symbols in b correspond to d = 0.

hydrogen temperatures the influence of impurities was also observable. The relaxation times in weak fields were about 50% shorter for sample MA than for sample JMC and in strong fields a 10% difference remained. For comparison, the τ versus H curve at T = 14.97 K is plotted in fig. 9a (symbol ◐). At liquid hydrogen temperatures the Argand diagrams for both samples are different also, no deviations for sample JMC, but an asymmetric broadening as indicated in fig. 2b for sample MA at weak fields, while above 15 kOe d = 0 within the experimental accuracy (fig. 9b).

Measurements were performed on sample 11.5% in order to examine whether the relaxation times depend on the concentration of manganese. Both at liquid helium and liquid hydrogen temperatures the relaxation times in strong magnetic fields

coincided with the relaxation times obtained on sample MA (figs. 8 and 9a). The deviations from semi-circles in the Argand diagrams were similar also. At liquid helium temperatures an asymmetric broadening was observed in weak magnetic fields, changing into a symmetric flattening at the strongest fields and at liquid hydrogen temperatures an asymmetric broadening at the weak magnetic fields, while above 15 kOe d = 0 again (fig. 9b).

c) *Manganese sulphate tetrahydrate.* The general formula of the sulphate tetrahydrates, which form a group of isomorphous monoclinic crystals, is $M''SO_4.4H_2O$ in which M'' is iron(II) or manganese; other compounds of the iron group occur in metastable form. The structure has been shown to be composed of isolated $M''_2(SO_4)_2.8H_2O$ ring molecules, linked to each other by a three dimensional network of hydrogen bonds. There are four molecules in the unit cell (axes a = 5.94 Å, b = 13.76 Å and c = 8.01 Å, $\beta = 90^o53'$) [33]. In manganese ammonium Tutton salt and manganese fluosilicate the splitting between the three doublets of the ground state is of the order of 0.1 cm^{-1} [31]. The zero field splitting in manganese sulphate tetrahydrate is not known, but in view of the analogous structure and nature of the crystalline field, it seems reasonable to assume a value of the same order of magnitude as in the above mentioned salts.

EPR measurements on manganese sulphate tetrahydrate, magnetically diluted with magnesium, demonstrated, at room temperature, a linear increase of the relaxation time upon decreasing the concentration of magnetic ions [26]. This effect was thought to confirm the Waller-Al'tshuler interaction mechanism. Turoff [27] reported EPR measurements of relaxation times at liquid helium temperatures on $Mn_{0.5}Mg_{0.5}SO_4.4H_2O$ and concluded a numerical agreement with the direct Waller-Al'tshuler relaxation process. Earlier non-resonance measurements on undiluted manganese sulphate tetrahydrate [28,29] did not differ essentially from results obtained on manganese fluosilicate and manganese Tutton salt, which are in agreement with the Kronig-Van Vleck theory. So, in contrast to the results from EPR methods, there was no reason to assume the Waller-Al'tshuler mechanism for the relaxation processes in the manganese sulphate. We performed measurements on manganese sulphate tetrahydrate in order to compare the direct process with that in the other manganese compounds.

A concentrated powdered sample was obtained by crushing a large crystal (sample 100% A). During the experiments it seemed necessary, as was also the case in the manganese compounds described above, to study another concentrated sample that was directly grown as a powder (sample 100% B). We did not succeed in obtaining a sample as Turoff used for his experiments, a dilution of

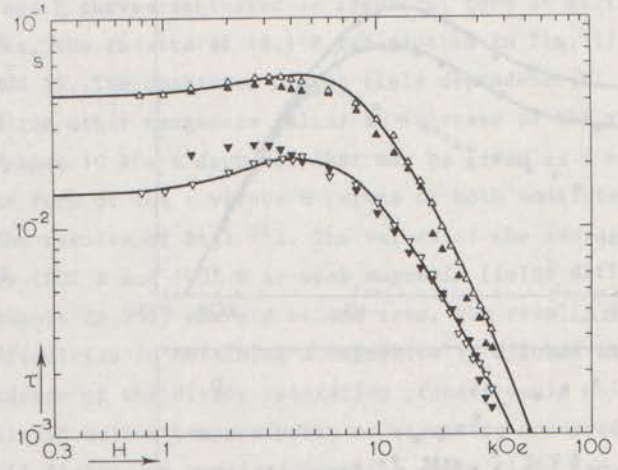

Fig. 10 Relaxation time as a function of external magnetic field for manganese sulphate tetrahydrate at T = 2.0 K (Δ, ▲) and T = 4.2 K (▽, ▼). Closed symbols: sample 100% A, open symbols: sample 95%. Full lines are computer fits according to eq.(53).

$MnSO_4.4H_2O$ with 50% $MgSO_4.4H_2O$, but this is not surprising as magnesium sulphate does not exist in a stable state [33]). We also tried the dilution with $ZnSO_4.4H_2O$. The result was not very successful either, our sample contained only 5% zinc sulphate (sample 95%).

The first measurements at liquid helium temperatures were performed on sample 100% A. At these temperatures, the plots of the differential susceptibilities in the Argand diagrams did not show semi-circles. At weak magnetic fields, a strong asymmetric broadening occurred as indicated in fig. 2b. On increasing the magnetic field, the asymmetry of the broadening diminished, but a symmetric flattening occurred (fig. 2c). The deviation parameter d amounted to approximately 0.3 in the whole field range. For T = 4.23 K and T = 2.00 K, the average relaxation times are given in fig. 10 (closed symbols). Below 4 kOe these times were almost field independent, while above 10 kOe they tended towards $\tau \propto H^{-2}$. The τ versus H curves showed a discontinuity at 30 kOe and 18 kOe (for T = 4.23

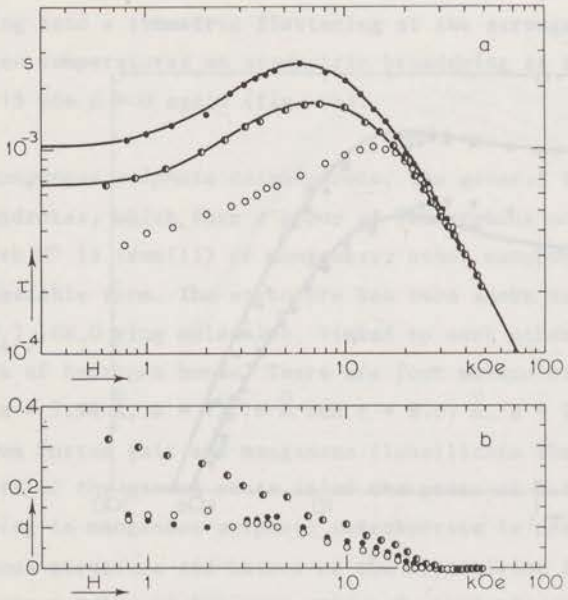

Fig. 11

Relaxation time (a) and deviation parameter (b) versus magnetic field for $MnSO_4.4H_2O$ at T = 14.1 K. ●: 100% A, ◐: 100% B, ○: 95%, ——— : computer fits according to eq.(53).

and 2.00 K, respectively). These discontinuities occurred at roughly the magnetic fields for which the observed Argand diagrams changed from the asymmetric to the symmetric case. The experiments on sample 100% A showed a time dependence of the curves in the Argand diagrams over a period of a week. As will be mentioned below, measurements on sample 95%, directly grown as a powder from an aqueous solution, did not show large deviations in the Argand diagrams. Therefore, the measurements were repeated on sample 100% B, a powder directly grown from an aqueous solution. However, the Argand diagrams in weak magnetic fields again showed a strong asymmetric broadening, similar to that in fig. 2b. The deviation parameter d was even larger and amounted to 0.4. We may conclude that the asymmetric broadening in the Argand diagrams for the undiluted samples is not related to the preparation method of the sample, but to other (unknown) physical or chemical impurities. The average relaxation times for sample 100% B are more or less the same as those of sample 100% A.

The measurements on both undiluted samples were extended to liquid hydrogen temperatures, as at these temperatures the observed relaxation times are not usually influenced by fast relaxation processes from impurities. However, in weak

magnetic fields, the susceptibilities in the Argand diagrams again demonstrated an asymmetric broadening. But with increasing magnetic field, the broadening diminished and above 25 kOe semi-circles were obtained. The broadening as a function of field is demonstrated by the deviation parameter d, as given in fig. 11b. The τ versus H curves exhibited an identical form at different liquid hydrogen temperatures, the results at 14.1 K are plotted in fig. 11a (●: 100% A, ◐: 100% B). The character of the field dependence of τ is identical to that observed in the other manganese salts: an increase of the relaxation times at weak fields and above 10 kOe a decrease that may be given as $\tau \propto H^{-1.7}$. In weak magnetic fields, the form of the τ versus H curves of both undiluted samples was in agreement with the results of Bijl [28]). The values of the average relaxation times of the samples 100% A and 100% B at weak magnetic fields differed by a factor of two, but above 25 kOe, where d became zero, the results coincided.

Due to the difficulties in obtaining a magnetically diluted sample, the concentration dependence of the direct relaxation process could only be studied at sample 95%. At liquid helium temperatures, no asymmetry occurred in the Argand diagrams, but a small flattening remained over the whole field range ($d \simeq 0.1$). As a consequence, the determination of relaxation times from these diagrams was more accurate than from the asymmetric Argand diagrams of the undiluted samples at liquid helium temperatures. At strong magnetic fields, approximately the same values for τ were found as for the samples 100% A and 100% B (open symbols in fig. 10). At liquid hydrogen temperatures, the relaxation times in magnetic fields below 10 kOe were a factor of 2 shorter than for 100% A and 100% B at these temperatures. The τ versus H curves (example in fig. 11a) are less smoothed than observed for the other samples, initially τ increases proportionally with $H^{0.5}$ until a maximum value is reached at H = 14 kOe. Above this field strength, the relaxation times decrease and finally they coincide with those of the undiluted samples. The deviation parameter was of the same order of magnitude as for sample 100% A (fig. 11b), d being zero above 20 kOe.

For the analysis of the above results the value of the internal field $(b/C)^{\frac{1}{2}}$ is needed. This value is not known accurately for $MnSO_4.4H_2O$ from the literature as it is for the manganese fluosilicate and manganese Tutton salt. At frequencies $\omega >> \tau^{-1}$ the adiabatic susceptibility, can be measured, related to the internal field according to eq.(41). The results obtained at 240 kHz between 2 and 20 K led to $b/C = (4.0 \pm 0.5) \times 10^6$ Oe^2 with $\theta = (-0.9 \pm 0.1)$ K. Earlier differential susceptibility measurements at low frequencies and temperatures between 14 and 300 K gave a larger value for the internal field [28,29]): $b/C = 6.2 \times 10^6$ Oe^2,

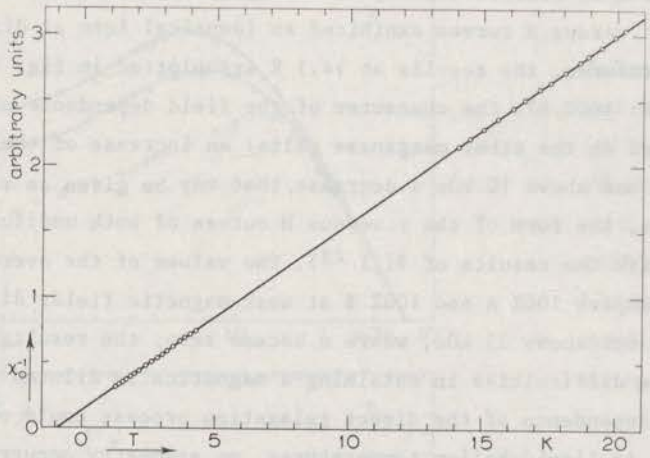

Fig. 12 χ_o^{-1} *as a function of temperature for powdered manganese sulphate tetrahydrate.*

but according to the asymmetric broadening of the Argand diagrams (fig. 2b), this result has not been obtained at frequencies high enough compared to τ^{-1}. Susceptibility measurements at 3 MHz and 77 K led to [34]): $b/C = 4.2 \times 10^6$ Oe^2, in agreement with the present results. The value of θ as given above was confirmed by direct static susceptibility measurements. The Curie-Weiss constant of manganese sulphate tetrahydrate as determined from χ_o^{-1} versus T (fig. 12) may be given as $\theta = (-0.90 \pm 0.05)$ K.

3.1.3 *Discussion.* The experimental results obtained on the three different manganese compounds, manganese fluosilicate, manganese Tutton salt and manganese sulphate tetrahydrate, showed an identical character with respect to the field dependence of the spin-lattice relaxation times. Both at liquid helium and liquid hydrogen temperatures, the relaxation times in weak magnetic fields increased with increasing magnetic field. Above a certain field value τ decreased continuously and approached $\tau \propto H^{-\alpha}$ with $\alpha \leqq 2$ at the strongest field values. Such a dependence of the relaxation time as a function of the external magnetic field suggests at least two relaxation processes operating in parallel. Therefore, the observed relaxation times will be compared with:

$$\tau_{obs}^{-1} = f(H) + cH^{\alpha}, \qquad (45)$$

the first term being predominant at weak magnetic fields, the other at strong fields. In the case that $g\mu_B H \ll kT$, the expressions for the direct relaxation process in manganese compounds, based on the Kronig-Van Vleck (KVV) as well as the Waller-Al'tshuler (WA) interaction mechanism (eqs.(26) and (18)), lead to the same simple relationship for the direct relaxation time: $\tau_{direct}^{-1} \propto H^2$. This is in agreement with our results in strong magnetic fields at liquid helium temperatures. At liquid hydrogen temperatures smaller exponents in the $\log \tau$ - $\log H$ graphs were observed ($\alpha \simeq 1.7$). This may be understood as at these temperatures the influence of the weak field relaxation processes, represented by f(H) in eq.(45), can not be neglected, even at 50 kOe. As a consequence, both terms of this equation have to be taken into account for the determination of the direct relaxation process at liquid hydrogen temperatures.

The expression for the relaxation time as given in eq.(44) is derived for a lattice with mutually isolated paramagnetic ions, giving rise to a field independent Raman relaxation time. In practice, the ions cannot be considered to be isolated if the external magnetic field is of the order of the internal field $(b/C)^{\frac{1}{2}}$. In that case the field dependence of the Raman process is described by the Brons-Van Vleck relation as given by eq.(28). For the hydrated manganese salts, the value of the internal magnetic field is of the order of 1 kOe [23,24]. As a consequence, the term f(H) of eq.(45) can be identified as the Brons-Van Vleck relation if the Raman process dominates the weak field relaxations. Upon increasing H, the Raman relaxation times increase with a factor 1/p, which is approximately 2. In our experiments the weak field relaxation process is often due to some fast relaxation mechanism, where the increase in τ at weak fields is over a factor of 2. For a detailed analysis of the direct relaxation process we need an adequate description of f(H) due to the fast relaxation mechanisms. In the next paragraph an attempt to derive such an expression on the basis of simple arguments is made without considering the details of the weak field relaxation processes. Having derived such an expression, analysis of the direct relaxation process at liquid hydrogen temperatures is possible.

a) *Weak field behaviour of the relaxation times.* A first attempt at a formal description of the temperature and field dependence of the relaxation times, observed in weak magnetic fields, was made by De Vries [24]. He extended the thermodynamical model of Casimir and Du Pré (section 2.1.1) by assuming two types

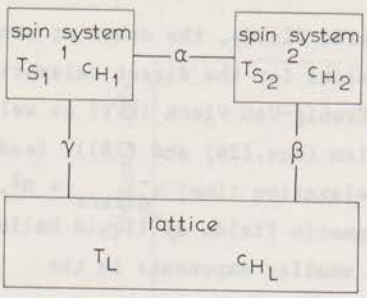

Fig. 13 Schematic diagram of the 'two spin system' model.

of spin systems. We will review his approach in a slightly more general form. The sample is supposed to contain two types of magnetic ions, represented by two spin systems which are each in internal equilibrium with spin temperature T_{S_1} and T_{S_2} and heat capacity c_{H_1} and c_{H_2}, resp., and a lattice system (temperature T_L and heat capacity c_{H_L}). In order to exclude phonon-bottleneck effects, c_{H_L} is supposed to be infinite, in other words, the energy exchange between the lattice and the cooling liquid is sufficient to keep T_L constant. The model is shown schematically in fig. 13. The two spin systems are coupled to each other via cross relaxation; both systems are able to exchange energy with the lattice system. Assuming each of the energy transfers in fig. 13 to be proportional to the temperature differences between the relevant systems, one may write:

$$dU_{S_1}/dt = c_{H_1} dT_{S_1}/dt = \alpha(T_{S_2} - T_{S_1}) + \gamma(T_L - T_{S_1}) \qquad (46a)$$

$$dU_{S_2}/dt = c_{H_2} dT_{S_2}/dt = \alpha(T_{S_1} - T_{S_2}) + \beta(T_L - T_{S_2}). \qquad (46b)$$

The thermal heat transfer coefficients between the different systems are represented by α, β and γ and are related to the relaxation times in a similar way as shown in section 2.1.1 by

$$\tau_{cross} = c_{H_1}/\alpha,\ \tau_{S_2} = c_{H_2}/\beta,\ \tau_{S_1} = c_{H_1}/\gamma.$$

We suppose the second spin system to consist of magnetic ions that behave differently from the ions in the first spin system. The origin of such ions may be found in the occurrence of chemical (other magnetic ions) or physical impurities

(crystal defects or dehydration, that may change the electrical crystalline field at the site of the magnetic ions), giving rise to fast relaxation centres. It seems reasonable to assume the number of these fast relaxation centres (N_2) to be small compared to the number of manganese ions in the first spin system (N_1). Thus, if the specific heats of the two spin systems are of the same order of magnitude, the heat capacity of the second spin system is much smaller than that of the first spin system, $c_{H_2}/c_{H_1} = N_2/N_1 << 1$. Furthermore, under our experimental conditions the quantities dT_{S_1}/dt and dT_{S_2}/dt are of the same order of magnitude. Then the change in the internal energy of the second spin system (dU_{S_2}/dt) may be neglected compared to that of the first spin system. So eq.(46b) becomes:

$$\alpha(T_{S_1} - T_{S_2}) + \beta(T_L - T_{S_2}) \approx 0,$$

or:

$$1 + \alpha/\beta = (T_{S_1} - T_L)/(T_{S_1} - T_{S_2}).$$

Now $T_{S_1} - T_{S_2}$ can be eliminated from eq.(46a):

$$c_{H_1} dT_{S_1}/dt = (1/\alpha + 1/\beta)^{-1}(T_L - T_{S_1}) + (1/\gamma)^{-1}(T_L - T_{S_1}),$$

or in terms of relaxation times:

$$dT_{S_1}/dt = \left[(\tau_{cross} + \tau_{S_2} c_{H_1}/c_{H_2})^{-1} + \tau_{S_1}^{-1}\right](T_L - T_{S_1}).$$

This expression describes the rate at which T_{S_1} returns to T_L, the relaxation rate is given by:

$$\tau^{-1} = (\tau_{cross} + \tau_{S_2} c_{H_1}/c_{H_2})^{-1} + \tau_{S_1}^{-1}. \qquad (47)$$

The first spin system transfers energy to the lattice along two parallel paths, one directly, the other via the fast relaxation centres included in the second spin system. From the symmetry in the eqs.(46) one would expect a relation for dT_{S_2}/dt also. Such an expression will be more complicated because no change in internal energy can be neglected. However, if the above assumption ($N_2 << N_1$) is true for our experiments, this implies that relaxation effects due to the variations in T_{S_2} will not be observable in the complex susceptibility and can be neglected for the further analysis. Consequently, the relaxation rate given in eq.(47) defines the relaxation time which is observed experimentally. If the

assumption concerning the second spin system is not correct a more complicated expression for the experimentally observed relaxation time is obtained, leading to three instead of two time constants. We used the simplified model because, as will be shown below, the observed relaxation times at weak magnetic fields are adequately described using eq.(47).

The 'two spin system' model, as reviewed above, was used by several authors in a rather restricted way. De Vries [24]) applied experimental data to eq.(47) to determine the unknown variables, and used these quantities to describe his other results. De Vroomen [35]) identified the second spin system to consist of copper pairs, and derived for this special case an expression for the weak field relaxation time. In order to analyze our present experimental results, we will consider an expression for the relaxation times as a function of magnetic field on the basis of the 'two spin system' model, in which the second spin system consists of the so-called fast relaxation centres. Detailed assumptions about the character of the fast relaxation centres will not be made.

From the first law of thermodynamics for magnetic systems that obey Curie's law, one may derive for the field dependence of the heat capacity of the spin system with spin temperature T_{S_1}:

$$c_{H_1} = (b + CH^2)/T_{S_1}^2 = (b/C + H^2)C/T_{S_1}^2 . \qquad (48)$$

The second spin system is supposed to consist of magnetic ions situated in such positions that the interactions among them or with their surroundings is different from the ions in the first spin system. Consequently the internal field value for these ions and the heat capacity will be different:

$$c_{H_2} = (b'/C' + H^2)C'/T_{S_2}^2 . \qquad (49)$$

Following the model of Casimir and Du Pré, the temperature differences between the systems are presumed to be small. From measurements on manganese Tutton salt it seems reasonable to assums $\tau_{cross} \ll \tau_{S_2}$ [24]); then substitution of eqs.(48) and (49) into eq.(47) leads to:

$$\tau_{obs}^{-1} = \tau_{S_2}^{-1} C'(b'/C' + H^2)/C(b/C + H^2) + \tau_{S_1}^{-1} . \qquad (50)$$

Comparing eq.(50) with the phenomenological description of the experimental results as given by eq.(45), one may identify the first term with f(H) representing the weak field behaviour of τ, and τ_{S_1} with the relaxation time of the direct process.

The first term of eq.(50) may be rewritten as:

$$\tau_{S_2}^{-1}(b'/b)\left[(b/C) + \{(b/C)/(b'/C')\}\,H^2\right]/(b/C + H^2). \qquad (51)$$

Comparison of eq.(51) and eq.(28) shows that the field dependence of τ as derived for the 'two spin system' model as well as for the Raman process (Brons-Van Vleck relation) can be represented by:

$$f(H) = f(0)(b/C + \varepsilon H^2)/(b/C + H^2). \qquad (52)$$

The similarity between the expressions means that eq.(50) can be used to examine all τ versus H curves. The coefficient ε can be either $p(\simeq 0.5)$ or $(b/C)/(b'/C')$, which may be considerably smaller than 0.5, while f(0) is $\tau^{-1}(0)$ or $(b'/b)\tau_{S_2}^{-1}$. The coefficient ε and the temperature dependence of f(0) are used to distinguish between a Raman process and fast impurity relaxations.

The model, as it has been discussed so far, is based on rather general suppositions. In fact, it is only assumed that the second spin system consists of a relatively small number of magnetic ions (possible manganese) that are in internal equilibrium and that the energy exchange between these ions and the bulk of manganese ions is rapid. In this way the 'two spin system' model leads to a single relaxation time, and thus to semi-circles in the Argand diagrams. The deviations in these diagrams, as observed for the different manganese compounds, show that the assumptions made in the model are too restrictive to give a complete description of the relaxation behaviour. The time constant of the relaxation process via the fast relaxation centres, the first term in eq.(47), will be different for each manganese ion in the crystal. A continuous distribution of relaxation times will occur that may cause a flattening or asymmetric broadening in the Argand diagrams. With increasing magnetic field the fast relaxation centres become less effective, and the deviations in the Argand diagrams will decrease. In fact this is in agreement with our experiments as can be seen in the figs. 6, 7, 9 and 11. The model given above for the fast relaxations is too simple to give a realistic description, especially at the very weak fields. At the fields where we can apply the model to correct the observed times, in order to obtain the coefficient of the direct process, the failures of the model become less important. In the next paragraph we will analyze the average relaxation times as a function of field with the simple 'two spin system' model, thereby demonstrating its usefulness, and we will briefly discuss the data for the fast relaxations thus obtained.

Table II

Constants determining the field dependence of the observed relaxation times in $MnSiF_6.6H_2O$ samples according to eq.(53).[#]

sample	T (K)	f(0) (x 10^2 s^{-1})	ε	A_{KVV} (x 10^{-11} $Oe^{-3}s^{-1}$)
C_1(H⊥c axis)	14.10	115	0.08	2.09
	14.91	145	0.08	2.11
	16.09	189	0.09	1.97
(H//c axis)	14.03	97	0.10	3.50
C_2(H//c axis)	14.03	96	0.10	3.62
	14.84	126	0.10	3.49
	16.02	171	0.11	3.33
P_1	2.06	10	0.04	2.2
	4.20	80	0.05	2.0
	14.09	84	0.32	1.8
	15.00	100	0.32	1.7
	16.00	112	0.33	1.7
P_2	1.96	1.1	0.14	1.50
	2.98	5.3	0.06	1.55
	4.20	13	0.09	1.40
	14.00	257	0.07	2.14
	14.99	329	0.07	2.09
	16.03	483	0.06	2.14
7%	14.08	31	0.53	1.16
	15.02	39	0.52	1.06
	15.96	49	0.52	0.99

[#] For the powdered samples b/C = 0.70 x 10^6 Oe^2 [23]), for the single crystals we used b/C = 1.50 x 10^6 Oe^2.

Table III

Constants determining the field dependence of the observed relaxation times in $Mn(NH_4)_2(SO_4)_2.6H_2O$ samples according to eq.(53).#

sample	T (K)	f(0) (x 10^1 s^{-1})	ε	A_{KVV} (x 10^{-11} $Oe^{-3}s^{-1}$)
JMC	2.02	1.4	0.22	1.12
	4.22	9.3	0.15	0.99
	14.20	62	0.39	0.92
	15.00	69	0.42	0.98
	16.00	103	0.39	1.01
MA	1.31	2.9	0.22	1.11
	1.98	7.1	0.14	1.40
	3.00	16	0.11	1.40
	4.20	25	0.12	1.21
	14.10	100	0.29	1.10
	14.97	117	0.30	1.11
	16.01	138	0.34	1.10
11.5%	2.05	1.7	0.06	1.58
	4.20	20	0.03	1.41
	14.05	110	0.30	1.08
	14.85	133	0.33	1.04
	16.05	145	0.40	1.03

$b/C = 0.58 \times 10^6$ Oe^2 [24].

b) *Analysis of the* $\tau(H)$ *curves*. Having established a model to describe the weak field behaviour of the relaxation times, a complete analysis of our experimental results is possible. By means of a least square computer programme, the τ versus H curves were fitted to eq.(50), with τ_{S_1} representing the direct relaxation time due to the KVV interaction mechanism (eq.(26)). So the computer fits are given by:

$$\tau^{-1} = f(0)(b/C + \varepsilon H^2)/(b/C + H^2) + A_{KVV}H^3\coth(g\mu_B H/2kT), \qquad (53)$$

Table IV

Constants determining the field dependence of the observed relaxation times in $MnSO_4.4H_2O$ samples according to eq.(53).#

sample	T (K)	f(0) ($\times 10^1$ s^{-1})	ε	A_{KVV} ($\times 10^{-11}$ $Oe^{-3}s^{-1}$)
100% A	2.00	2.5	0.36	0.8
	4.23	4.4	0.70	0.8
	14.10	96	0.23	0.95
	15.96	175	0.20	0.96
100% B	14.03	148	0.27	0.88
	14.95	170	0.27	0.88
	16.00	219	0.26	0.88
95%	2.04	2.3	0.41	0.65
	4.25	6.7	0.40	0.74
	14.06			0.8
	15.92			0.8

b/C: see 3.1.2c.

where f(0), ε and A_{KVV} are the parameters to be determined. As can be seen from the examples drawn in figures 5 to 11, these computer fits provide a good description of the observed $\tau(H)$ curves (except in the case of 95% $MnSO_4.4H_2O$ at liquid hydrogen temperatures). The values of f(0) and A_{KVV} are listed in the tables II, III and IV for the three manganese compounds. The parameters ε are given in these tables also, in order to enable a numerical estimate for the relaxation times if the quoted values for b/C are used. It has to be noted that in the case where the static susceptibility is described by a Curie-Weiss law (eq.(3)), the internal fields in eq.(53) have to be replaced by $(b/C)/(T/T-\theta)^3$. This follows directly from eq.(41). The coefficients of the direct process will be discussed in the next paragraph, we will now focus our attention on the weak field relaxation behaviour.

In order to distinguish between a Raman relaxation process and impurity relaxations at weak fields, one may consider the temperature dependence of f(0)

together with the coefficient ε. For the single crystals of manganese fluosilicate f(0) approaches a T^5 dependence, but the coefficient ε differs considerably from the value 0.5 as expected for the Raman relaxation process. None of the other coefficients f(0) (all powdered samples) reaches a T^5 dependence, but rather $f(0) \propto T^\beta$ with $1<\beta<4$. Earlier results on manganese fluosilicate and manganese Tutton salt showed that an analogous temperature dependence is characteristic for relaxations via chemical or physical impurities [23,24]. A powdered sample, obtained from spectroscopically pure chemicals, did not differ essentially from the ones grown from analar chemicals ($Mn(NH_4)_2(SO_4)_2.6H_2O$, samples JMC and MA), while on the other hand a different way of sample preparation changes the observed relaxation times (cf. $MnSiF_6.6H_2O$, samples P_1 and P_2). From the above it may be concluded that physical impurities are of major importance for the weak field relaxations.

The computer fits demonstrate that the simple 'two spin system' model gives an adequate description for the observed relaxation times in the case of weak field impurity relaxations in the manganese salts. In fact, this conclusion is of rather general validity as in the majority of cases of weak fields the behaviour of τ, observed in concentrated magnetic materials, can be fitted to an expression given by eq.(50) [36,37].

c) *The direct relaxation process.* The observed field dependences of the relaxation times at strong magnetic fields for the various manganese salts are interpreted in terms of the direct relaxation process. The coefficients A_{KVV} of this direct process were given in the last column of the tables II, III and IV. Several samples were studied at liquid helium as well as at liquid hydrogen temperatures. In general the coefficients A_{KVV} from both series of measurements are not identical. It has to be noted that there is a remarkable difference between the strong field relaxation times from measurements at liquid hydrogen and liquid helium temperatures: the former are obtained from semi-circles in the Argand diagrams, while the latter come from flattened curves in these diagrams (av. $d \simeq 0.2$ below $T = 4.2$ K and above $H = 20$ kOe in the three manganese compounds). This flattening must be attributed to the influence of the phonon bottleneck. It is known that the use of powdered samples with an average crystal diameter of 0.1 mm minimizes this influence, but does not exclude it [18]. In practice, severe effects of the phonon bottleneck are observed if $\tau<10^{-3}$ s [18,37] and this is just about the case with manganese fluosilicate powders. Our measurements (fig. 7) show that in these samples a deviation from $\tau^{-1} \propto H^3\coth(g\mu_B H/2kT)$ occurs at the strongest fields, accompanied by an increasing d value. The direct process

relaxation times which are larger than 10^{-3} s, may be influenced by phonon-bottleneck effects ($d \neq 0$) but not in such a way that deviations from the expected field dependence are observed; in this case only the constant A_{KVV} may be affected. For a numerical comparison with theory we exclude the possible inaccuracy due to the effect of the phonon bottleneck by restricting ourselves to the results at liquid hydrogen temperatures. The relaxation times at liquid helium temperatures are used to demonstrate that our $\tau(H)$ curves that tend towards $\tau^{-1} \propto H^2$ at liquid hydrogen temperatures have indeed to be attributed to the direct process.

The single crystals of manganese fluosilicate were examined in order to study the possible influence of the direction of the external magnetic field on the coefficient A_{KVV}. As can be seen in table II, a slight dependence on orientation exists. The coefficient for $H \perp c$ axis is almost identical to the results for the powdered samples, as is to be expected if the dependence is sinusoidal for instance. The influence of chemical impurities on the direct process was tested with the manganese Tutton salt, the compound that is known to be the most sensitive to these impurities [24]). The difference between the coefficients of sample JMC and sample MA is only 10%, which we believe to be too small for further consideration here.

The results for the various powdered manganese samples will now be compared with the theoretical calculations. Blume and Orbach [11]) predicted, on the basis of the KVV interaction mechanism, for the direct spin-lattice relaxation time of Mn^{2+} ions in a cubic environment (Mn^{2+} in MgO):

$$\tau^{-1} = 0.13 \times 10^{-6}\ TH^2\ s^{-1}, \qquad (54)$$

for the case that $g\mu_B H \ll kT$. If this condition is not fulfilled, eq.(54) has to be written as:

$$\tau^{-1} = 0.9 \times 10^{-11}\ H^3 \coth(g\mu_B H/2kT)\ s^{-1}. \qquad (55)$$

Eq.(55) suggests the coefficients A_{KVV} in the tables II to IV to be of the correct order of magnitude, but some constants used in the calculations have to be altered slightly for Mn^{2+} ions in the hydrated salts. The velocity of sound (v), entering to the fifth power in the theoretical expression for A_{KVV}, is about 3×10^5 cm/s in the hydrated salts instead of 5×10^5 cm/s in the case of MgO. The density (ρ) of the three manganese compounds we studied, is within 10% of 2 g/cm^3 (3.7 g/cm^3 for MgO). Considering these alterations eq.(55) becomes:

$$\tau^{-1} = 20 \times 10^{-11}\ H^3 \coth(g\mu_B H/2kT)\ s^{-1}$$

for hydrated manganese salts. This result differs from an earlier estimate [25]) because more reasonable values for v and ρ are included in the present calculation. The above estimate remains a rather crude order of magnitude calculation, as the detailed crystalline fields for the manganese ions in the examined samples has yet to be considered. Moreover, the KVV interaction mechanism is calculated on the basis of a point-charge model and the rôle of covalency effects which may lengthen the relaxation times [38,39]) is not considered. The influence of covalency will be studied in more detail in section 3.2.

Another description for the direct process in manganese compounds may be obtained with the WA interaction mechanism, as suggested by the measurements of Turoff [27]). The modulation of the dipolar interaction, which is the important link in the energy exchange due to the WA mechanism, may be effective in the case of large magnetic moments that are present in large concentrations. Manganese compounds fulfil this requirement, thus the WA theory may apply to the above measurements and the two terms of eq.(18) have to be used in analyzing the $\tau(H)$ curves. From eq.(18) it is clear that only the analysis with the two spin WA mechanism yields values for the coefficient of the direct process that differ from the results as given in the last column of the tables II to IV. We recall the average values in table V ($A_{WA\ I}$), together with the average coefficients $A_{WA\ II}$ from the computer fits with the two spin WA mechanism. Both coefficients $A_{WA\ I}$ and $A_{WA\ II}$ can be calculated (eqs.(19)). Apart from the values for ρ and v as given above, the quantity Z/r_o^6 has to be determined, r_o being the equilibrium distance between nearest neighbour magnetic ions and Z the number of these nearest neighbours. From the available data on the crystal structures [30,32,33]) we calculated Z/r_o^6 to be 1.0×10^{44}, 0.7×10^{44} and 4.0×10^{44} cm^{-6} for manganese fluosilicate, manganese Tutton salt and manganese sulphate respectively. Using the above quantities, the coefficients $A_{WA\ I}$ and $A_{WA\ II}$ as given in eqs.(19) are calculated (table V). A remarkable difference can be seen between these coefficients for the three manganese compounds, while our experiments led to more or less identical values. $A_{WA\ I}$ and $A_{WA\ II}$ are linearly concentration dependent, but hardly any change in the relaxation times was observed for 7% manganese fluosilicate and 11.5% manganese Tutton salt. Manganese sulphate could not be diluted magnetically, so the concentration dependence of a possible WA interaction mechanism could not be examined.

The discrepancies between the observed coefficients and the ones calculated

Table V

Coefficients of the direct process due to the Waller-Al'tshuler interaction mechanism.

	$A_{WA\ I}$ ($\times 10^{-11}$ $Oe^{-3}s^{-1}$)		$A_{WA\ II}$ ($\times 10^{-11}$ $Oe^{-3}s^{-1}$)	
	average exp. value	calculated with eq.(19a)	average exp. value	calculated with eq.(19b)
$MnSiF_6.6H_2O$	1.9	0.006	3.9	0.40
$Mn(NH_4)_2(SO_4)_2.6H_2O$	1.0	0.004	2.0	0.28
$MnSO_4.4H_2O$	0.9	0.024	1.8	1.61

from eqs.(19) together with the non-existing concentration dependence of the direct process relaxation time, are in favour to a description with the KVV interaction mechanism in the case of manganese fluosilicate and manganese Tutton salt. For manganese sulphate a distinction cannot be made. Earlier investigations on the direct spin-lattice relaxation process in manganese sulphate were performed with resonance techniques [27]. These results were attributed to the WA mechanism, but our τ versus H curves in fig. 10 show that these resonance experiments (H = 3 kOe) must be related to the fast impurity relaxations discussed above. From the similarity between the relaxation times in the three manganese compounds at strong fields, it seems rather artificial to describe the relaxation behaviour in manganese sulphate with a WA direct relaxation process.

3.1.4 *Conclusion.* The weak field behaviour of the relaxation times in manganese fluosilicate, manganese Tutton salt and manganese sulphate tetrahydrate must be ascribed to the influence of fast relaxing impurities. In performing a detailed analysis of the direct relaxation process at strong fields, an adequate description of the relaxation times at weak fields is obtained with a simple 'two spin system' model. It has been demonstrated that the direct process is best studied at liquid hydrogen temperatures and may be averaged to:

$$\tau^{-1} = 1.9 \times 10^{-11}\ H^3 \coth(g\mu_B H/2kT)\ s^{-1} \text{ for } MnSiF_6.6H_2O,$$

$$\tau^{-1} = 1.0 \times 10^{-11}\ H^3 \coth(g\mu_B H/2kT)\ s^{-1} \text{ for } Mn(NH_4)_2(SO_4)_2.6H_2O \text{ and}$$

$$\tau^{-1} = 0.9 \times 10^{-11}\ H^3 \coth(g\mu_B H/2kT)\ s^{-1} \text{ for } MnSO_4.4H_2O.$$

These direct processes are best described with the Kronig-Van Vleck interaction mechanism. The crude order of magnitude calculation gives a reasonable agreement with the above experimental results. We return to this calculation in section 3.2, where the influence of covalency on the direct process is investigated.

3.2 *Spin-lattice relaxation in manganese cesium double chloride*

3.2.1 *Introduction.* In the discussion of the direct spin-lattice relaxation time for the hydrated manganese salts (section 3.1), it was pointed out that the point charge model may be a rather crude simplification in the description of the crystalline field. It was suggested that considering covalency effects may lead to a better numerical agreement with experiment. Some authors predict a lengthening of the direct spin-lattice relaxation times upon increasing covalency [38,39]. In order to examine such an effect we studied the direct relaxation process in manganese cesium double chloride, which is known to have a 13% covalent bonding of the manganese ion with the surrounding chlorine ions.

3.2.2 *Experimental results.* Crystals of cesium manganese double chloride (Cs_3MnCl_5) are tetragonal with four molecules in a unit cell (a = 9.214 Å, c = 14.908 Å) [40]. The structure of the isomorphous Cs_3CoCl_5 has been determined in detail [41,42]. The compound should be thought of as a double salt of the composition $Cs_2MnCl_4.CsCl$. Each manganese ion is surrounded by a tetrahedron of chlorine ions causing a large cubic crystalline field with a small tetragonal distortion. The other chlorine atoms have only cesium neighbours. ESR measurements at liquid nitrogen temperature on 0.5×10^{-2} at.% Mn^{2+} in Cs_3ZnCl_5 show that the $^6S_{5/2}$ ground state of the manganese ion is split into three doublets at 0.024, 0.006 and -0.030 cm^{-1} [43]. From the magnitude of the hyperfine coupling constant a covalency of 13% is concluded for the manganese-chlorine bonds [43].

The samples were prepared by fusing together CsCl and $MnCl_2$ (molar ratio 3:1). After cooling down to room temperature the polycrystalline mass was crushed to a powder with an average crystal diameter of 0.1 mm. Measurements can only be

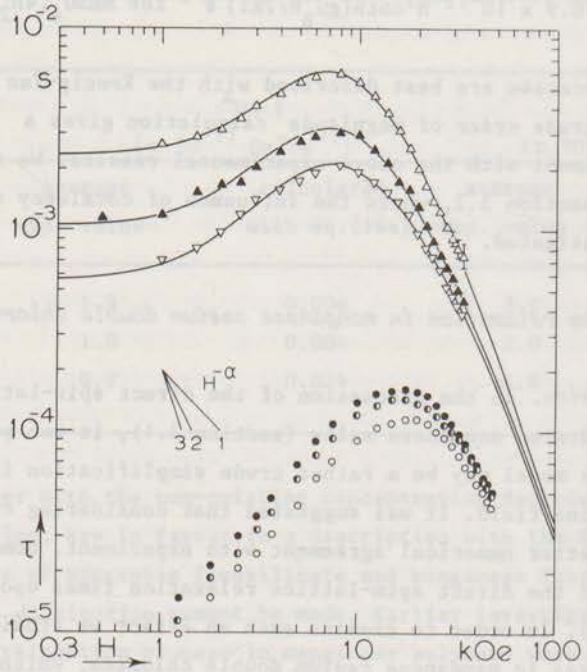

Fig. 14 Relaxation time τ as a function of external magnetic field for manganese cesium double chloride. △ : T = 2.00 K, ▲ : T = 2.99 K, ▽ : T = 4.19 K; ● : T = 14.01 K, ◐ : T = 14.92 K, ○ : T = 16.20 K. Full lines are computer fits according to eq.(53).

performed immediately after preparing the samples due to the fast disintegration of the compound. As a consequence the quoted relaxation times are of two different samples that were prepared in a similar way from identical chemicals.

The field dependence of the relaxation times was determined at liquid helium and liquid hydrogen temperatures. At liquid helium temperatures the usual form of the $\tau(H)$ curves was observed, an increase of τ at weak fields and a decrease above 8 kOe. At the strongest fields τ tends to the usual H^{-2} dependence (fig. 14, triangles). The semi-circles in the Argand diagrams were flattened in the whole field range (example in fig. 2b), with a deviation parameter d decreasing from 0.35 in weak fields to 0.15 at 30 kOe. At liquid hydrogen temperatures the weak

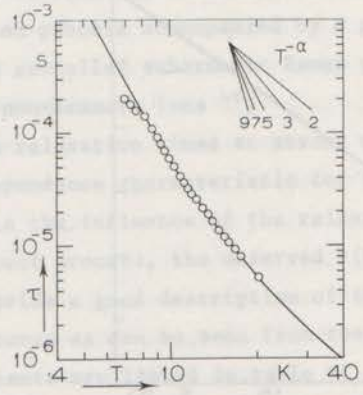

Fig. 15

Relaxation time as a function of temperature for Cs_3MnCl_5 at H = 2 kOe.

——: $\tau^{-1} = 5.4 \times 10^{-2}\ T^5 J_4(65/T)\ s^{-1}$.

field relaxation behaviour has a character, different from the usually observed Brons-Van Vleck type τ(H) curves. Between 1 and 10 kOe, the observed relaxation times increase linearly over a decade in time interval (fig. 14, circles). A maximum is reached at approximately 20 kOe, while above that field value τ decreases continuously with $\tau \propto H^{-1.8}$ at the strongest fields. Deviations from semi-circles in the Argand diagrams were not observed over the whole field range (d = 0).

A second sample was needed to examine the temperature dependence of the relaxation times at weak fields. The relaxation times of this sample at liquid helium temperatures and strong fields were verified to coincide numerically with the results reported above. At weak fields larger deviations in the Argand diagrams occurred at these temperatures, but the character of the τ(H) curves was identical to that measured on the first sample. Above 8 K, the Argand diagrams became semi-circles, and a reliable temperature dependence of τ at 2 kOe was determined above this temperature. The results are plotted in fig. 15, the τ(T) curve may be characterised by $\tau \propto T^{-\beta}$, with at the steepest part β equals 4.

In the determination of τ from susceptibility measurements, one also defines the adiabatic susceptibility χ_{ad} yielding the internal field value (eq.(41)). From the field and temperature dependence of χ_{ad} at 240 kHz between 1.2 and 20 K we found $b/C = (2.6 \pm 0.1) \times 10^6\ Oe^2$ with $\theta = (-0.7 \pm 0.2)$ K. This yields $b/R = 0.14\ K^2$, if the Curie constant is assumed to be given by eq.(2) with S = 5/2 and

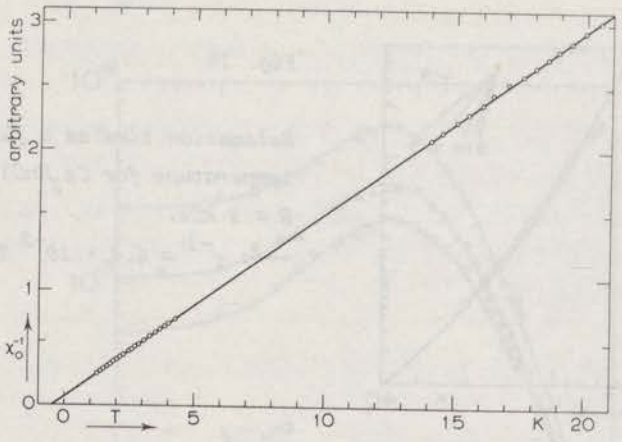

Fig. 16 χ_o^{-1} *as a function of temperature for powdered* Cs_3MnCl_5.

g = 2. This result of b/R is in fair agreement with the value of 0.16 K^2 as extrapolated from specific heat measurements below 2 K [44]). The Curie-Weiss constant θ was determined also by direct measurement of the static susceptibility between 1.2 and 20 K (fig. 16) yielding θ = (-0.5 ± 0.1) K. Earlier susceptibility measurements below 4 K gave θ = (-0.9 ± 0.1) K [44]).

3.2.3 *Discussion.* As mentioned above, the splitting between the doublets of the ground state of the Mn^{2+} ion in Cs_3MnCl_5 is of the order of 0.05 cm^{-1} and thus much smaller than kT in our experiments. Accordingly, one may expect the spin-lattice relaxation times to show field and temperature dependences as predicted for multilevel systems (eq.(44)).

Our results above 8 K at an external magnetic field of 2 kOe are adequately described by $\tau^{-1} = 5.4 \times 10^{-2}\ T^5 J_4(\Theta_D/T)\ s^{-1}$, with Θ_D = 65 K (full line in fig. 15). The value of the Debije temperature is of the same order of magnitude as the value of 70 K as reported from relaxation measurements on the isomorphous Cs_3CoCl_5 [45]). Although the temperature dependence of τ suggests that the Raman process is the predominant relaxation mechanism in weak fields, the τ(H) curve can not be fitted to the Brons-Van Vleck relation as is usual for Raman relaxation processes. As mentioned above, the relaxation times below 10 kOe increase linearly with the magnetic field. An explanation for this field behaviour can not be given. The

Raman process may be obscured by some fast relaxation process, in which case usually deviations in the Argand diagrams are observed, but our experiments show d = 0. From the literature we know of only one possibility for a T^5 Raman relaxation process accompanied by a positive slope in the log τ – log H curve, but this so-called anharmonic Raman process is expected to be effective in the case of non-Kramers ions [46]).

The relaxation times at strong magnetic fields tend towards the quadratic field dependence characteristic for the direct relaxation process. In order to eliminate the influence of the relaxation mechanism at weak magnetic fields on this direct process, the observed τ(H) curves are fitted to eq.(53). The computer fits provide a good description of the observed τ(H) curves at liquid helium temperatures as can be seen from the full lines in fig. 14. The resulting coefficients are listed in table VI. As far as the weak field behaviour is concerned, table VI shows the coefficient f(0) to be proportional to $T^{-1.8}$, at small values of ε, two features that are characteristic for relaxation processes via fast relaxing impurity centres [23,24]). Such fast relaxations were expected to occur, as the deviations in the Argand diagrams were quite large. At liquid hydrogen temperatures a similar analysis of the τ(H) curves is impossible, as the linear increase of τ upon H can not be described with f(H) as given in eq.(52).

Table VI

Constants determining the field dependence of the observed relaxation times in Cs_3MnCl_5 according to eq.(53).

T (K)	f(0) (x 10^2 s^{-1})	ε	A (x 10^{-11} $Oe^{-3}s^{-1}$)
2.00	4.2	0.18	2.90
2.99	10	0.17	3.40
4.19	18	0.15	2.90
14.01			3.8
14.92			3.8
16.20			4.0

A numerical estimate for the direct process at liquid hydrogen temperatures was obtained by taking into account only the relaxation times above 30 kOe. These estimates are given in table VI also. The difference between the coefficients

obtained from the two temperature regions is more or less identical to the differences occurring for the three manganese compounds described in the previous section.

If one considers the numerical values for A as given in table VI, it is noticeable that these coefficients are larger than the values of A as observed for the manganese compounds mentioned in section 3.1. So instead of increasing τ and thus decreasing A due to covalency, the observed effect is just the opposite. Let us consider the expected behaviour in more detail.

a) *The effect of covalent bonding.* The magnitude of the covalent bonding may be obtained from the hyperfine coupling coefficient. The covalency in Cs_3MnCl_5 was demonstrated to be 13% [43]). If we assume the linear dependence between hyperfine coupling coefficient and covalency as measured by Matumura [47]) to be correct for the hydrated manganese compounds studied, manganese fluosilicate and manganese Tutton salt have a covalency of approximately 4½%. The hyperfine coupling in manganese sulphate is not known and we will omit this compound in our further analysis.

Blume and Orbach [11]) calculated the coefficient A of the direct process for Mn^{2+} in MgO in the case of a purely ionic bonding as was mentioned already in section 3.1.3c. Mn^{2+} in MgO is known to have 8% covalency [47]). However, various authors suggested the influence of this covalency on the direct spin-lattice relaxation time in this substance to be negligible [48,49]). Other calculations concerning the influence of covalency on the direct relaxation process were performed for an octahedral complex with one magnetic ion [38]) and more specifically, for Ti^{3+} in alums [39]). These approaches lead to strongly increasing relaxation times upon increasing covalency, and thus to a decreasing coefficient A. Our measurements on Cs_3MnCl_5 show a clear shortening of the direct process, and thus an increasing A, with respect to the results obtained on the less covalent hydrated manganese salts, in contrast to the theoretical predictions. This situation leads us to reconsider the crude order of magnitude calculation for the coefficient of the direct process on the basis of the point charge model as given in 3.1.3c.

b) *Refined calculation of A with the point charge model.* The coefficient of the direct process A contains as a crucial variable the velocity of sound in the crystal, v, entering into A as v^{-5} (eq.(12)). In the order of magnitude calculation in the preceding section we estimated $v = 3 \times 10^5$ cm s^{-1} for the hydrated manganese salts. The dependence of A on the velocity of sound is a

consequence of the long wave approximation in the phonon description of the lattice vibrations. For the phonon distribution the Debije model is assumed. The coefficient A may be re-expressed in terms of the Debije temperature, as Θ_D and v are directly related to each other by eq.(11). Accordingly, on this assumption, the coefficient A becomes proportional to $M^{-5/3}\rho^{2/3}\Theta_D^{-5}$, in which M is the molecular weight and ρ the density of the crystal. The Debije temperature may be derived from various types of measurements. We elected to choose the values observed in the Raman relaxation process, because these values correspond to the phonon system as it is effective in the relaxation mechanisms. For $Mn(NH_4)_2(SO_4)_2.6H_2O$ from the literature Θ_D = 280 K [22], but a value of 145 K seems more reasonable for ammonium Tutton salts (cf. chapter IV and ref. 50). The values of Θ_D, M and ρ for the various compounds are listed in table VII.

Table VII

	Θ_D (K)	M (g)	ρ [51] (g/cm^3)	$A_{calculated}$ ($Oe^{-3}s^{-1}$)	$A_{experimental}$ ($Oe^{-3}s^{-1}$)
$MnSiF_6.6H_2O$	140 [23]	305	1.90	19.5×10^{-11}	1.9×10^{-11}
$Mn(NH_4)_2(SO_4)_2.6H_2O$	145	391	1.83	10.0×10^{-11}	1.0×10^{-11}
Cs_3MnCl_5	65	631	3.4	4.0×10^{-9}	3.9×10^{-11}

The coefficient A contains several matrix elements which may also differ for the various compounds. At present, we will neglect these differences compared to the variation in $M^{-5/3}\rho^{2/3}\Theta_D^{-5}$ on the substance. The matrix elements for the different compounds are assumed to have the value calculated for Mn^{2+} in MgO using the point charge model. So, in this way the coefficients A of the direct process for the various manganese compounds can be calculated without the influence of covalency. The results are given in table VII, together with the experimentally determined values. In comparing these two sets of coefficients, it is noticeable that the experimentally observed A values are smaller than those calculated. This difference is about a factor of 10 for the manganese compounds with a 4½% covalency and about 100 for Cs_3MnCl_5 having a covalency of 13%. At first sight this increased difference between $A_{calculated}$ and $A_{experimental}$ for Cs_3MnCl_5 may be seen as a confirmation of the effect of covalency on the direct relaxation times. However, the doubtful assumption in the above discussion is the neglection of the difference between the occurring matrix elements. The crystal field in $MnSiF_6.6H_2O$ is cubic with a trigonal

distortion [30]), while the crystal field at the site of the Mn^{2+} ions in the ammonium Tutton salt is cubic with a tetragonal distortion [32]). Both samples have about the same covalency. The difference between $A_{calc.}$ and $A_{exp.}$ is found to be a factor of 10 for these two samples, thus supporting our assumption that variation in the symmetry of the crystalline field does not influence the coefficients A in these salts. The crystalline field at the site of the Mn^{2+} ions in Cs_3MnCl_5 is also cubic with a small tetragonal distortion. Therefore, we suppose our initial assumption concerning the crystalline field, having no influence on the matrix elements, to be correct. The conclusion must be that the factor of 100 difference between $A_{calc.}$ and $A_{exp.}$ for Cs_3MnCl_5 does in fact demonstrate the lengthening effect of increasing covalency on the direct process relaxation times.

3.2.4 *Conclusion.* The temperature dependence of the relaxation times in manganese cesium double chloride at weak magnetic fields shows, above 8 K, a $T^5 J_4(\Theta_D/T)$ shape, that is characteristic for the Raman process in multilevel systems. Instead of a Brons-Van Vleck relation as is usual for the field dependence of the Raman relaxation time, τ increases linearly with H below 10 kOe. In strong magnetic fields, the direct relaxation process for multilevel systems is observed both at liquid helium and liquid hydrogen temperatures and can be given as:

$$\tau^{-1} = 3.9 \times 10^{-11} H^3 \coth(g\mu_B H/2kT)\ s^{-1}.$$

Numerically this result is even larger than the values reported in section 3.1. At first sight this seems to contradict the theoretical predictions about the effect of covalency on the relaxation. However, a refined discussion of the coefficient A of the direct process with the point charge model for the various manganese compounds, taking into account the variations in the parameters Θ_D, ρ and M, demonstrated the lengthening effect of covalency on the direct relaxation process in Cs_3MnCl_5.

3.3 *Spin-lattice relaxation in three hydrated chromium salts*

3.3.1 *Introduction.* The investigation of the direct spin-lattice relaxation process in various manganese compounds clearly demonstrated the applicability of the relaxation theory for multilevel systems. In the present section we will examine whether this theory does also apply to chromium salts. The $^4F_{3/2}$ ground state of the Cr^{3+} ion in hydrated salts is split into two doublets with

a zero field energy separation in the order of 0.1 cm^{-1}, which is much smaller than kT under our experimental conditions.

3.3.2 *Experimental results.* The experiments were performed on three chromium compounds. Cesium chromium alum will be discussed in a), while measurements on guanidinium chromium sulphate hexahydrate and guanidinium chromium selenate hexahydrate will be given in b).

a) *Cesium chromium alum.* The alums provide an extensive series of isomorphous cubic crystals with general formula $M'M''(S'O_4)_2.12H_2O$, in which M' is a monovalent cation (K, NH_4, Cs, etc.), M'' a trivalent cation (e.g. Al) and S' is S or Se. The crystal structure of a large number of alums has been investigated, showing that three types occur depending on the radius of the monovalent ion [52]. There are four molecules in a unit cell, each trivalent ion is surrounded by an octahedron of six water molecules. In the compound cesium chromium alum ($CsCr(SO_4)_2.12H_2O$) this octahedron has a small trigonal distortion along one of the body diagonals of the unit cube [53]. The electrical crystalline field lifts the degeneracy of the Cr^{3+} ground state ($^4F_{3/2}$), under our experimental conditions only two doublets are effectively populated. The zero field splitting between these doublets is 0.133 cm^{-1}, the effective g value 1.98 [54].

Previous experiments on chromium alums do not show clearly which processes are involved in the spin-lattice relaxation mechanism. The most relevant results until now, all obtained at weak magnetic fields, were reviewed recently [36]. The temperature dependence of the spin-lattice relaxation times below 4.2 K in the earlier papers may be given as $\tau \propto T^{-\beta}$ with $1<\beta<4$. Above liquid helium temperatures $\tau(T)$ could not be determined satisfactorily. The dependence of the relaxation time on the external magnetic field was examined below 5 kOe only. The importance of cross-relaxation processes in cesium chromium alum was demonstrated [55]. The present equipment enables a study of $\tau(T)$ above 4.2 K, while $\tau(H)$ can be determined in magnetic fields up to 50 kOe at liquid helium and liquid hydrogen temperatures.

The cesium chromium alum was chosen for our experiments because this alum is more stable then the frequently used potassium chromium alum [56]. Accordingly, effects due to a changing crystal structure, as observed in hydrated manganese salts (paragraph 3.1.2), did not influence the present results. The experiments were performed on powdered samples (average crystal diameter 0.1 mm) in order to minimize the influence of the phonon bottleneck at liquid helium temperatures [18]. One sample was pure cesium chromium alum (sample 100%), two others were mixed crystals, part of the chromium being replaced by aluminium: $CsCr_xAl_{1-x}(SO_4)_2.12H_2O$,

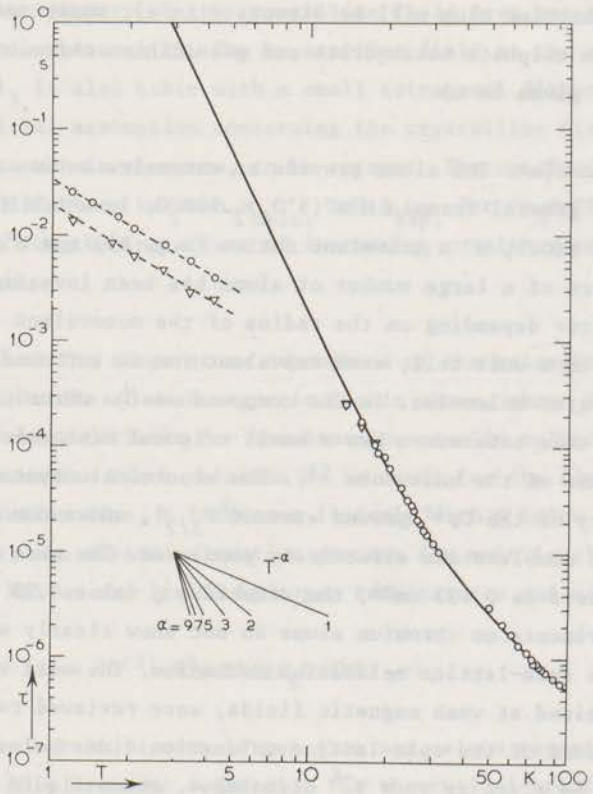

Fig. 17 The relaxation time τ as a function of temperature for cesium chromium alum samples at H = 4 kOe. ○ : sample 100%, ▽ : sample 2.6%, ——: $\tau^{-1} = 2.3 \times 10^{-4}\ T^5 J_4(145/T)\ s^{-1}$.

with x = 0.059 (sample 5.9%) and x = 0.026 (sample 2.6%).

The temperature dependence of the relaxation times was determined on the samples 100% and 2.6% at an external magnetic field of 4 kOe between 1.2 and 100 K (fig. 17). At liquid helium temperatures the relaxation times on both samples may be described by $\tau \propto T^{-1.4}$, but the absolute values of τ for both samples differ by a factor of two. In the Argand diagrams of sample 100% an asymmetric broadening at the high frequency side was observed (example in fig. 2b),

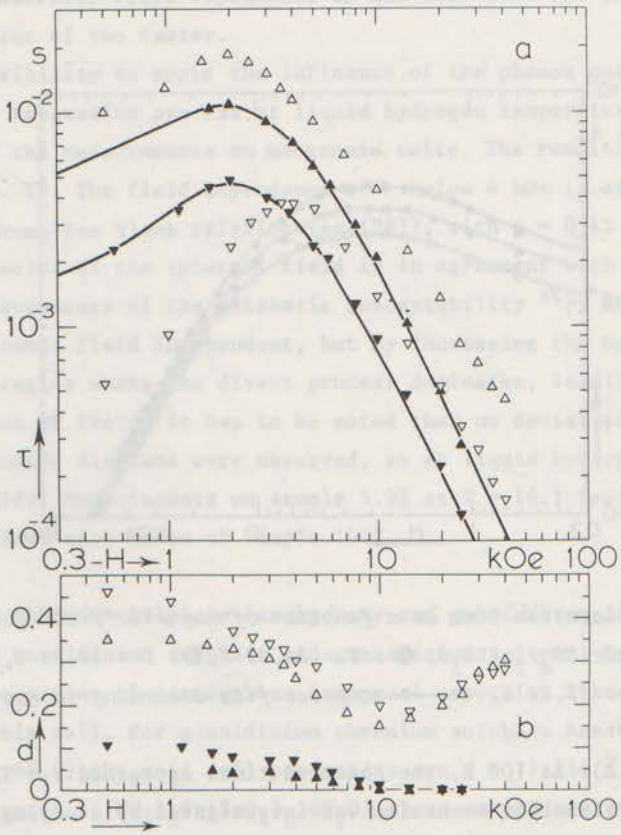

Fig. 18 Relaxation time (a) and deviation parameter (b) as a function of external magnetic field for cesium chromium alum samples at T = 2.0 K (△, ▲) and T = 4.2 K (▽, ▼). Open symbols: sample 100%, closed symbols: sample 5.9%, full lines: computer fits according to eq.(53).

with a deviation parameter d of 0.30. The asymmetry in the Argand diagrams was considerably smaller for sample 2.6%, d being about 0.05. At liquid hydrogen temperatures the relaxation times for both samples coincide and can be given as $\tau \propto T^{-3.5}$. At these temperatures, semi-circles in the Argand diagrams were observed for both the 100% and 2.6% samples. The temperature dependence of the relaxation time was determined above 20 K on sample 100% only, using the running

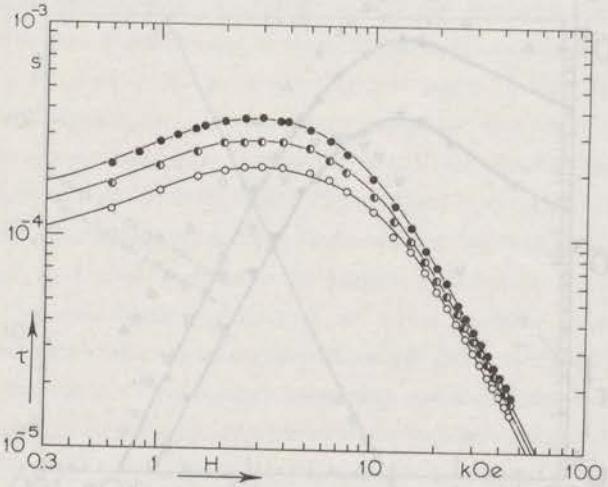

Fig. 19 Relaxation time as a function of magnetic field for 100% $CsCr(SO_4)_2 \cdot 12H_2O$. ● : T = 14.08 K, ◐: T = 14.94 K, ○: T = 15.84 K, ——: computer fits according to eq.(53).

method (par. 2.2.3). At 100 K, the observed times aproached $\tau \propto T^{-2}$.

The direct relaxation mechanism was investigated by studying the field dependence of τ up to strong magnetic fields. At liquid helium temperatures and in weak magnetic fields, the average relaxation times for sample 100% increased with increasing magnetic field (fig. 18a, open symbols). A maximum value is reached at approximately 4 kOe, while at stronger fields τ decreases again. Above 10 kOe, the relaxation times approach $\tau \propto H^{-2.0}$, but above 20 kOe the negative slope in the log τ - log H graph becomes smaller. With increasing magnetic field, the asymmetry of the semi-circles in the Argand diagrams initially diminished, but above 10 kOe a symmetric flattening occurred which increased upon increasing the field. This behaviour, demonstrated by the deviation parameter d as a function of magnetic field in fig. 18b, suggests an increasing influence of the phonon bottleneck on the direct process at strong fields. In order to reduce this influence the measurements at liquid helium temperatures were repeated on the diluted samples 5.9% and 2.6%. The relaxation times for both samples are almost identical, the results for sample 5.9% being inserted

in fig. 18a (closed symbols). The deviations in the Argand diagrams disappeared above 10 kOe (fig. 18b, closed symbols). In this field region the observed times showed a quadratic field dependence as was also seen for sample 100%, but τ is about a factor of two faster.

Another possibility to avoid the influence of the phonon bottleneck is to study the direct relaxation process at liquid hydrogen temperatures, as was demonstrated for the measurements on manganese salts. The resulting $\tau(H)$ curves are given in fig. 19. The field dependence of τ below 4 kOe is adequately described by a Brons-Van Vleck relation (eq.(28)), with $p = 0.45$ and $b/C = 0.47 \times 10^6$ Oe^2. This value of the internal field is in agreement with the result derived from measurements of the adiabatic susceptibility [36]. Above the internal field value, τ becomes field independent, but by increasing the magnetic field one reaches the region where the direct process dominates, leading to a decrease of τ as a function of field. It has to be noted that no deviations from semi-circles in the Argand diagrams were observed, so at liquid hydrogen temperatures $d = 0$ at all fields. Measurements on sample 5.9% at T = 14.1 K yielded relaxation times that coincided with those of sample 100%.

b) *Guanidinium chromium sulphate hexahydrate and guanidinium chromium selenate hexahydrate*. The guanidinium sulphate and guanidinium selenate hexahydrates form an extensive series of isomorphous hexagonal crystals. There are three molecules in a unit cell. For guanidinium chromium sulphate hexahydrate ($C(NH_2)_3Cr(SO_4)_2.6H_2O$) the unit cell parameters are a = 11.754 Å and c = 9.041 Å [57]. For the selenate ($C(NH_2)_3Cr(SeO_4)_2.6H_2O$) these parameters are about 5% larger. The chromium ions are surrounded by a nearly regular octahedron of six water molecules, causing a cubic electrical crystalline field with a small trigonal distortion. On substituting selenate for sulphate the trigonal distortion increases [58]. Only two of the three molecules in the unit cell are crystallographically and magnetically equivalent. The EPR spectra for the Cr^{3+} ions in the aluminium isomorphs yield a splitting between the doublets (2D) of 0.214 and 0.164 cm^{-1} for the Cr^{3+} ions at the two different sites in the sulphate and 0.370 and 0.262 cm^{-1} in the selenate [59,60].

Single crystals were grown by slow evaporation of the requisite aqueous solutions [58]. The selenate was examined as a powdered sample with an average crystal diameter of 0.1 mm (sample GCrSeH), the sulphate as a single crystal (sample GCrSH).

For GCrSeH the field dependence of the relaxation times was determined at 2.0 and 4.2 K and at 14.1 K. The relaxation times at 2.0 K are almost field

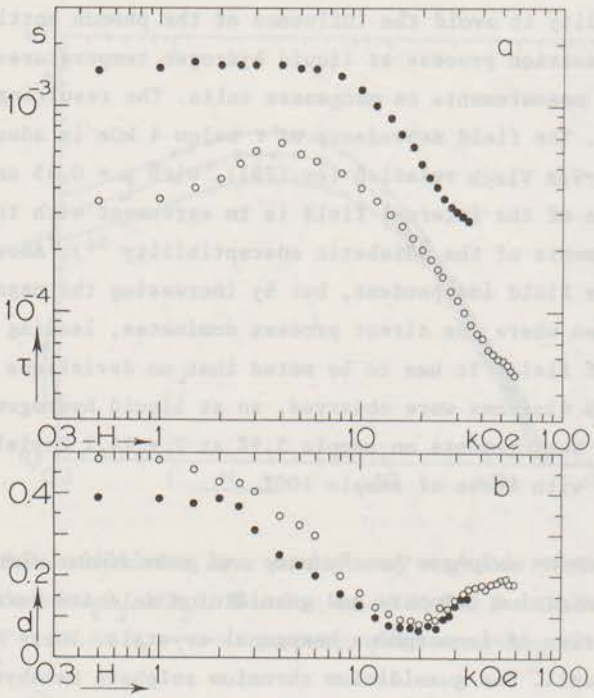

Fig. 20 Relaxation time (a) and deviation parameter (b) as a function of magnetic field for powdered guanidinium chromium selenate hexahydrate. ● : T = 2.00 K, ○: T = 4.24 K.

independent below 6 kOe, above this field value τ decreases and tends towards $\tau \propto H^{-1.6}$ (fig. 20a). The relaxation times at the strongest fields become larger than expected from $\tau \propto H^{-1.6}$. At T = 4.2 K the same character of the τ(H) curve is observed at strong fields, but below 4 kOe τ increases with increasing magnetic field. The Argand diagrams at the liquid helium temperatures show a symmetric flattening of the semi-circles over the whole field range, the deviation parameter d has a minimal value at about 20 kOe (fig. 20b). The behaviour of the τ(H) curves above 10 kOe, together with the increasing d values, is characteristic of a direct relaxation process obscured by phonon-bottleneck effects. The direct spin-lattice relaxation process may be observed without these effects at liquid hydrogen temperatures. The relaxation times observed at T = 14.1 K (fig. 21,

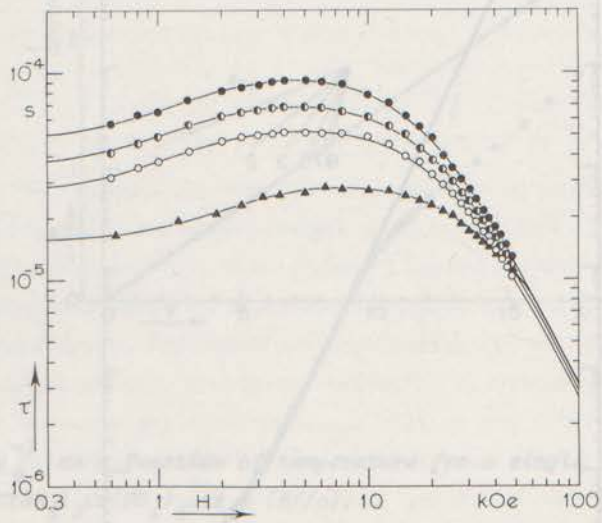

Fig. 21 Relaxation time as a function of magnetic field for powdered $C(NH_2)_3Cr(SeO_4)_2.6H_2O$ (triangles) and a single crystal of $C(NH_2)_3Cr(SO_4)_2.6H_2O$ with H//c (circles). ▲ : T = 14.01 K, ● : T = 14.06 K, ◐ : T = 14.99 K, ○ : T = 15.92 K, ——— : computer fits according to eq.(53).

symbol ▲) increase below 10 kOe according to a Brons-Van Vleck relation with p = 0.5 and b/C = 2.9 x 10^6 Oe^2. Above 15 kOe, τ becomes shorter and tends towards $\tau \propto H^{-1.0}$ at the strongest fields. At this temperature no deviations from semi-circles in the Argand diagrams were observed. Apparently, our maximum magnetic field of 50 kOe is not strong enough to reach the H^{-2} dependence of the direct relaxation time in GCrSeH, so no further measurements were performed on this sample at liquid hydrogen temperatures.

A preliminary measurement on a powdered sample of GCrSH showed a time dependence of the curves in the Argand diagrams, with corresponding changing relaxation times, as observed for powdered manganese compounds (par. 3.1.2). Therefore the relaxation behaviour was studied on a single crystal of GCrSH with the external magnetic field parallel to the crystallographic c axis. As

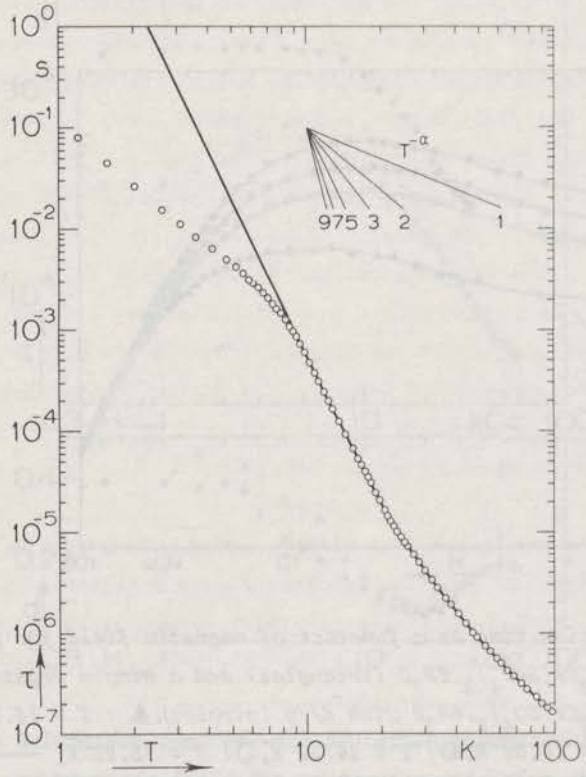

Fig. 22 Relaxation time as a function of temperature for a single crystal of guanidinium chromium sulphate hexahydrate (H//c) at H = 4 kOe. ———: $\tau^{-1} = 6.6 \times 10^{-4}\ T^5 J_4(145/T)\ s^{-1}$.

the influence of the phonon bottleneck is disastrous in large crystals at liquid helium temperatures, the field dependence of τ was studied at liquid hydrogen temperatures only (fig. 21, circles). The form of the $\tau(H)$ curves in weak fields is identical to a Brons-Van Vleck relation with p = 0.5 and $b/C = 0.96 \times 10^6$ Oe^2. The numerical values of τ at 14.1 K and weak fields are a factor of 3 larger than for the selenate. Above 10 kOe, the relaxation time decreases continuously and can be given at the strongest fields as $\tau \propto H^{-2.0}$. No deviations from semi-circles in the Argand diagrams were observed (d = 0).

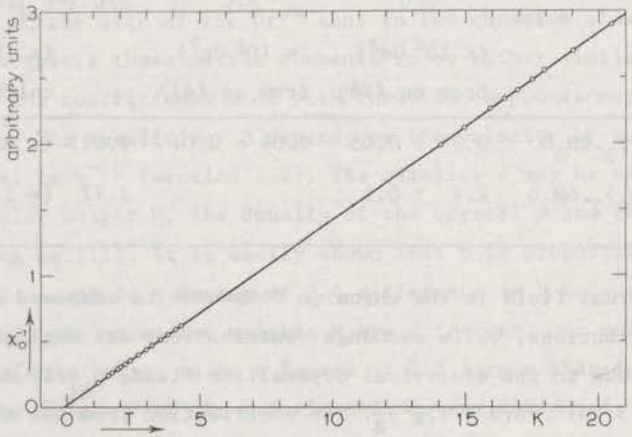

Fig. 23 χ_o^{-1} *as a function of temperature for a single crystal of* $C(NH_2)_3Cr(SO_4)_2.6H_2O$ *(H//c).*

The form of the weak field behaviour of τ according to a Brons-Van Vleck relation with p = 0.5 suggests the Raman process to be dominant at weak magnetic fields. To examine this Raman process in more detail, the temperature dependence of the relaxation times has been studied at an external magnetic field of 4 kOe between 1.2 and 100 K (fig. 22). At liquid helium temperatures, $\tau(T)$ is adequately described by $T^{-2.0}$. Above 10 K, the relaxation times exhibit $\tau \propto T^{-4.0}$ tending towards $T^{-2.0}$ at 100 K.

The internal field values for GCrSH and GCrSeH are not yet known from literature as for the cesium chromium alum. The values of b/C, following from the Brons-Van Vleck relations (eq.(28)) at liquid hydrogen temperatures, are given in table VIII. The internal field value can be obtained also from adiabatic susceptibility measurements as a function of magnetic field and temperature (eq.(41)). The result of such measurements for GCrSH at 240 kHz is given in the table also. In the derivation of this value we obtained $\theta = (-0.13 \pm 0.03)$ K. Direct measurements of the zero field susceptibility χ_o as a function of temperature (fig. 23) indeed yield a Curie-Weiss behaviour, with $\theta = (-0.14 \pm 0.01)$ K.

Table VIII

	b/C ($\times 10^6$ Oe^2) from eq.(28)	b/C ($\times 10^6$ Oe^2) from eq.(41)	b/C ($=b_{el}/C + b_{dip}/C$) ($\times 10^6$ Oe^2) calculated
$C(NH_2)_3Cr(SO_4)_2.6H_2O$	0.96 ± 0.05	1.04 ± 0.01	1.025 (= 0.927 + 0.098)
$C(NH_2)_3Cr(SeO_4)_2.6H_2O$	2.9 ± 0.1		2.77 (= 2.68 + 0.085)

The internal field in the chromium compounds is composed of electric and dipolar contributions, while exchange contributions are negligible [61,62]. The contribution due to the electrical crystalline field, b_{el}/C, can be calculated from $b_{el}/C = 3(2D)^2/4S(S + 1)g^2\mu_B^2$. The contribution from the dipole-dipole interactions, b_{dip}/C, is calculated from the available crystallographic data, this procedure being described in detail in ref. 63. The values for b/C calculated in this way (table VIII) are in fair agreement with the measured values.

From our experimental results, $b/R = 0.023$ K^2 for GCrSH and $b/R = 0.06$ K^2 for GCrSeH are obtained. We do not known of any specific heat measurements with which to compare these results.

3.3.3 *Discussion.* As mentioned above the zero field splitting of the Cr^{3+} ground state in the hydrated salts we studied is of the order of 0.1 cm^{-1}, which is small compared to kT in our experiments. The spin-lattice relaxation times may show the field and temperature dependence characteristic for a multilevel system (eq.(44)). Successively, the Raman process in weak fields, and the direct process that dominates at strong fields will be discussed.

a) *The Raman relaxation process.* Above 10 K, the temperature dependence of the observed relaxation times at an external magnetic field of 4 kOe may be given for the samples 2.6% and 100% $CsCr(SO_4)_2.12H_2O$ as $\tau^{-1} = 2.3 \times 10^{-4}$ $T^5J_4(145/T)$ s^{-1} and for $C(NH_2)_3Cr(SO_4)_2.6H_2O$ as $\tau^{-1} = 6.6 \times 10^{-4}$ $T^5J_4(145/T)$ s^{-1} (full lines in figs. 17 and 22). The field dependence of τ below 5 kOe at these temperatures is described adequately by a Brons-Van Vleck relation in all cases. The expressions mentioned above do not correspond to the strong field limit at which eq.(44) is derived. Extrapolation of the result at 4 kOe to strong magnetic fields using the Brons-Van Vleck relation yields the Raman relaxation time to be

$\tau^{-1}_{Raman} = BT^5J_4(145/T)$ with $B = 2.2 \times 10^{-4}$ $K^{-5}s^{-1}$ for $CsCr(SO_4)_2.12H_2O$ and $B = 6.3 \times 10^{-4}$ $K^{-5}s^{-1}$ for $C(NH_2)_3Cr(SO_4)_2.6H_2O$.

The coefficient B contains several matrix elements. The similarity of the crystalline fields at the site of the Cr^{3+} ions in the chromium alum and the chromium sulphate suggests these matrix elements to be rather similar also. The difference between the coefficients B of both chromium compounds may be ascribed to other influences. The coefficient B depends on the velocity of sound in the crystal proportional to v^{-10} (section 1.2). The quantity v may be expressed in terms of the molecular weight M, the density of the crystal ρ and the Debije temperature Θ_D using eq.(11). It is easily shown that B is proportional to $M^{-10/3}\rho^{4/3}\Theta_D^{-10}$. This leads to a factor of 3.4 difference in B between the sulphate and the alum, as only the molecular weights M are different. Our measurements show B in the chromium sulphate to be a factor of 2.8 larger than in the chromium alum. In view of the accuracy of the experimental determination of Θ_D, which is about 3%, this measured difference factor between B in the alum and the sulphate is in agreement with the difference as expected from the factor $M^{-10/3}$.

b) *The direct relaxation process.* The direct process relaxation rate for a multilevel system is expected to show a field dependence proportional to H^2, tending towards H^3 for $g\mu_B H \gtrsim 2kT$. The quadratic field dependence of τ^{-1} is approached in 100% cesium chromium alum at liquid helium temperatures at about 10 kOe, but the relaxation time is lengthened with respect to this field dependence at the strongest fields. This lengthening of τ is accompanied by increasing deviations from semi-circles in the Argand diagrams. These effects are characteristic of the influence of the phonon bottleneck on the direct process. At weak magnetic fields short-circuiting impurity relaxations obscure the direct process. The influence of these fast relaxations decreases with increasing magnetic field, and thus d decreases (see also section 3.1). So the observed relaxation time is, at weak magnetic fields, smaller than τ_{direct} due to fast relaxations, and, at strong fields, larger than τ_{direct} under the influence of phonon bottleneck. At some intermediate field strength the observed relaxation time must equal the direct process relaxation time. This field value may be found as the magnetic field where d(H) reaches the minimal value. This so-called 'interpolation method' has been used successfully for the determination of the coefficient of the direct process in the case where the direct relaxation time is obscured by the phonon bottleneck at strong magnetic fields[18]). In our measurements on 100% $CsCr(SO_4)_2.12H_2O$ a minimal d value is reached at T = 4.23 K

Table IX

Constants determining the field dependence of the observed relaxation times in $CsCr(SO_4)_2.12H_2O$ samples according to eq.(53).#

sample	T (K)	f(0) ($\times 10^2\ s^{-1}$)	ε	A ($\times 10^{-11}\ Oe^{-3}s^{-1}$)
100%	2.10			6
	4.23			8
	14.08	61	0.39	12.5
	14.94	79	0.39	12.7
	15.84	102	0.41	13.0
5.9%	2.09	2.2	0.28	14.3
	4.21	6.3	0.19	16.8
	14.05	88	0.4	13
2.6%	4.24	32	0.05	15.4

$b/C = 0.47 \times 10^6\ Oe^2$ 36).

for H = 14 kOe, and at T = 2.10 K for H = 10 kOe (fig. 18). From the corresponding relaxation times the coefficient A of the direct process, as given in table IX, is calculated.

Effects of the phonon bottleneck are not observed for the sample 100% $CsCr(SO_4)_2.12H_2O$ at liquid hydrogen temperatures. Above 30 kOe the observed relaxation time is proportional to H^{-2}, and d = 0. The $\tau(H)$ curves have been fitted to eq.(53) in order to subtract the Raman process, which is effective in weak fields, from the observed time constants. The computer fits thus obtained provide a good description of the observed relaxation times (full lines in fig. 19), the resulting coefficients are listed in table IX also.

The measurements for the samples 5.9% and 2.6% cesium chromium alum show a clear H^{-2} dependence of τ above 10 kOe, where d becomes zero also. Thus the phonon bottleneck is obviously not effective in these magnetically diluted samples. This enables the determination of the coefficient of the direct process using a computer fit with eq.(53) to the observed $\tau(H)$ curves. As an

example the fits to the results on sample 5.9% are given in fig. 18 (full lines), the resulting coefficients are given in table IX.

The coefficients A in table IX enable a test of the reliability of the interpolation method. The A values for sample 100% from the measurements at liquid helium temperatures using the interpolation method are about a factor of two smaller than A, obtained from the computer fit to the measurements at liquid hydrogen temperatures. It has to be noted that the minimal d value at liquid helium temperatures amounts to 0.2. This implies that the observed relaxation times must be considered as average ones over a distribution of relaxation times, the difference between the upper and lower limit being at least a factor of 10^{64}). The resulting time constants for the direct process with the interpolation method differ only by a factor of two from the results obtained from perfect semi-circles. Thus the A values obtained with the interpolation method are shown to be reliable, a more accurate value will be obtained when the minimal deviation parameter is smaller than 0.2.

We will now focus our attention on the direct process in the guanidinium chromium compounds. The steepest slope that is reached in the log τ - log H graphs for GCrSeH at liquid helium temperatures amounts to -1.6, and the corresponding d(H) graphs increase strongly above 20 kOe (fig. 20). This demonstrates the considerable influence of the phonon bottleneck on the relaxation behaviour at strong fields in this sample. The coefficient A of the direct process is determined using the interpolation method, the resulting A values are given in table X. A verification of these A values could not be

Table X

Constants determining the field dependence of the observed relaxation times in guanidinium chromium selenate and guanidinium chromium sulphate hexahydrate according to eq.(53).#

sample	T (K)	f(0) ($\times 10^3$ s^{-1})	ε	A ($\times 10^{-11}$ $Oe^{-3}s^{-1}$)
GCrSeH	4.24			20
	2.09			17
	14.06	63	0.53	12
GCrSH	14.10	20	0.48	13.6
	14.99	27	0.49	13.5
	15.92	36	0.49	13.7

b/C = see 3.3.2b.

obtained properly from the $\tau(H)$ curves at liquid hydrogen temperatures, because at the maximum field of 47.5 kOe a clear H^{-2} dependence of τ is still not reached. A computer fit with eq.(53) is used in order to extrapolate the observed $\tau(H)$ curve at T = 14.06 K towards strong fields (full line in fig. 21). The resulting A value as quoted in table X has an accuracy of about 25%.

In order to avoid inaccuracies due to the phonon bottleneck at liquid helium temperatures, and possible influences of physical impurities in powdered samples (cf. manganese salts) in determining A for GCrSH, the direct process is studied on a single crystal of this compound at liquid hydrogen temperatures. The observed $\tau(H)$ curves have been fitted to eq.(53) as shown in fig. 21 (full lines), the resulting coefficients are listed in table X also. The A values in this table demonstrate that the single crystal of GCrSH (H//c axis) yields almost identical results as obtained on the powdered sample of GCrSeH.

In the numerical analysis of the direct process in chromium compounds we will concentrate on the results obtained at liquid hydrogen temperatures in the undiluted samples. The observed difference in the Raman relaxation times between the chromium alum and the chromium sulphate is not present in the direct relaxation times. Following the same arguments as with the Raman process one would expect that the coefficient A of the sulphate is a factor of 1.8 larger than of the alum due to the different molecular weights. Our experiments show this factor to be only 1.1. As mentioned above, two inequivalent Cr^{3+} ions with different zero field splittings between the ground doublets occur in the chromium sulphate. Such an effect may have influence on the direct process as only a specific band of phonons participates. A direct comparison between the A values may therefore be opportune, as inequivalent Cr^{3+} sites do not occur in the alum.

A thorough calculation of the direct relaxation time is known for Cr^{3+} in Al_2O_3 [65]). One obtains for a powdered sample $A = 0.3 \times 10^{-11}$ $Oe^{-3}s^{-1}$. In this calculation empirical spin-lattice interaction parameters are used, thus covalency effects are included automatically. For the hydrated chromium compounds we can only estimate the order of magnitude of A due to the complexity of the matrix elements in these salts. A reasonable value for the velocity of sound in Al_2O_3 is $v = 5 \times 10^5$ cm s^{-1}. Application of the Debije temperature, as determined with the Raman process, in eq.(11) yields $v = 1.8 \times 10^5$ cm s^{-1} for the hydrated chromium salts. Taking the density of the crystal 2.1 g cm^{-3} (4.0 g cm^{-3} for Al_2O_3), we obtain for the hydrated chromium compounds $A = 90 \times 10^{-11}$ $Oe^{-3}s^{-1}$. For an order of magnitude estimate the agreement with the experimental results is satisfactory.

3.3.4 *Conclusion.* The theoretical predictions for the spin-lattice relaxation times in multilevel systems are verified experimentally in hydrated chromium salts. Above approximately 8 K the Raman relaxation process is observed in weak fields with the characteristic $T^5J_4(\Theta_D/T)$ dependence. In strong magnetic fields the direct relaxation process is operative at liquid helium and liquid hydrogen temperatures. The reduction of the influence of the phonon bottleneck at liquid helium temperatures in magnetically diluted samples, and at temperatures above 14 K in undiluted samples, is observed. Especially, the measurements at liquid hydrogen temperatures are demonstrated to yield accurate values for the direct relaxation times. As a result, the relaxation times in $CsCr(SO_4)_2.12H_2O$ may be given as:

$$\tau^{-1} = 2.2 \times 10^{-4}\ T^5J_4(145/T) + 12.7 \times 10^{-11}\ H^3\coth(g\mu_B H/2kT)\ s^{-1}$$

and in $C(NH_2)_3Cr(SO_4)_2.6H_2O$ as:

$$\tau^{-1} = 6.3 \times 10^{-4}\ T^5J_4(145/T) + 13.6 \times 10^{-11}\ H^3\coth(g\mu_B H/2kT)\ s^{-1},$$

but the influence of fast relaxing impurities may obscure these relaxation times at weak magnetic fields.

3.4 *Some concluding remarks on the spin-lattice relaxation in multilevel systems*

The characteristic field and temperature dependences as predicted for the spin-lattice relaxation times in multilevel systems were verified experimentally in various manganese and chromium compounds. The Raman relaxation process ($\tau^{-1} = BT^5J_4(\Theta_D/T)$) in these salts is operative in general above approximately 10 K in weak magnetic fields. The direct relaxation process ($\tau^{-1} = AH^3\coth(g\mu_B H/2kT)$) was observed at liquid helium and at liquid hydrogen temperatures in strong fields. It was shown that the disturbing influence of the phonon bottleneck, which reduced the accuracy of determining the direct process at liquid helium temperatures, is not present at liquid hydrogen temperatures. From our measurements we were able to demonstrate the reliability of the so-called interpolation method, which has been used for the determination of the direct process in cases where the direct relaxation time is obscured by the phonon bottleneck.

The crucial parameters, which are the decisive factors for the magnitude of the coefficient A in the direct process, are the velocity of sound in the

crystal and the matrix elements of the spin-lattice interaction. The velocity of sound may be re-expressed in terms of the molecular weight M, the density of the crystal ρ and the Debije temperature Θ_D. These quantities account for the observed difference in the direct relaxation times among e.g. the hydrated manganese salts, the matrix elements being of equal order of magnitude. These matrix elements are expected to vary with degree of covalent bonding. Such an influence that causes a lengthening of the direct process was seen in the manganese cesium double chloride.

A comparison between the coefficients A of the direct process in the hydrated manganese salts with those of the chromium compounds shows the former to be smaller. The matrix elements for the direct process in the Mn^{2+} compounds remain about a factor of 10 smaller than those of the Cr^{3+} salts after the influence of the values of M, ρ and Θ_D on A is taken into account. The ground state of the Mn^{2+} ion is ^6S, thus the orbital angular momentum L is zero. In the theory of Kronig and Van Vleck the spin-orbit coupling is the essential link in the interaction between spins and lattice vibrations. In order to find non-zero matrix elements in the orbit-lattice interaction it is necessary for an S state ion to mix excited states, with non-zero angular momentum, into the ground state using spin-orbit coupling. For Cr^{3+} the ground state is ^4F, thus L = 3. In an octahedral environment as in the hydrated salts the ground state is an orbital singlet with all excited states lying higher in energy by amounts large compared with the spin-orbit coupling. The orbital angular momentum is then said to be 'quenched'. Thus, also in this case, non-zero matrix elements of the orbit-lattice interaction are obtained after mixing in of excited states via the spin-orbit coupling. Although at first sight the situation for an S state ion is not very different from that of an ion with quenched orbital momentum, the admixture of L = 3 states may be quite strong and thus responsible for the larger matrix elements in the chromium salts. On the other hand, we do not know experimentally the influence of covalency in these salts, so a thorough numerical comparison between the manganese and the chromium salts is rather premature. Blume and Orbach [11]) predicted the relaxation times for Mn^{2+} to be a factor of 100 larger than for other iron group salts. Our present results do not support this crude order of magnitude estimate. Theoretical predictions of the numerical value of the coefficients of the direct process can not be made on the basis of simple parameters only, due to the complexity of the occurring matrix elements.

Summarizing, the direct relaxation process may be given in the high temperature approximation as $\tau^{-1} = A'TH^2$ with $A' \simeq 1\ kOe^{-2}K^{-1}s^{-1}$ for manganese salts and $A' \simeq 10\ kOe^{-2}K^{-1}s^{-1}$ for chromium salts.

CHAPTER IV

SPIN-LATTICE RELAXATION IN COBALT TUTTON SALTS

4.1 *Introduction*

The Tutton salts form monoclinic crystals with two molecules in a unit cell [32]. The general formula for the cobalt Tutton salts is $Co(M')_2(SO_4)_2.6H_2O$ in which M' is a monovalent cation (NH_4, K, Cs, etc.). The unit cell parameters of cobalt ammonium Tutton salt are: a = 9.25 Å, c = 6.24 Å and $\beta = 106^{o}56'$ [66]. Each cobalt ion is surrounded by an octahedron of six water molecules, resulting in a nearly tetragonal electrical crystalline field [67]. The symmetry axes of the crystal field at the site of the two cobalt ions in the unit cell have different directions with respect to the crystallographic axes. The $^4F_{9/2}$ ground state of the free cobalt ion is split into six doublets under the influence of the combined effect of the tetragonal crystal field and the spin-orbit coupling. The lowest doublet lies some hundreds of degrees below the other doublets [68], thus for experiments at low temperatures the cobalt Tutton salt may be considered as having an isolated Kramers doublet with effective spin $\frac{1}{2}$. Electron spin resonance experiments at 20 K on cobalt Tutton salts, magnetically diluted with zinc [67], yield the g values with respect to the crystal field axes as given in table XI.

Table XI

	g_x	g_y	g_z
$Co(NH_4)_2(SO_4)_2.6H_2O$	3.06	3.06	6.45
$CoK_2(SO_4)_2.6H_2O$	2.50	3.35	6.56

These values are not known for the cesium salt. As can be seen in tabel XI, the ammonium salt has an axial symmetry, while the potassium salt deviates from axial symmetry. The average g value for powdered samples becomes 4.49 in both salts.

Kronig and Van Vleck derived for the spin-lattice relaxation time of an isolated Kramers doublet (chapter I):

$$\tau^{-1} = AH^5\coth(g\mu_B H/2kT) + BH^0T^9J_8(\Theta_D/T) + CH^2T^7J_6(\Theta_D/T). \qquad (56)$$

The first term represents the direct relaxation process, which leads to $\tau_{dir}^{-1} \propto TH^4$ if $g\mu_B H \ll kT$. The second term is the expression for the Raman relaxation time with the characteristic temperature dependence occurring due to the 'Van Vleck cancellation'. The third term represents a second, field dependent, Raman process, which may exist because the 'Van Vleck cancellation' is avoided in the presence of an external magnetic field. Since the earliest investigations on spin-lattice relaxation phenomena, many experiments have been performed on cobalt Tutton salts, but no experimental verification of the theoretical predictions was obtained until 1973 [69]. In this paper, the observation of the $T^9 J_8(\Theta_D/T)$ Raman process in weak magnetic fields is reported for cobalt ammonium and cobalt potassium Tutton salt. The relaxation time at strong magnetic fields and liquid helium temperatures was observed to be proportional to $H^{-\alpha}$ with $\alpha<4$. It was demonstrated, that this behaviour is characteristic of a direct relaxation process, strongly affected by phonon-bottleneck effects. The apparent $\tau \propto H^{-4}$ dependence of the direct process was verified in zinc ammonium Tutton salt containing 2% cobalt, thus avoiding the phonon bottleneck.

The difficulties in studying the direct relaxation process at liquid helium temperatures are easily overcome at liquid hydrogen temperatures, where the phonon bottleneck is not present (chapter III). At these temperatures, the $T^9 J_8(\Theta_D/T)$ Raman process is effective in weak magnetic fields [69]. This process is field independent if $H \gg (b/C)^{\frac{1}{2}}$ (Brons-Van Vleck relation, eq.(28)), thus one may expect the direct process ($\tau \propto H^{-4}$) to dominate the (field independent) Raman process above a certain field value. Initially, investigations at liquid hydrogen temperatures and strong magnetic fields could be performed only with a nitrogen cooled pulse magnet (H_{max} = 32 kOe). The first results for powdered $Co(NH_4)_2(SO_4)_2.6H_2O$ are shown in fig. 24; a decrease of τ at the strongest fields is clearly observed. If this decrease is caused by the direct process, it is expected that the shortening of τ at T = 17 K occurs at a stronger field than at 14 K, because the Raman relaxation time decreases proportionally with T^{-9}, while $\tau_{dir} \propto T^{-1}$. This difference between the curves at 14 and 17 K was not seen in the experiments given in fig. 24. From these measurements one might conclude that the mechanism causing the shortening of the relaxation times above 20 kOe is almost as strongly temperature dependent as the $T^9 J_8(\Theta_D/T)$ Raman process. A possibility to cause such a behaviour would be the occurrence of the field dependent Raman process ($\tau^{-1} \propto H^2 T^7 J_6(\Theta_D/T)$). The maximum field of the pulse magnet was not strong enough to decide between the field dependent processes.

It was expected to gain more decisive information by extending the measurements towards 90 kOe, using the pulsed field magnet at the Natuurkundig

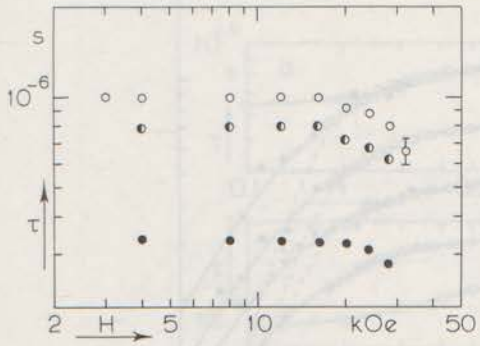

Fig. 24

The relaxation time as a function of magnetic field obtained with a nitrogen-cooled pulse magnet for powdered cobalt ammonium Tutton salt. ○: T = 14.1 K, ◐: T = 14.9 K, ●: T = 17.0 K.

Laboratorium of the University of Amsterdam [70]). The results obtained on powdered $Co(NH_4)_2(SO_4)_2.6H_2O$ are given in fig. 25 (closed symbols), more detailed information is given in ref. 71. The pulsed field experiments were influenced by mechanical resonance in the measuring coils, which reduced the accuracy. During the experiments in Amsterdam a superconducting magnet with a separate inner cryostat became available (H_{max} = 34 kOe), which enabled an accurate determination of $\tau(H)$ over a wide range of temperatures. Some of these results are given in fig. 25 also (open symbols). At weak magnetic fields the observed relaxation times are field independent, while above 20 kOe again a clear decrease of τ is observed. Therefore, the $\tau(H)$ curves from the experiments with the superconducting magnet were analyzed as a sum of two parallel processes, one being field independent, the other alternatively chosen as $\tau \propto H^{-4}$ or $\tau \propto H^{-2}$. As can be seen in fig. 25 the best fit with a least square computer programme is obtained with the quadratic field dependence (full lines). The relaxation times from the pulsed field experiments agree nicely with the extrapolation of those computer fits. A description of the observed shortening of τ above 20 kOe with $\tau \propto H^{-4}$ is less adequate (broken lines), so one may conclude that the field dependent Raman relaxation process is the likely cause of the strong field behaviour of τ.

For a unique verification of this process in cobalt Tutton salts, considering also its temperature dependence, an extensive determination of $\tau(H)$ above 35 kOe is required. In order to do so, the existing 50 kOe superconducting magnet was

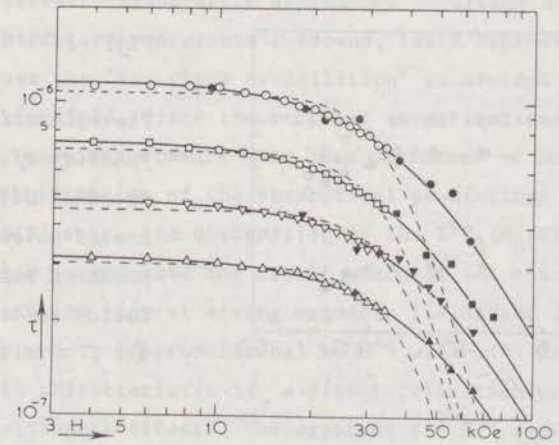

Fig. 25 *Relaxation time as a function of magnetic field for powdered* $Co(NH_4)_2(SO_4)_2.6H_2O$. ○, ●: *T = 14.1 K,* □, ■: *T = 15.0 K,* ▽, ▼: *T = 16.0 K,* △, ▲: *T = 17.0 K. Open symbols represent the relaxation times obtained with a superconducting magnet (Leiden), closed symbols refer to measurements in pulsed fields (Amsterdam). The full lines represent a computer fit with a quadratic field term, the broken lines are computer fits with* H^4 *at strong fields.*

modified so that a separate inner cryostat could be inserted (chapter II). In the next section we will review the detailed investigation with this magnet on a series of three cobalt Tutton salts. At a later stage it was even possible to use a 110 kOe magnet [72]), which gave us a nice opportunity to demonstrate the reliability of our results obtained below 50 kOe.

4.2 *Experimental results*

Measurements were performed on cobalt ammonium, cobalt potassium and cobalt cesium Tutton salt at liquid hydrogen temperatures and strong magnetic fields. During the analysis of the experimental results, it was felt that a study of the field independent Raman process and the direct process for our samples would also be significant. Previously, these processes in concentrated cobalt Tutton salts have

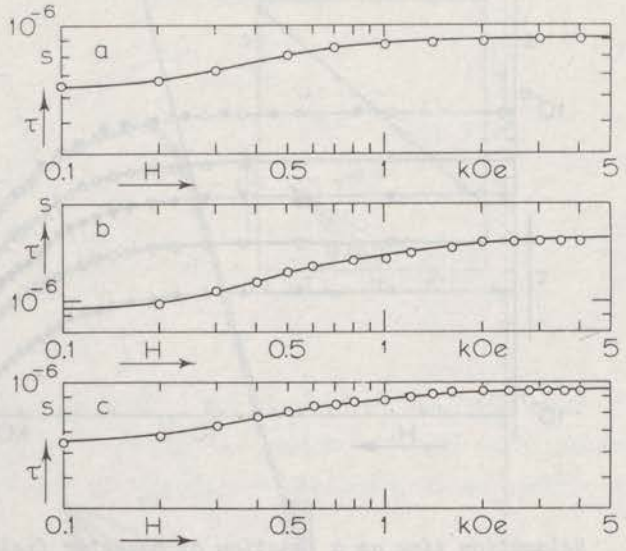

Fig. 26 Relaxation time as a function of magnetic field at T = 14.1 K for $Co(NH_4)_2(SO_4)_2.6H_2O$ (a), $CoK_2(SO_4)_2.6H_2O$ (b) and $CoCs_2(SO_4)_2.6H_2O$ (c). The full lines represent Brons-Van Vleck relations (eq.(28)) with b/C = 17.2 × 10^4 Oe^2.

been studied for $Co(NH_4)_2(SO_4)_2.6H_2O$ only [69]). Most of the present experiments were performed on powdered samples. The average crystal diameter was 0.1 mm, obtained by crushing a powder that came out of the solution as crystallites of about 0.5 mm diameter. For the preparation we used pro analysi chemicals (samples PA). In determining the direct process we needed samples from spectroscopically pure chemicals (samples SP). A survey of the measurements will be given successively for $Co(NH_4)_2(SO_4)_2.6H_2O$, $CoK_2(SO_4)_2.6H_2O$ and $CoCs_2(SO_4)_2.6H_2O$.

4.2.1 *Cobalt ammonium Tutton salt.* An extensive series of τ(H) curves for sample PA was determined at temperatures between 14 and 17 K in magnetic fields up to 47.5 kOe. Above 17 K the relaxation times in strong fields became too short to be measured with the present experimental equipment. At weak fields,

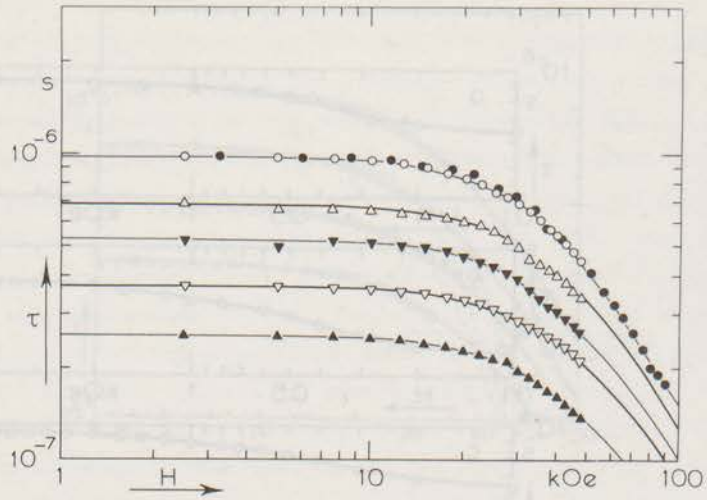

Fig. 27 Relaxation time as a function of magnetic field for cobalt ammonium Tutton salt. Closed circles: sample SP, other symbols: sample PA. ●, ○: T = 14.1 K, △: T = 14.79 K, ▼: T = 15.52 K, ▽: T = 16.02 K, ▲: T = 16.98 K. Full lines are computer fits according to $\tau^{-1} = B' + C'H^2$ *(eq.(57)).*

the τ(H) curves are adequately described by a Brons-Van Vleck relation (eq.(28)) with p = 0.7 and b/C = 17.2 x 10^4 Oe^2. As an example, the result at T = 14.1 K is given in fig. 26a. The value of the internal field is identical to the result from earlier susceptibility measurements [69]). Some of the τ(H) curves above 2 kOe are given in fig. 27. From 2 up to 10 kOe τ is constant, but above 10 kOe the relaxation times decrease continuously. Around our strongest field of 47.5 kOe the field dependence of the relaxation time may be given as $\tau \propto H^{-1.0}$. All reported relaxation times were obtained from semi-circles in the Argand diagrams. At a later stage of the experiments it became possible to measure a few τ(H) curves up to 100 kOe. This was done in order to show the reliability of the results described above. The actual check measurement, this time on the pure sample SP, is also inserted in fig. 27. No relevant differences were observed between sample SP and PA. The inverse proportional decrease of τ with H continues, approaching $\tau \propto H^{-2}$ at 95 kOe.

During the analysis of the above results it appeared useful to measure the

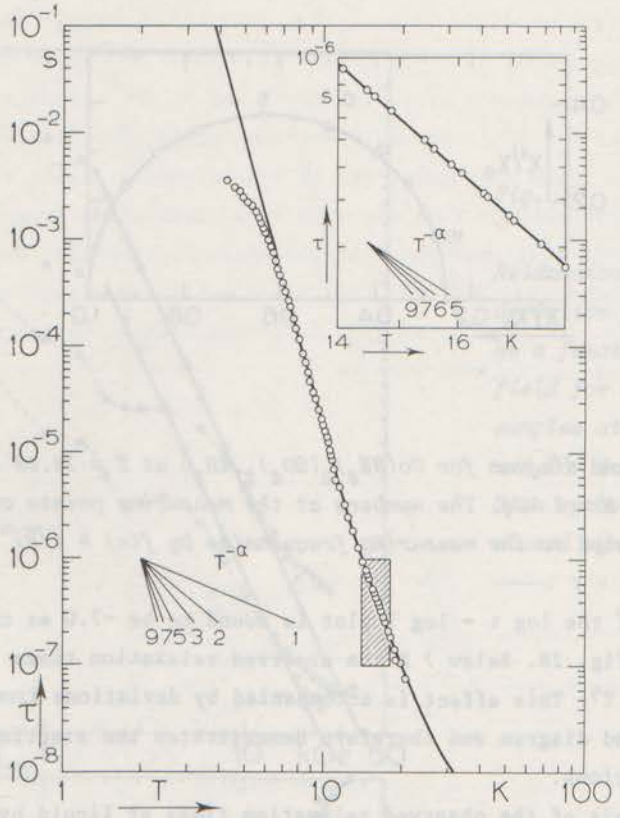

Fig. 28 Relaxation time as a function of temperature for $Co(NH_4)_2(SO_4)_2.6H_2O$ (sample PA) at H = 1 kOe.
———: $\tau^{-1} \propto T^9 J_8(145/T)$.

T^9 Raman process as observed earlier [69]) in more detail. This was done for sample PA between 4.2 and 20.4 K at an external magnetic field of 1 kOe (fig. 28). Between 4 and 14 K the so-called running method (chapter II) was used. Between 7 and 10 K the expected T^9 dependence of the relaxation rate is observed, at higher temperatures the observed exponent decreases. The results from the 'running method' rely on single frequency measurements. Between 14 and 18 K the full Argand diagrams were measured in detail (d = 0, example in fig. 29)

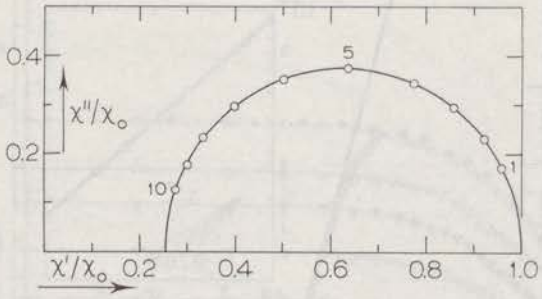

Fig. 29 Argand diagram for $Co(NH_4)_2(SO_4)_2.6H_2O$ at T = 14.09 K and H = 1 kOe. The numbers at the measuring points are related to the measuring frequencies by $f(n) = (\sqrt{2})^n \times 30$ kHz.

and the exponent of the log τ - log T plot is found to be -7.0 as can be seen from the inset of fig. 28. Below 7 K the observed relaxation times start to deviate from $\tau^{-1} \propto T^9$. This effect is accompanied by deviations from a semi-circle in the Argand diagram and therefore demonstrates the starting influence of impurity relaxations.

For the analysis of the observed relaxation times at liquid hydrogen temperatures the numerical value of the direct process relaxation time was also needed. From the earlier measurements [69]) one may obtain an estimate for the direct process, but at present the accuracy of the determination is higher and we wanted to be sure that the values we used did apply for the samples that were studied. Therefore, $\tau(H)$ was measured at various liquid helium temperatures in magnetic fields up to 34 kOe. As an example the results for sample PA at T = 4.21 and 1.97 K are given in fig. 30a (closed symbols). The relaxation times decrease irregularly with the magnetic field, a steepest slope in the log τ - log H graph being reached at about 10 kOe ($\tau \propto H^{-1.8}$). Deviations from semi-circles in the Argand diagrams were observed over the whole field range. The deviation parameter d decreases irregularly in weak fields also, while above 10 kOe a strong increase is observed (fig. 30b, closed symbols). The behaviour of $\tau(H)$ and d(H) in weak fields was measured earlier [18,69]) and was demonstrated to be due to the influence of chemical impurities. To exclude this effect the above measurements were

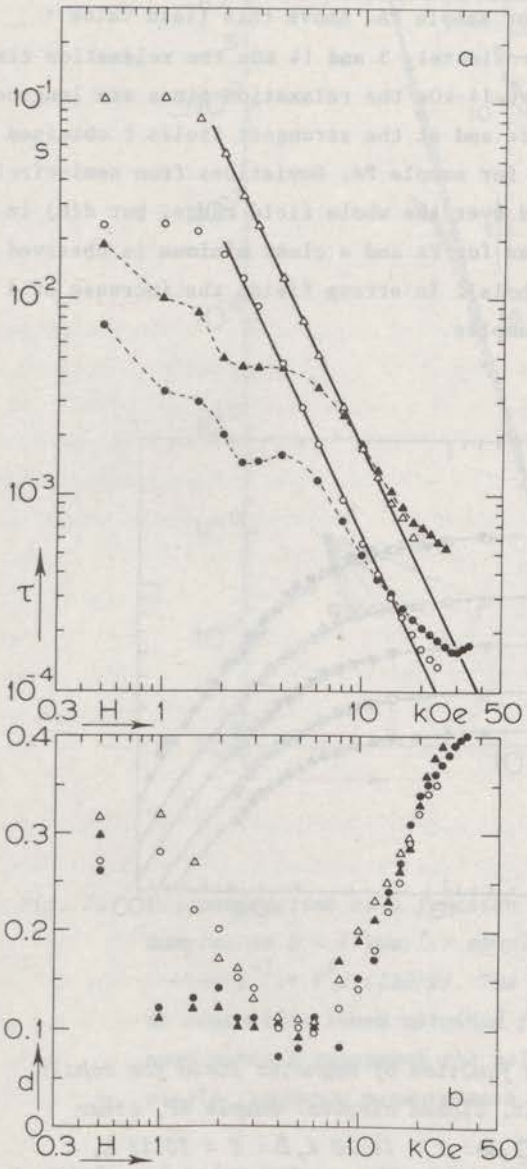

Fig. 30

Relaxation time (a) and deviation parameter (b) as a function of magnetic field for $Co(NH_4)_2(SO_4)_2 \cdot 6H_2O$ *samples at T = 2.0 K (△, ▲) and T = 4.2 K (○, ●). Open symbols: sample SP, closed symbols: sample PA,* ——: $\tau \propto H^{-2.1}$.

repeated on the spectroscopically pure sample SP. We studied this sample at various temperatures, as an example the results at T = 4.20 and 2.00 K are given in fig. 30 (open symbols). Below 2 kOe, τ is field independent and about an order of magnitude longer than for sample PA. Above this field value τ decreases continuously. Between approximately 3 and 14 kOe the relaxation times can be given as $\tau^{-1} \propto T^{1.2}H^{2.1}$. Above 14 kOe the relaxation times are lengthened with respect to this field dependence and at the strongest fields τ obtained on sample SP becomes even shorter than for sample PA. Deviations from semi-circles in the Argand diagrams were observed over the whole field range, but d(H) in weak fields is now more smoothed than for PA and a clear minimum is observed at about 5 kOe (fig. 30b, open symbols). In strong fields the increase of d is more or less identical in both samples.

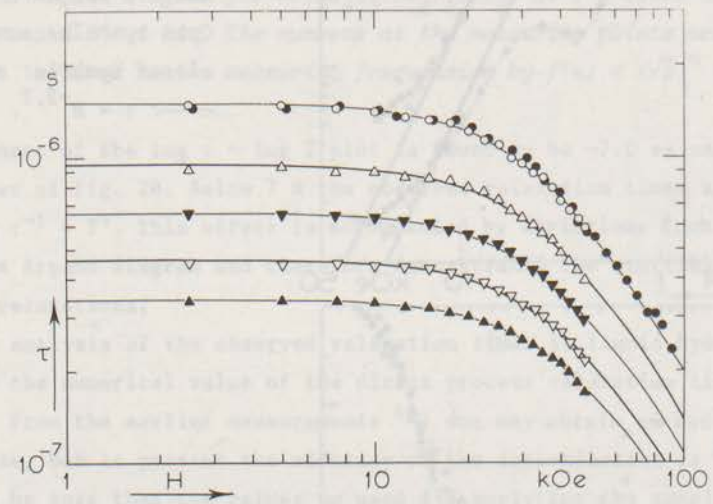

Fig. 31 Relaxation time as a function of magnetic field for cobalt potassium Tutton salt. Closed circles: sample SP, other symbols: sample PA. ○, ●: T = 14.10 K, △: T = 15.18 K, ▼: T = 16.06 K, ▽: T = 17.01 K, ▲: T = 18.01 K, ———: computer fits according to eq.(57).

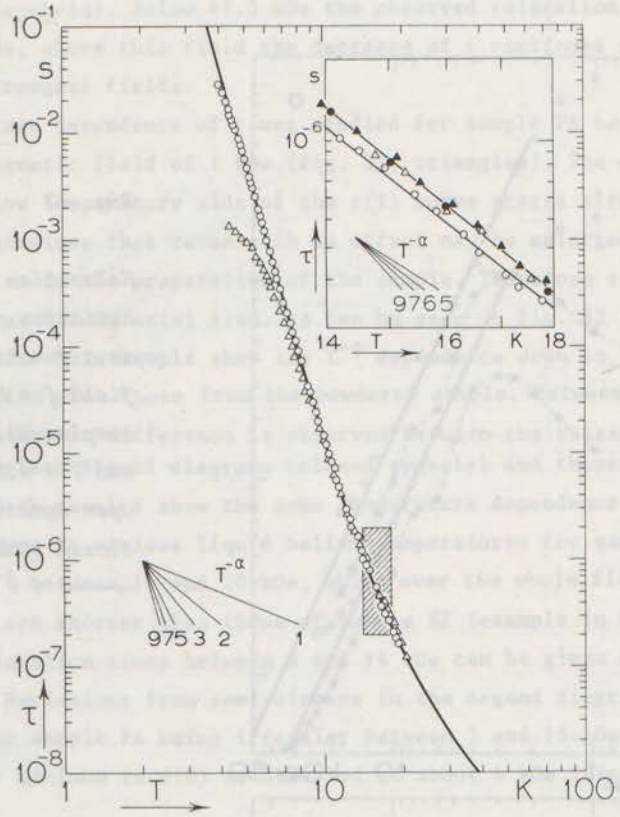

Fig. 32 Relaxation time as a function of temperature for $CoK_2(SO_4)_2.6H_2O$ samples at H = 1 kOe. Δ: sample PA, ○: single crystal (H//K_3), ——: $\tau^{-1} \propto T^9 J_8(120/T)$. The closed symbols in the inset refer to relaxation times obtained from complete Argand diagrams, the open symbols represent the relaxation times as obtained from single frequency measurements.

4.2.2 *Cobalt potassium Tutton salt.* Similar measurements to those mentioned above were performed on cobalt potassium Tutton salt. At liquid hydrogen temperatures τ increases in weak magnetic fields according to a Brons-Van Vleck relation with p = 0.6 and b/C = 17.2 x 10^4 Oe^2 (example in fig. 26b). A set of τ(H) curves above 2 kOe for sample PA is shown in fig. 31, the only difference between the

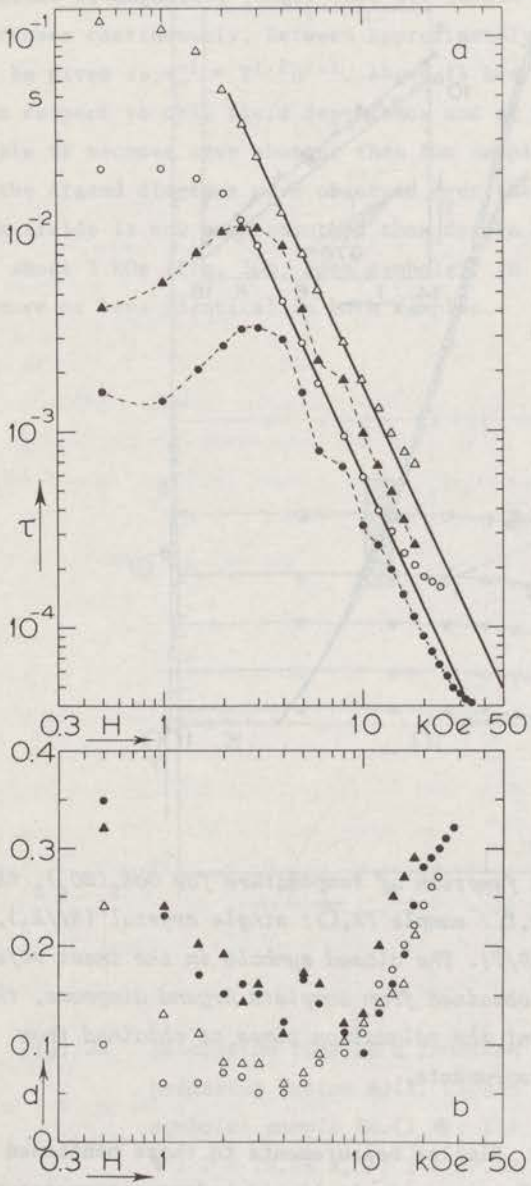

Fig. 33

Relaxation time (a) and deviation parameter (b) as a function of magnetic field for $CoK_2(SO_4)_2.6H_2O$ *samples at T = 2.0 K (Δ, ▲) and T = 4.2 K (○, ●). Open symbols: samples SP, closed symbols: sample PA,* ———: $\tau \propto H^{-2.2}$.

cobalt ammonium Tutton salt being that τ is about a factor of 1.5 longer in the potassium salt. A check measurement up to 95 kOe was performed on sample SP (fig. 31, closed symbols). Below 47.5 kOe the observed relaxation times for both SP and PA coincide, above this field the decrease of τ continues approaching $\tau \propto H^{-2}$ at the strongest fields.

The temperature dependence of τ was studied for sample PA between 4 and 20 K at an external magnetic field of 1 kOe (fig. 32, triangles). The deviation from $\tau^{-1} \propto T^9$ on the low temperature side of the $\tau(T)$ curve starts already below 9 K. The impurity relaxations that cause such an effect may be enlarged by the crushing of the crystallites in the preparation of the sample. Therefore $\tau(T)$ is determined on a single crystal ($H//K_3$ axis) also. As can be seen in fig. 32 (circles) the relaxation times for this sample show the T^{-9} dependence down to 4.5 K, above 9 K the results coincide with those from the powdered sample. Between 14 and 18 K (inset of fig. 32) a systematic difference is observed between the relaxation times obtained from complete Argand diagrams (closed symbols) and those from the running method. Both results show the same temperature dependence ($\tau \propto T^{-6.2}$).

The $\tau(H)$ curves at various liquid helium temperatures for sample PA reach at most $\tau^{-1} \propto H^{2.3}$ between 14 and 20 kOe, while over the whole field range the relaxation times are shorter than those of sample SP (example in fig. 33a). For sample SP the relaxation times between 3 and 14 kOe can be given by $\tau^{-1} \propto T^{1.5}H^{2.2}$. For both samples deviations from semi-circles in the Argand diagrams have been observed, d(H) for sample PA being irregular between 2 and 15 kOe, while for sample SP a clear minimum in d(H) is observed at about 4 kOe (fig. 33b).

4.2.3 *Cobalt cesium Tutton salt.* Measurements at liquid hydrogen temperatures on cobalt cesium Tutton salt revealed identical $\tau(H)$ curves as observed for the ammonium and potassium Tutton salt, with a Brons-Van Vleck relation ($p = 0.7$, $b/C = 17.2 \times 10^4$ Oe^2) in weak fields (example in fig. 26c) and decreasing relaxation times in strong fields tending towards H^{-2} (fig. 34, open symbols). A series of $\tau(H)$ curves was determined for sample SP also (fig. 34, closed symbols). Below 10 kOe, τ is about 10% longer than for PA, above 25 kOe the relaxation times for both samples coincide.

The relaxation time as a function of temperature was studied on sample PA between 4 and 20 K at H = 1 kOe (fig. 35, triangles). In order to reduce the influence of physical impurities at the lowest temperatures this measurement was repeated on a single crystal with $H//K_3$ axis (fig. 35, circles). Below 7 K the relaxation times for the single crystal become longer than for sample PA, above this temperature they coincide. Between 14 and 18 K, τ is proportional to $T^{-6.5}$ for both samples (inset in fig. 35). The shape of the $\tau(T)$ curve is identical

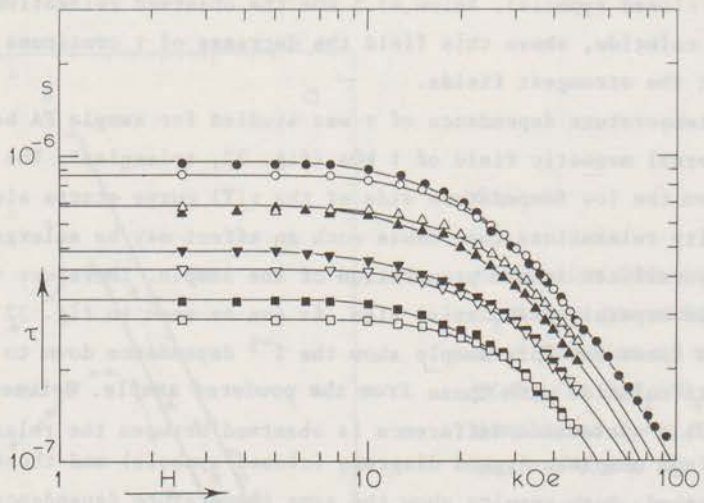

Fig. 34 Relaxation time as a function of magnetic field for cobalt cesium Tutton salt. Closed symbols: sample SP, open symbols: sample PA. ○ ,● : T = 14.11 K,△: T = 14.76 K,▲: T = 15.01 K, ▽,▼ : T = 16.00 K,□ ,■ : T = 16.95 K, ——: computer fits according to eq.(57).

to those observed for the ammonium and the potassium salts.

Some of the $\tau(H)$ curves obtained at liquid helium temperatures for the samples PA and SP are given in fig. 36. The relaxation times for sample PA reach at most $\tau^{-1} \propto H^{2.3}$ at about 10 kOe, while for sample SP the relaxation times between 4 and 10 kOe can be given as $\tau^{-1} \propto T^{1.7}H^{2.4}$. The shape of the $d(H)$ curves is identical to that observed for the other cobalt Tutton salts.

4.3 *Discussion.*

The various results obtained on the cobalt ammonium, the cobalt potassium and the cobalt cesium Tutton salts show a striking similarity. The observed $\tau(T)$ and $\tau(H)$ curves are similar for the three compounds. We shall discuss the results for the three compounds together.

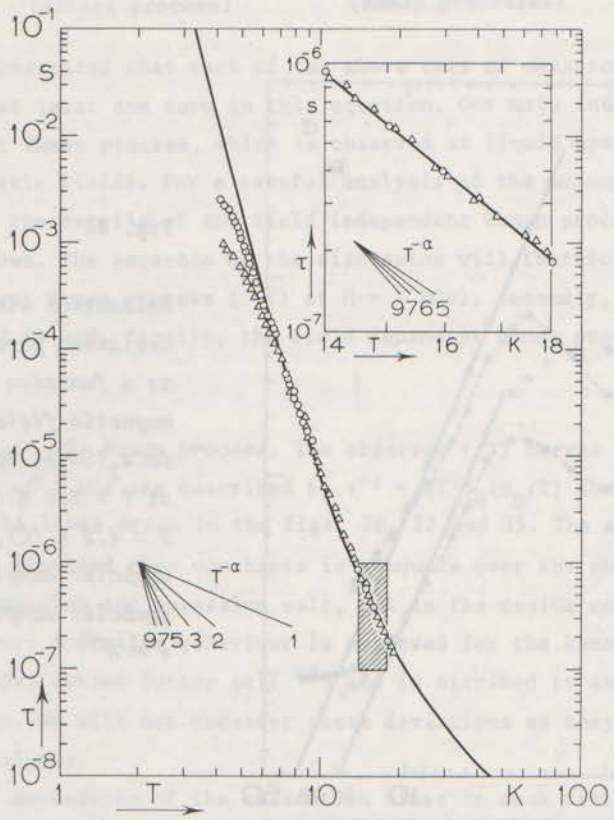

Fig. 35 Relaxation time as a function of temperature for $CoCs_2(SO_4)_2.6H_2O$ samples at H = 1 kOe. Δ: sample PA, ○: single crystal (H//K_3), ——: $\tau^{-1} \propto T^9 J_8(95/T)$.

The investigations may be divided into three typical sets of measurements:

- the relaxation time as a function of magnetic field at liquid hydrogen temperatures,
- the relaxation time as a function of temperature between 4 and 21 K at an external magnetic field of 1 kOe,
- the relaxation time as a function of magnetic field at liquid helium temperatures.

The expression for the spin-lattice relaxation time in cobalt Tutton salts was expected to be as given in eq.(56):

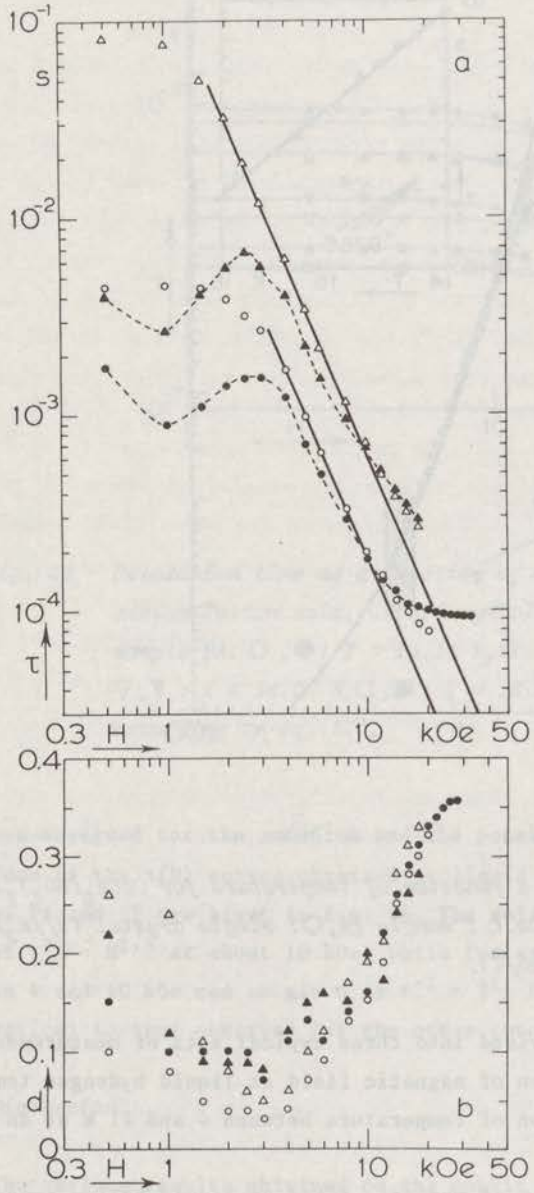

Fig. 36

Relaxation time (a) and deviation parameter (b) as a function of external magnetic field for $CoCs_2(SO_4)_2.6H_2O$ *samples at T = 2.0 K (△, ▲) and T = 4.2 K (○, ●). Open symbols: sample SP, closed symbols: sample PA, ———:* $\tau \propto H^{-2.4}$.

$$\tau^{-1} = AH^5\coth(g\mu_B H/2kT) + BH^0T^9J_8(\Theta_D/T) + CH^2T^7J_6(\Theta_D/T).$$

(direct process) (Raman processes)

It will be demonstrated that each of the above sets of measurements shows the occurrence of at least one term in this equation. Our main interest lies in the field dependent Raman process, which is observed at liquid hydrogen temperatures in strong magnetic fields. For a careful analysis of the measurements it is essential that the details of the field independent Raman process and of the direct process are known. The sequence of the discussion will therefore be, firstly, the field independent Raman process ($\tau(T)$ at H = 1 kOe), secondly, the direct process ($\tau(H)$ below 4.2 K) and, finally, the field dependent Raman process ($\tau(H)$ between 14 and 18 K.

4.3.1 *The $T^9J_8(\Theta_D/T)$ Raman process.* The observed $\tau(T)$ curves at an external magnetic field of 1 kOe are described by $\tau^{-1} = BT^9J_8(\Theta_D/T)$ above about 7 K, as can be seen by the full lines drawn in the figs. 28, 32 and 35. The agreement between these curves and the observed time constants is adequate over the whole temperature range in the ammonium and potassium salt, but in the cesium compound small deviations occur. A similar behaviour is observed for the Raman relaxation process in copper cesium Tutton salt [50]) and is ascribed to anomalies in the phonon spectrum. We will not consider these deviations as they do not influence our further analysis.

The field dependence of the relaxation times in weak fields at liquid hydrogen temperatures fulfils the Brons-Van Vleck relation for the three compounds, as was mentioned above (examples in fig. 26). Thus, both the field and temperature dependence of τ are in agreement with that of the $T^9J_8(\Theta_D/T)$ Raman process. The measured $\tau(T)$ curves are extrapolated to strong fields according to the observed Brons-Van Vleck relations. Then the actual numerical values of the parameters in the strong field approximation of eq.(56) become:

$B = 1.5 \times 10^{-9}\ K^{-9}s^{-1}$ and $\Theta_D = 145$ K for $Co(NH_4)_2(SO_4)_2.6H_2O$,

$B = 2.1 \times 10^{-9}\ K^{-9}s^{-1}$ and $\Theta_D = 120$ K for $CoK_2(SO_4)_2.6H_2O$ and

$B = 6.9 \times 10^{-9}\ K^{-9}s^{-1}$ and $\Theta_D = 95$ K for $CoCs_2(SO_4)_2.6H_2O$

for both the powdered samples and the single crystals.

From these results the matrix elements occurring in the coefficients B may be compared with each other by elimination of the other parameters. The complete expression for the coefficient B can be derived from the general relation for the Raman relaxation time as given in eq.(14), which has to be adapted to the specific case of an isolated Kramers doublet (section 1.3.2). The velocity of sound in this expression is eliminated with eq.(11) and one finally obtains:

$$B = 2.3 \times 10^{5} \, (N^{10/3} \hbar^{3} / k \rho^{-4/3} M^{10/3} \Theta_D^{10} \Delta_c^{4}) \, | \sum_{jj'} \langle -a/2|V_j|-c/2\rangle\langle -c/2|V_j|a/2\rangle |^2 .$$

The values of M, the molecular weight, and ρ, the density of the crystal, are listed in table XII. The distance between the lowest doublet and the other doublets, Δ_c, is reported to be a few hundreds of degrees [68]). An accurate value for the samples we studied is not known, but we assume it to be equal to 350 K for the three cobalt Tutton salts. The matrix elements as estimated with the values of B and Θ_D as mentioned above, are given in table XII. As can be seen in this table, the matrix element for the ammonium salt is about a factor of 2 greater than for the two other compounds. A further discussion will be given after considering the aspects of the other relaxation processes in the cobalt Tutton salts.

Table XII

	ρ [51]) ($g\ cm^{-3}$)	M (g)	matrix elements (erg^2) from T^9J_8 Raman process	direct process	$H^2T^7J_6$ Raman process
$Co(NH_4)_2(SO_4)_2.6H_2O$	1.91	395	1.3×10^{-26}	4.0×10^{-14}	1.9×10^{-15}
$CoK_2(SO_4)_2.6H_2O$	2.22	437	0.6×10^{-26}	3.2×10^{-14}	0.8×10^{-15}
$CoCs_2(SO_4)_2.6H_2O$	2.70	625	0.6×10^{-26}	4.1×10^{-14}	0.7×10^{-15}

4.3.2 *The direct relaxation process.* Previous experiments at liquid helium temperatures revealed $\tau^{-1}_{direct} = 0.13\ TH^4\ s^{-1}$ (H in kOe) for cobalt ammonium Tutton salt [69]). Extrapolation of this result towards liquid hydrogen temperatures shows that the direct process relaxation time equals the time constant of the, field independent, $T^9J_8(\Theta_D/T)$ Raman process at a magnetic field of about 27 kOe at T = 14 K. This would imply that above this field value the observed time constants must show the influence of the direct process. The measurements given in fig. 25 did already demonstrate that the direct process was not seen at liquid hydrogen temperatures. In order to verify that the numerical value given above for the

direct process applies for our samples, the field dependence of τ at liquid helium temperatures for the three cobalt Tutton salts was studied.

The $\tau(H)$ and the corresponding d(H) curves as obtained from our experiments at liquid helium temperatures (figs. 30, 33 and 36) clearly show the features of a bottlenecked direct process. The expected $\tau \propto H^{-4}$ dependence is not reached and the deviation parameter d increases strongly above 5 kOe. We applied the interpolation method (see section 3.3) in order to obtain a reliable estimate for the coefficient A of the direct process. The results are given in table XIII.

Table XIII

Coefficients A($kOe^{-3}K^{-1}s^{-1}$) of the direct process in cobalt Tutton salts obtained using the interpolation method.

	sample PA	sample SP
$Co(NH_4)_2(SO_4)_2.6H_2O$	0.10	0.10
$CoK_2(SO_4)_2.6H_2O$	0.06	0.15
$CoCs_2(SO_4)_2.6H_2O$	0.40	0.50

In this determination we used the simplified expression for the direct relaxation process ($\tau^{-1} = ATH^4$) which is only valid in the case that $g\mu_B H \ll kT$. Under our experimental conditions this simplification is correct within 5%, which lies within the accuracy of the determination of A. The accuracy in A for the samples PA is only 20% due to the anomalous behaviour of d(H) in weak fields. The A values for the samples SP are considered to be 10% accurate. For the ammonium and the cesium salt the values do not differ essentially between the PA and the SP samples, the resulting A values for the two potassium samples showing a considerable difference. The actual d values for this compound, especially for sample PA, remain higher than in the other substances, so a wider distribution of relaxation times is expected to occur. The values of A for the ammonium and the potassium (SP) salt are in fair agreement with the earlier experiments [69], no previous result is known for the cobalt cesium Tutton salt.

From the A values in table XIII the matrix elements of the direct process for the three compounds can be calculated. The expression for A is given by (chapter I):

$$A = 3.4 \times 10^3 \, (g^4 \mu_B^4 N^5 / 3\hbar / M^5 / 3\rho^{-2} / 3 k^4 \Theta_D^5 \Delta_c^2) \, | \sum_j \langle -c/2|J|a/2\rangle\langle a/2|V_j|c/2\rangle |^2 .$$

The resulting values for the matrix elements are given in table XII, showing

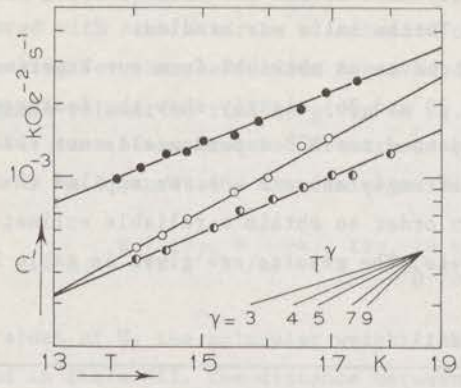

Fig. 37

Coefficients C', obtained from the computer fits with $\tau^{-1} = B' + C'H^2$ *to the observed* $\tau(H)$ *curves, as a function of temperature (double logarithmic scale).* ○ : $Co(NH_4)_2(SO_4)_2.6H_2O$, ◐ : $CoK_2(SO_4)_2.6H_2O$, ● : $CoCs_2(SO_4)_2.6H_2O$.

that the value for the potassium salt (sample SP) is about 20% smaller than for the other compounds.

4.3.3 *The* $H^2T^7J_6(\Theta_D/T)$ *Raman process.* At liquid hydrogen temperatures τ starts to decrease continuously above approximately 10 kOe and tends towards H^{-2} at the strongest fields. This behaviour of $\tau(H)$ is identical for the three cobalt Tutton salts (figs. 27, 31 and 34). In the further analysis of these $\tau(H)$ curves we omit the decrease of τ below 2 kOe according to the Brons-Van Vleck relation. The shape of the observed $\tau(H)$ curves suggests that the T^9 Raman process is dominated at strong fields by another relaxation process with a time constant that decreases with increasing magnetic field. The processes that are known to show such a behaviour are the direct process with $\tau \propto H^{-4}T^{-1}$ and the Raman process with $\tau \propto H^{-2}T^{-7}J_6^{-1}(\Theta_D/T)$. Preliminary measurements on cobalt ammonium Tutton salt (cf. fig. 25) demonstrated the field dependence of τ^{-1} to be more a H^2 than a H^4 dependence. Therefore a description with the field dependent Raman process with its striking field and temperature dependence must account for the observed field dependence at strong fields.

The observed $\tau(H)$ curves are fitted to an expression consisting of two terms, one being field independent, the other proportional to H^2. This fit was provided by a computer programme according to

$$\tau^{-1} = B' + C'H^2 \qquad (57)$$

and yields an adequate description of the observed $\tau(H)$ curves (full lines in figs. 27, 31 and 34). The resulting coefficients B' depend on temperature proportionally with $T^9J_8(\Theta_D/T)$, characteristic of the Raman process observed in

Table XIV

Various values of γ ($=-d(\log \tau)/d(\log T)$) calculated from $\tau^{-1} = T^7 J_6(\Theta_D/T)$.

γ	Θ_D/T	γ	Θ_D/T
2.1	0.92	5.2	7.1
2.5	2.1	5.6	8.0
3.0	3.1	6.0	9.0
3.5	4.0	6.3	10.0
4.1	5.1	6.7	12.1
4.7	6.1	6.9	14.4

weak fields. As this process has been discussed in section 4.3.1, we can now concentrate on the coefficients C'.

The coefficient C' is expected to be proportional to $T^7 J_6(\Theta_D/T)$, if the conclusion in the preliminary results, to attribute this process to the field dependent Raman relaxation process, is correct. The integral $J_6(\Theta_D/T)$ causes the temperature dependence of C' to vary from T^7 at $T \lesssim 0.1\Theta_D$ towards T^2 at $T > \Theta_D$. The coefficients C' are plotted on a double logarithmic scale against the temperature (fig. 37). From this figure it is seen that our temperature interval is far too small to notice the above mentioned variation in the exponent. Our results may be given as $C' \propto T^\gamma$ with $\gamma = 5.5$, 4.3 and 3.9 for the ammonium, potassium and cesium salt, respectively. Such strongly temperature dependent coefficients C' do suggest the $H^2T^7J_6(\Theta_D/T)$ Raman process to be the cause of the strong field relaxation behaviour. The exponent γ is directly related to the value of Θ_D/T for temperatures $0.1\ \Theta_D < T < \Theta_D$, as can be calculated from the temperature derivative of the curve $T^7 J_6(\Theta_D/T)$. This dependence is shown in table XIV. From a more comprehensive version of this table the reported γ values suggest the Debije temperatures as given in table XV. These results are about 20% smaller than the values reported in 4.3.1, which are also given in this table. In spite of these differences in Θ_D, both the field and temperature dependence of the observed relaxation times at strong fields are in fair agreement with the prediction for a $H^2T^7J_6(\Theta_D/T)$ Raman process. The Debije temperatures from the $T^9J_8(\Theta_D/T)$ Raman process were determined over a larger interval in T, and may therefore be considered as more reliable. Using these values (first column of table XV) the results at strong fields can be given as $\tau^{-1} = CH^2T^7J_6(\Theta_D/T)$

Table XV

Debije temperatures for cobalt Tutton salts as obtained from the Raman processes.

	from $T^9J_8(\Theta_D/T)$	from $H^2T^7J_6(\Theta_D/T)$
	Θ_D(K)	Θ_D(K)
$Co(NH_4)_2(SO_4)_2.6H_2O$	145	125
$CoK_2(SO_4)_2.6H_2O$	120	85
$CoCs_2(SO_4)_2.6H_2O$	95	75

with

$C = 6.3 \times 10^{-15}$ $kOe^{-2}K^{-7}s^{-1}$ for $Co(NH_4)_2(SO_4)_2.6H_2O$,

$C = 6.5 \times 10^{-15}$ $kOe^{-2}K^{-7}s^{-1}$ for $CoK_2(SO_4)_2.6H_2O$ and

$C = 2.2 \times 10^{-14}$ $kOe^{-2}K^{-7}s^{-1}$ for $CoCs_2(SO_4)_2.6H_2O$.

The complete expression for the coefficient C is (chapter I):

$$C = 2.3 \times 10^{5} \, (g^2 \mu_B^2 N^{10/3} \hbar^3 / k^3 \rho^{-4/3} M^{10/3} \Theta_D^{10} \Delta_c^2) \, |\sum_{jj'} \langle -a/2|V_{jj'}|a/2\rangle|^2.$$

Substituting all quantities for the various compounds, the values of the matrix elements given in table XII are obtained. The matrix element for the ammonium salt is about a factor of 2 larger than for the other two compounds. The same difference is observed for the matrix elements as calculated from the $T^9J_8(\Theta_D/T)$ Raman process. This suggests a similarity between the potassium and the cesium salt which is not present with the ammonium compound. In the potassium salt there is a departure from axial symmetry of the tetragonal crystalline field at the site of the Co^{2+} ion, which is not present with the ammonium salt, as reported in section 4.1. The symmetry in the cobalt cesium Tutton salt is not known, but the above suggests it to be similar to that in the potassium salt. We did not bring into the discussion the matrix elements as obtained from the direct process in view of the accuracy of the A values obtained with the interpolation method.

4.3.4 *Additional comments on the direct process in cobalt Tutton salts.* So far we have not considered the fact that the difficulties in studying the direct

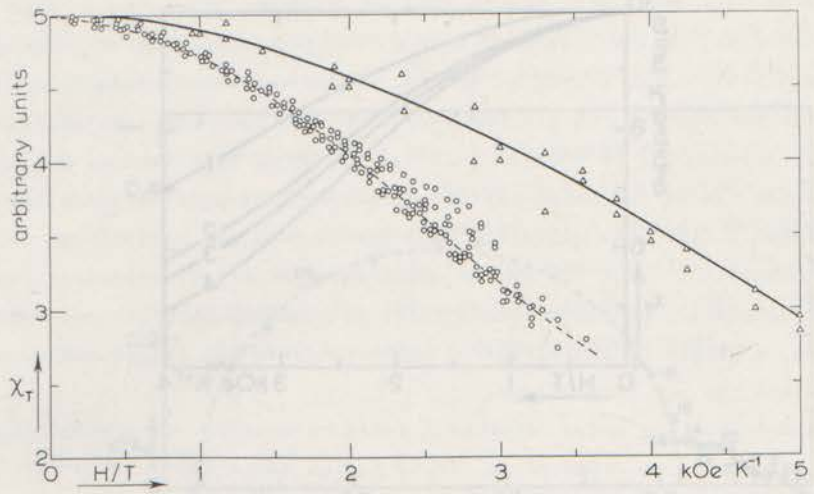

Fig. 38 The isothermal susceptibility χ_T as a function of H/T for $Co(NH_4)_2(SO_4)_2.6H_2O$ as obtained from the semi-circles in the Argand diagrams at liquid hydrogen temperatures (○) and liquid helium temperatures (△). The full line represents χ_T as calculated [64]) with g = 4.49.

relaxation process at liquid helium temperatures were expected to be overcome at liquid hydrogen temperatures (chapter III). Extrapolation of the direct process relaxation time as obtained from our measurements at liquid helium temperatures (4.3.2) to T = 14 K shows that this direct process should be more effective than the observed Raman processes above 29 kOe for $Co(NH_4)_2(SO_4)_2.6H_2O$, above 24 kOe for $CoK_2(SO_4)_2.6H_2O$ and above 19 kOe for $CoCs_2(SO_4)_2.6H_2O$. It was demonstrated above (section 4.3.3) that there is no indication for the direct process to be included in the observed $\tau(H)$ curves at liquid hydrogen temperatures, nor can the observed temperature dependence of τ account for this process. The question remains as to why we did not observe the direct process at liquid hydrogen temperatures.

So far we did not mention that another relaxation process exists at liquid hydrogen temperatures, operating parallel to the above discussed Raman processes, but causing minor susceptibility variations. It is worth to study this extra

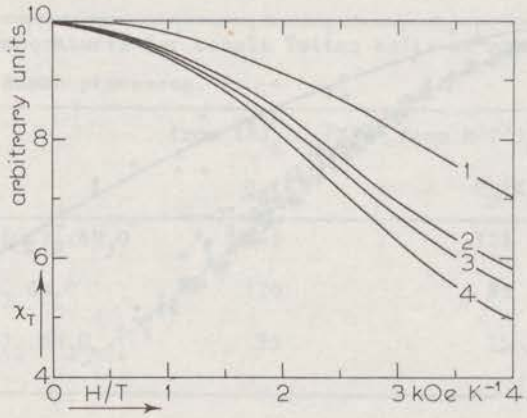

Fig. 39 A comparison of χ_T as obtained from the semi-circles in the Argand diagrams at liquid hydrogen temperatures for $Co(NH_4)_2(SO_4)_2.6H_2O$ (curve 4), $CoK_2(SO_4)_2.6H_2O$ (3) and $CoCs_2(SO_4)_2.6H_2O$ (2) with the calculation from ref. 64 with g = 4.49 (curve 1).

process in more detail, in view of the fact that the direct process was not seen at the liquid hydrogen temperatures. The existence of the extra relaxation process was found from a careful analysis of the Argand diagrams. The quoted relaxation times at liquid hydrogen temperatures (figs. 27, 31 and 34) were obtained from semi-circles in these diagrams. Extrapolation of these semi-circles to χ' at frequencies $\omega \ll \tau^{-1}$ yields the isothermal susceptibility χ_T (section 2.1.1). The thus obtained values for χ_T at various liquid hydrogen and liquid helium temperatures are plotted as a function of H/T in fig. 38 for $Co(NH_4)_2(SO_4)_2 \cdot 6H_2O$. This isothermal susceptibility χ_T can also be derived from the Curie-Weiss law in combination with a Brillouin function for the saturation [64]). The thus calculated χ_T(H/T) curve, using g = 4.49 for powdered cobalt Tutton salt, is inserted in fig. 38 (full line). As can be seen in this figure, the isothermal susceptibilities determined at liquid hydrogen temperatures lie considerably below the calculated line, while the results obtained at liquid helium temperatures are in good agreement with this theoretical curve. This agreement means that our

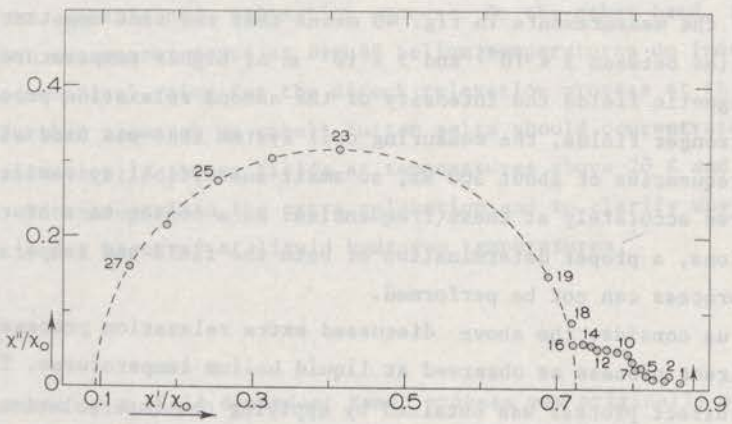

Fig. 40 Argand diagram for $Co(NH_4)_2(SO_4)_2.6H_2O$ at T = 14.05 K and H = 35 kOe. The numbers at the measuring points are related to the measuring frequency according to $f(n) = (\sqrt{2})^n \times 82.9$ Hz. The broken line represents a semi-circle. ↑ : χ_T calculated from ref. 64.

powdered samples may indeed be considered as randomly oriented crystallites with g = 4.49. A similar effect is seen in the measurements of χ_T on the other cobalt Tutton salts. The discrepancy between the average experimental results at liquid hydrogen temperatures for the three compounds (full lines 2, 3 and 4) and the calculated curve 1 can be seen in fig. 39. Such differences can only be ascribed to the occurrence of another relaxation process at liquid hydrogen temperatures, which means that our initial estimates for the susceptibility in the case $\omega << \tau^{-1}$ do not yield really the isothermal susceptibility χ_T.

In order to examine the existence of such an extra relaxation process, the susceptibility measurements at liquid hydrogen temperatures were extended to much lower frequencies. It was found that the Argand diagrams showed, apart from the large semi-circles around 200 kHz from which the Raman relaxation times were determined, also a small asymmetric broadening on the low frequency side. Measuring down to 100 Hz, the χ' values reached the theoretical χ_T, while small

χ'' values occurred. Such a behaviour was observed for the three compounds we studied, as an example we give the Argand diagram for cobalt ammonium Tutton salt at T = 14.05 K and H = 35 kOe in fig. 40. However, the curve in this figure is too smoothed at the low frequency side to determine the time constant of the second relaxation process properly. Rather, we indicate its order of magnitude, which for the measurements in fig. 40 means that the time constant of the second process lies between 3×10^{-5} and 3×10^{-6} s. At higher temperatures and/or weaker magnetic fields the intensity of the second relaxation process decreases. In the stronger fields, the measuring coil system that was used starts to cut off at frequencies of about 500 Hz, so small susceptibility variations can not be measured accurately at these frequencies. As a consequence of these experimental restrictions, a proper determination of both the field and temperature dependence of this process can not be performed.

Let us consider the above discussed extra relaxation process in relation to the direct process as observed at liquid helium temperatures. The coefficient A of the direct process was obtained by applying the interpolation method to the results at liquid helium temperatures. In doing so, it was assumed that the direct relaxation time is proportional to $T^{-1}H^{-4}$, a dependence that was justified by the observation of this H^{-4} dependence in magnetically diluted cobalt Tutton salts [69]). Several rare earth Kramers ions, if present in small concentrations, show the TH^4 dependence of the direct relaxation process, while, if such ions occur in larger concentrations, the dependence of τ^{-1} was demonstrated to be as TH^2 [73,74,75]). Such a behaviour was predicted theoretically by Baker and Ford [73]), who ascribed it to relaxations via forbidden transitions between hyperfine levels. Cobalt has a nuclear spin of 7/2, so according to Baker and Ford, a $\tau^{-1} \propto TH^2$ direct process is possible if the cobalt ions occur in large concentrations. If this is true, applying the interpolation method with a TH^4 direct process, is wrong and one should reanalyze the results discussed in section 4.3.2 in terms of a TH^2 direct relaxation process. We performed this analysis and found the so-obtained direct relaxation process to extrapolate to relaxation times at liquid hydrogen temperatures that fall within the range indicated above for the extra relaxation mechanism. In order to make the above suppositions more definite, Flokstra and Van der Marel at the Technische Hogeschool Twente studied $\tau(H)$ of cobalt ammonium Tutton salt at liquid helium temperatures, as their experiment enables a study of the direct relaxation process in the presence of the phonon bottleneck [76]). Their preliminary results clearly show the H^{-4} dependence for the direct process relaxation times of undiluted cobalt ammonium Tutton salt, with a coefficient A that is in numerical agreement with our result from the

interpolation method [77]). So the just mentioned possible occurrence of a TH^2 direct process in concentrated cobalt Tutton salt is not justified.

Instead of determining the direct relaxation process from the low frequency side of the Argand diagrams at liquid hydrogen temperatures, our measurements introduce another, unexplained, relaxation process. On the other hand, it is demonstrated that our measurements at liquid helium temperatures do indeed give a reliable numerical value for the direct relaxation process at these temperatures. Further research on cobalt Tutton salts should concentrate on the study of the relaxation in strong fields at temperatures above 20 K and between 4 and 14 K, in order to explain the extra relaxation and to clarify why the direct process is not observed at liquid hydrogen temperatures.

4.4 *Conclusion*

The occurrence of a field dependent Raman process was originally predicted by Kronig in 1939 [8]). The first experimental verification was found in three cobalt Tutton salts from the striking field and temperature dependence of the observed time constants at liquid hydrogen temperatures and strong magnetic fields. Numerically this process can be given as $\tau^{-1} = CH^2T^7J_6(\Theta_D/T)$ with

$$C = 6.3 \times 10^{-15}\ \text{kOe}^{-2}\text{K}^{-7}\text{s}^{-1} \text{ and } \Theta_D = 145\ \text{K for } Co(NH_4)_2(SO_4)_2.6H_2O,$$

$$C = 6.5 \times 10^{-15}\ \text{kOe}^{-2}\text{K}^{-7}\text{s}^{-1} \text{ and } \Theta_D = 120\ \text{K for } CoK_2(SO_4)_2.6H_2O \text{ and}$$

$$C = 2.2 \times 10^{-14}\ \text{kOe}^{-2}\text{K}^{-7}\text{s}^{-1} \text{ and } \Theta_D = 95\ \text{K for } CoCs_2(SO_4)_2.6H_2O.$$

A proper TH^4 dependence, as expected for the direct process relaxation rate in Co^{2+} compounds at liquid helium temperatures, is obscured by the phonon bottleneck. The direct process was examined with the interpolation method and turned out to be in numerical agreement with the result on diluted samples. The detailed analysis of the susceptibilities at liquid hydrogen temperatures showed the occurrence of another relaxation mechanism at strong fields with relaxation times that are approximately a factor of 100 longer than for the Raman processes. A definite conclusion concerning this mechanism is, as yet, not possible.

REFERENCES

1) Van Vleck, J.H., The Theory of Electric and Magnetic Susceptibilities, Oxford University Press (1932).
2) Hebel, L.C. and Slichter, C.P., Phys. Rev. 113 (1959) 1504.
3) Verstelle, J.C. and Curtis, D.A., Handbuch der Physik (1968) Bd. 18/1.
4) Ziman, J.M., Electrons and Phonons, Oxford University Press (1960).
5) Orbach, R., Proc. Roy. Soc. A264 (1961) 458.
6) Waller, I., Z. Physik 79 (1932) 370.
7) Al'tshuler, S.A., Izv. Akad. Nauk SSSR, 20 (1956) 1207.
8) Kronig, R. de L., Physica 6 (1939) 33.
9) Van Vleck, J.H., Phys. Rev. 57 (1940) 426.
10) Kramers, H.A., Proc. Kon. Ned. Akad. Wetenschap. 33 (1930) 959.
11) Blume, M. and Orbach, R., Phys. Rev. 127 (1962) 1587.
12) Brons, F., thesis, Groningen 1938.
13) Orbach, R., Proc. Roy. Soc. A264 (1961) 485.
14) Casimir, H.B.G. and Du Pré, F.K., Physica 5 (1938) 507; (Commun. Kamerlingh Onnes Lab., Leiden Suppl. No. 85a).
15) Huber, D.L., Phys. Rev. B3 (1971) 836.
16) Cole, K.S. and Cole, R.H., J. Chem. Phys. 9 (1941) 341.
17) Tromp, H.R.C. and Van Duyneveldt, A.J., Physica 45 (1969) 445; (Commun. Leiden No. 376a).
18) Roest, J.A., Van Duyneveldt, A.J., Van der Bilt, A. and Gorter, C.J., Physica 64 (1973) 306; (Commun. Leiden No. 400a).
19) Stoneham, A.M., Proc. Phys. Soc. 86 (1965) 1163.
20) De Vries, A.J. and Livius, J.W.M., Appl. sci. Res. 17 (1967) 31; (Commun. Leiden No. 349a).
21) Orbach, R. and Blume, M., Phys. Rev. Letters 8 (1962) 478.
22) Gorter, C.J. and Van Duyneveldt, A.J., Proc. XIIIth Conf. Low Temperature Physics, Boulder (1972) 621.
23) Van Duyneveldt, A.J., Tromp, H.R.C. and Gorter, C.J., Physica 45 (1969) 272; (Commun. Leiden No. 374b).
24) De Vries, A.J., Livius, J.W.M., Curtis, D.A., Van Duyneveldt, A.J. and Gorter, C.J., Physica 36 (1967) 65; (Commun. Leiden No. 356a).
25) Van Duyneveldt, A.J., Pouw, C.L.M. and Breur, W., Physica 57 (1972) 205; (Commun. Leiden No. 387b).

26) Sitnikov, K.P., thesis, Kazan State University 1954.
27) Turoff, R.D., Coulter, R., Irish, J., Sundquist, M. and Buchner, E., Phys. Rev. 164 (1967) 406.
28) Bijl, D., Physica 16 (1950) 269; (Commun. Leiden No. 280b).
29) Teunissen, P. and Gorter, C.J., Physica 7 (1940) 33.
30) Kodera, E., Torii, A., Osaki, K. and Watanabé, T., J. Phys. Soc. Japan 32 (1972) 863.
31) Bleaney, B. and Ingram, D.J.E., Proc. Roy. Soc. A208 (1951) 143.
32) Hofman, W., Z. Krist. 78 (1931) 279.
33) Baur, W.H., Acta Cryst. 15 (1962) 815, 17 (1964) 863.
34) Starr, C., Phys. Rev. 60 (1941) 241.
35) De Vroomen, A.C., Lijphart, E.E. and Poulis, N.J., Physica 47 (1970) 458; (Commun. Leiden No. 377b).
36) Eijkelhof, H.M.C., Pouw, C.L.M. and Van Duyneveldt, A.J., Physica 62 (1972) 257; (Commun. Leiden No. 395b).
37) Soeteman, J., Bevaart, L. and Van Duyneveldt, A.J., Physica 74 (1974) 126; (Commun. Leiden No. 407a).
38) Ovchinnikov, I.V., Sov. Phys. Solid State 5 (1964) 1378.
39) Cianchi, L., Lett. Nuovo Cimento 1 (1971) 723.
40) IJdo, D.J.W., thesis, Leiden 1960.
41) Powell, H.M. and Wells, A.F., J. Chem. Soc. 62 (1935) 359.
42) Figgis, B.N., Gerloch, M. and Mason, R., Acta Cryst. 17 (1964) 506.
43) Henning, J.C.M. and Bongers, P.F., J. Phys. Chem. Solids 27 (1966) 745.
44) Blöte, H.W.J. and Huiskamp, W.J., Physica 53 (1971) 445; (Commun. Leiden No. 386a).
45) Roest, J.A., thesis, Leiden 1972.
46) Walker, M.B. and Williams, F.I.B., Can. J. Phys. 48 (1970) 355.
47) Matumura, O., J. Phys. Soc. Japan 14 (1959) 108.
48) Kondo, J., Progr. Theor. Phys. 28 (1962) 1026.
49) Sharma, R.R., Das, T.P. and Orbach, R., Phys. Rev. 155 (1967) 338.
50) Soeteman, J., thesis, Leiden 1974.
51) Handbook of Chemistry and Physics, Weast, R.C. (Ed.), Cleveland (1968).
52) Lipson, H. and Beevers, C.A., Proc. Roy. Soc. A148 (1935) 664.
53) Bagguley, D.M.S. and Griffiths, J.H.E., Proc. Roy. Soc. A204 (1951) 188.
54) Bleaney, B., Proc. Roy. Soc. A204 (1951) 203.
55) Van Duyneveldt, A.J., Tromp, H.R.C. and Gorter, C.J., Physica 38 (1968) 205; (Commun. Leiden No. 361c).

56) Guillien, R., C R Acad. Sci. 209 (1939) 21.
57) Schein, B.J.B., Lingafelter, E.C. and Stewart, J.M., J. Chem. Phys. 47 (1967) 5183.
58) Carlin, R.L. and Walker, I,M., J. Chem. Phys. 46 (1967) 3921.
59) Burns, G., Phys. Rev. 123 (1961) 1634.
60) Schwartz, R.W. and Carlin, R.L., J. Am. Chem. Soc. 92 (1970) 6763.
61) De Vrijer, F.W., thesis, Leiden 1951.
62) Gataullin, O.F., Zaripov, M.M., Mosina, L.V., Ryzhmanov, Y.V. and Yablokov, Y.V., Proc. XVIIIth Colloque AMPERE (1974) 455.
63) Hillaert, J.G.A., thesis, Leiden 1973.
64) Van den Broek, J., thesis, Leiden 1960.
65) Donoho, P.L., Phys. Rev. 133 (1964) A1080.
66) Rau, V.G. and Kurkutova, E.N., Sov. Phys. Crystallogr. 17 (1973) 997.
67) Bleaney, B. and Ingram, D.J.E., Proc. Roy. Soc. A208 (1951) 143.
68) Abragam, A. and Pryce, M.H.L., Proc. Roy. Soc. A206 (1951) 173.
69) Roest, J.A., Van Duyneveldt, A.J., Van der Bilt, A. and Gorter, C.J., Physica 64 (1973) 324; (Commun. Leiden No. 400b).
70) Roeland, L.W., Muller, F.A. and Gersdorf, R., Proc. Conf. Champs Magnétiques Intenses, Grenoble (1966) 175.
71) Van Duyneveldt, A.J., Pouw, C.L.M. and Breur, W., Phys. Stat. Sol. (b) 55 (1973) K63.
72) Metselaar, J.W., Jordaan, H.A., Schutter, J.W. and De Klerk, D., Cryogenics 10 (1970) 220; (Commun. Leiden No. 378c).
73) Baker, J.M. and Ford, N.C., Phys. Rev. 136 (1964) A1692.
74) Rimai, L., Bierig, R.W. and Silverman, B.D., Phys. Rev. 146 (1966) 222.
75) Breur, W. and Fain, S.C., Intern. J. Magnetism 2 (1972) 145.
76) Flokstra, J., Gerritsma, G.J., Hartemink, G.A. and Van der Marel, L.C., Physica 77 (1974) 99.
77) Flokstra, J., private communication.

SAMENVATTING

De eerste metingen op het gebied van spin-roosterrelaxatie zijn verricht met de zogenaamde niet-resonante technieken, waarbij de differentiële susceptibiliteit gemeten wordt bij relatief lage frekwenties (<10 MHz). De eenvoudige theorie zoals die afgeleid kan worden voor spin-roosterrelaxatieverschijnselen is alleen geldig voor geïsoleerde ionen. Deze situatie wordt het beste benaderd in magnetisch zeer verdunde materialen, terwijl de niet-resonante meetmethode juist geschikt is voor meer geconcentreerde stoffen. De ontwikkeling van de moderne elektronika maakte het gebruik van resonante technieken om de spin-roosterrelaxatie te bestuderen mogelijk. Met deze methodes zijn de theoretische voorspellingen regelmatig bevestigd in de magnetisch zeer verdunde materialen. De resonante technieken, die in het frekwentiegebied van de mikrogolven werken, zijn echter meestal beperkt tot een aantal specifieke magneetvelden. Bij de niet-resonante meetmethode is men niet gebonden aan een vaste keuze voor het magneetveld en deze methode is daarom erg geschikt voor het bepalen van de veldafhankelijkheid van relaxatietijden, speciaal sinds de toepassing van supergeleidende spoelen het mogelijk maakt dit bij sterke magneetvelden te doen. In sterke magneetvelden is de koppeling tussen de paramagnetische ionen en het veld groter dan die tussen de ionen onderling en daarom kan men onder deze experimentele omstandigheden ook de magnetisch geconcentreerde stoffen opgebouwd denken uit geïsoleerde ionen, zodat het vergelijken met de theorie mogelijk wordt.

Sinds de toepassing van sterke magneetvelden is de niet-resonante methode met succes aangewend voor het onderzoek van het directe spin-roosterrelaxatieproces in geconcentreerde stoffen. Maar de bepaling van dit proces kan beïnvloed worden door het optreden van de zogenaamde 'phonon bottleneck'. Dit effect ontstaat doordat bij de temperaturen van vloeibaar helium de roostertrillingen niet altijd in staat zijn tot een snel energietransport tussen het magnetische spinsysteem en de koelvloeistof. Deze 'bottleneck' zal niet aanwezig zijn als de experimenten bij hogere temperaturen, bijvoorbeeld bij temperaturen van vloeibaar waterstof, gedaan worden. Bij hogere temperaturen is de warmtecapaciteit van het systeem van roostertrillingen groter, zodat dit systeem minder beïnvloed wordt door het energietransport tussen spinsysteem en roostertrillingen. In dit proefschrift zijn metingen met een niet-resonante meetmethode van spin-roosterrelaxatietijden in enige mangaan-, chroom- en cobaltzouten beschreven, waarbij het onderzoek van de veldafhan-

kelijkheid van de relaxatietijden in sterke magneetvelden zich voor het eerst concentreerde op het temperatuurgebied van vloeibaar waterstof.

In hoofdstuk I wordt een overzicht gegeven van de mikroskopische theorie van de paramagnetische spin-roosterrelaxatie. De temperatuur- en veldafhankelijkheden van relaxatietijden in diverse gevallen worden besproken. In hoofdstuk II wordt aangegeven hoe uit susceptibiliteitsmetingen de spin-roosterrelaxatietijd bepaald kan worden. Het thermodynamische model van Casimir en Du Pré leidt tot een relatie tussen de relaxatietijd en de susceptibiliteit. Tot slot wordt in dit hoofdstuk een overzicht gegeven van de beschikbare meetapparatuur, te zamen met enkele gegevens over de gebruikte magneten.

In hoofdstuk III worden de metingen aan een aantal mangaan- en chroomzouten beschreven. In deze zouten kunnen de magnetische spins zich bij lage temperaturen over meer dan twee energieniveaus verdelen. Voor de spin-roosterrelaxatietijden in deze zogenaamde 'multilevel' systemen zijn karakteristieke temperatuur- en veldafhankelijkheden voorspeld, die experimenteel bevestigd zijn in de onderzochte mangaan- en chroomzouten. Het Ramanproces is waargenomen boven 10 K in zwakke magneetvelden, het directe proces in sterke magneetvelden bij temperaturen van vloeibaar helium én van vloeibaar waterstof. Er is aangetoond dat de storende invloed van de 'phonon bottleneck', die de nauwkeurigheid van de bepaling van het directe proces bij temperaturen van vloeibaar helium vermindert, niet aanwezig is boven 14 K. De grootte van de coëfficiënt van het directe proces wordt bepaald door de geluidssnelheid in het kristal en door de matrixelementen van de spin-roosterinteractie. De geluidssnelheid kan uitgedrukt worden in het molecuulgewicht, de dichtheid van het kristal en de Debijetemperatuur. De verschillende waarden van deze grootheden voor $MnSiF_6.6H_2O$, $Mn(NH_4)_2(SO_4)_2.6H_2O$ en $MnSO_4.4H_2O$ verklaren de waargenomen verschillen in het directe proces tussen deze drie mangaanzouten. De waarde van de matrixelementen hangt onder andere af van de mate van covalente binding van het magnetische ion met de omringende ionen. Een toename van de covalentie leidt tot een verlenging van het directe proces. Dit effect is geconstateerd voor Cs_3MnCl_5. De relaxatietijden van het directe proces en het Ramanproces voor de onderzochte chroomzouten, $CsCr(SO_4)_2.12H_2O$, $C(NH_2)_3Cr(Se_4)_2.6H_2O$ en $C(NH_2)_3Cr(SO_4)_2.6H_2O$, hebben dezelfde veld- en temperatuurafhankelijkheden als in de mangaanzouten, hetgeen aantoont dat ook de chroomzouten tot de 'multilevel' systemen gerekend moeten worden. De spin-roosterrelaxatietijden in de chroomzouten zijn korter dan in de onderzochte mangaanzouten.

In hoofdstuk IV tenslotte worden de metingen van relaxatietijden aan drie geconcentreerde cobalttuttonzouten beschreven. De cobaltzouten onderscheiden zich

van de eerder genoemde 'multilevel' systemen doordat slechts twee energieniveaus bezet zijn. De voor zo'n eenvoudiger systeem afgeleide temperatuur- en veldafhankelijkheden van de relaxatietijden voor het directe en het (veldonafhankelijke) Ramanproces zijn reeds eerder bevestigd voor een aantal cobaltzouten. Metingen van de veldafhankelijkheid van de relaxatietijden bij temperaturen van vloeibaar helium toonden aan dat het directe proces sterk beïnvloed wordt door de 'phonon bottleneck'. Voor $Co(NH_4)_2(SO_4)_2.6H_2O$, $CoK_2(SO_4)_2.6H_2O$ en $CoCs_2(SO_4)_2.6H_2O$ is het directe proces bepaald met toepassing van de zogenaamde interpolatiemethode. Extrapolatie van het gevonden directe proces naar hogere temperaturen doet verwachten dat dit proces ook boven 14 K waargenomen kan worden zonder de storende invloed van de 'phonon bottleneck'. Daarom zijn de spin-roosterrelaxatietijden voor de drie cobalttuttonzouten gemeten bij temperaturen van vloeibaar waterstof in magneetvelden tot 100 kOe. In zwakke magneetvelden wordt het veldonafhankelijke Ramanproces waargenomen. De veld- en temperatuurafhankelijkheid van de relaxatietijden in sterke magneetvelden kan niet aan het directe proces worden toegeschreven, maar vormt de eerste experimentele bevestiging van een veldafhankelijk Ramanproces, dat reeds in 1939 door Kronig voorspeld was. Uit de numerieke waarden van de coëfficiënten van beide Ramanprocessen kunnen de matrixelementen voor de drie cobaltzouten berekend worden. Voor het kalium- en het caesiumzout geeft dit identieke waarden, terwijl de matrixelementen voor het ammoniumzout ongeveer twee maal zo groot zijn als in deze twee zouten.

Op verzoek van de faculteit der Wiskunde en Natuurwetenschappen volgt hier een overzicht van mijn studie.

In juli 1965 behaalde ik het diploma Gymnasium β aan het St. Maartenslyceum te Voorburg, waarna ik de natuurkundestudie aan de Rijksuniversiteit te Leiden aanving. In november 1968 legde ik het kandidaatsexamen natuur- en wiskunde met bijvak sterrekunde af. Daarna begonnen mijn werkzaamheden op het Kamerlingh Onnes Laboratorium in de werkgroep 'Paramagnetische Relaxatie' van prof. dr. C.J. Gorter, waarvan de dagelijkse leiding berustte bij dr. A.J. van Duyneveldt. In december 1971 volgde het doctoraalexamen in de experimentele natuurkunde met als bijvak sociologie. Het Ministerie van Onderwijs en Wetenschappen verleende mij een promotiebeurs. In januari 1973 werd ik aangesteld als wetenschappelijk medewerker. Sinds september 1970 was ik tevens werkzaam op het natuurkundepraktikum voor prekandidaten. Thans ben ik leraar natuurkunde te Doetinchem.

Dit proefschrift is tot stand gekomen dankzij de medewerking van velen. In de eerste plaats dient dr. A.J. van Duyneveldt genoemd te worden, die mij het vak van de experimentele natuurkunde geleerd heeft. Zijn inzet en enthousiasme zijn voor mij een grote stimulans geweest. De samenwerking met hem is bepalend geweest voor de vorm en inhoud van dit proefschrift. De belangstelling die prof. dr. N.J. Poulis getoond heeft, heb ik zeer op prijs gesteld. De samenwerking binnen de werkgroep met drs. H.M.C. Eijkelhof en dr. J. Soeteman is altijd prettig geweest. Bij het verkrijgen en verwerken van de meetresultaten werd ik in meerdere of mindere mate bijgestaan door drs. A. van der Bilt, H.A. Groenendijk en J.P.C. Vreugdenhil. Technische assistentie werd altijd vlot en vaardig verleend door J. Bij. Het glastechnische gedeelte werd verzorgd door C.J. van Klink en L. van As. De cryogene afdeling zorgde altijd voor de benodigde hoeveelheden koelvloeistoffen. De meeste preparaten werden vervaardigd door mevr. M.A. Otten-Scholten, de guanidiniumpreparaten werden ter beschikking gesteld door prof. dr. R.L. Carlin. De figuren in dit proefschrift werden alle getekend en op foto gezet door W.F. Tegelaar. Het manuscript werd nauwgezet getypt door mevr. J.G.M. ten Hoorn-Kool. De Engelse tekst werd kritisch gelezen door Ir. P.D. Biggs.

STELLINGEN

behorende bij het proefschrift van

C.L.M. POUW

22 oktober 1975

1) Het directe spin-roosterrelaxatieproces in geconcentreerde paramagnetische stoffen kan met niet-resonante meettechnieken worden bestudeerd in sterke magneetvelden. Deze experimenten dienen bij voorkeur te worden gedaan bij hogere temperaturen dan die van vloeibaar helium.

Dit proefschrift, hoofdstuk III.

2) Om de invloed van covalentie op paramagnetische spin-roosterrelaxatie experimenteel vast te stellen, is een onderzoek van het directe proces in een aantal Mn^{2+}-verbindingen met verschillende mate van covalentie voor het magnetische ion gewenst. De coëfficiënten A van het directe proces voor de verschillende verbindingen mogen echter niet rechtstreeks met elkaar worden vergeleken.

Dit proefschrift, hoofdstuk III.

3) De wijze waarop Higuchi en Tanaka de concentratie-afhankelijkheid van infrarood bandbreedtes van enkele nitroverbindingen interpreteren, is onjuist.

S. Higuchi en S. Tanaka, Spectrochim. Acta 31A (1975) 1003.

4) De beschrijving van de "avalanche" doorslag van een halfgeleiderdiode met een zogenaamde kritische veldsterkte gaat aan het wezenlijke karakter ervan voorbij.

A.S. Grove, Physics and Technology of Semiconductor Devices.

5) Bij het produceren van zuivere orthowaterstof met gebruikmaking van preferentiële adsorptie kan, zonder noemenswaardig verlies aan zuiverheid, een aanzienlijk grotere opbrengst verkregen worden door een eenvoudige wijziging in de door Depatie en Mills beschreven procedure.

D.A. Depatie en R.L. Mills, Rev. Sci. Instr. 39 (1968) 105.

6) Villa en Hatfield beschrijven het door hen waargenomen EPR-spectrum van koperionen in bis(N,N-diëthyldithiocarbamaat)zink met behulp van S=1 koperparen. Zowel tegen de resultaten van de experimenten als tegen de conclusies kunnen overwegende bezwaren worden ingebracht.

J.F. Villa en W.E. Hatfield, Inorg. Chim. Acta 5 (1971) 145.

7) Voor het Raman spin-roosterrelaxatieproces van niet-Kramers ionen, waarbij de magnetische spins zich over meer dan twee energieniveaus kunnen verdelen (niet-Kramers "multilevel" systemen), is eenvoudig af te leiden dat de relaxatietijd evenredig is met $H^{-2}T^{-3}J_2^{-1}(\Theta_D/T)$.

Dit proefschrift, hoofdstuk I.

8) Het verdient aanbeveling het eventuele optreden van korte-afstandsordening in vloeibare, binaire legeringen in bepaalde gevallen te bestuderen met behulp van diffuse neutronenverstrooiing.

J. Vrijen en C. van Dijk, Proc. of the NATO Advanced Study Institute, Geilo (1975) 43.

9) Het functioneren van gemeentelijke loodsdiensten naast de Rijksloodsdienst, zoals momenteel het geval is in het Waterweggebied, is ondoelmatig.

10) Het is gewenst om kinderen van ouders die aan coronaire hartziekten lijden, regelmatig te laten controleren op een verhoogd cholesterolgehalte en een verhoogde bloeddruk.

11) De wettelijke verplichting om voor een benoeming in een onderwijsfunctie een "bewijs van goed gedrag" te kunnen overleggen, is in strijd met de Universele Verklaring van de Rechten van de Mens.